

Hydrostatic and Hydrodynamic

Evaluation of a

Suction-Stabilized Float

by

Luis Vendrell

A Thesis Presented in Partial Fulfillment
of the Requirements for the Degree
Master of Science in Technology

Approved April 2013 by the
Graduate Supervisory Committee:

Sangram Redkar
Bradley Rogers
John Rajadas

ARIZONA STATE UNIVERSITY

May 2013

ABSTRACT

This report examines the hydrostatic and hydrodynamic properties of a floating platform that uses a stability method known as Suction-Stabilization. This method differs from conventional methods of stabilization in that it utilizes an internal volume to raise the effective metacentric height through an inverse free surface effect. The specific case used in this report is a Suction-Stabilized Float meant for use in a backyard pool application. However, the analyses described in it are applicable to uses outside that of a pool, such as in a deep-sea wind turbine application. This report shows that Suction-Stabilization increases the stability of the float in both static and dynamic situations.

DEDICATION

This is dedicated to my beautiful wife, Crystal, and my two amazing children, Zackary and Eva. It is also dedicated to my mother, Lynn Thornburgh, and my father, Rudolph Vendrell, who funded the majority of my higher education.

ACKNOWLEDGMENTS

I would like to acknowledge and give infinite thanks to Professor Sangram Redkar for his amazing support and help in this project. He opened his office and met with me, for hours, to discuss the problems I encountered and helped me to overcome those obstacles. Without his guidance and willingness to help, I can honestly say I would not be graduating this semester. In addition, I would like to thank Professor Bradley Rogers and Professor John Rajadas who agreed to sit on my committee and help me graduate even after four years away from the program.

In that same vein, I want to thank my manager, Bob DeKruyff, who allowed me the time to work on this project, allowed me to use the office when I needed it, and read through this report and gave incredible feedback.

Lastly, I would like to make it painfully clear that without the time afforded to me by my family this project would never have reached a conclusion in the period allotted. Thanks to my wife and children for allowing me the time away from the house and thanks to my mother for watching the children when it was needed.

TABLE OF CONTENTS

	Page
LIST OF TABLES.....	vi
LIST OF FIGURES	vii
CHAPTER	
1 INTRODUCTION.....	1
2 LITERATURE REVIEW.....	5
3 BACKGROUND INFORMATION	11
4 BASELINE GEOMETRY	15
Baseline Geometry of the SSF.....	15
Coordinate System	18
5 HYDROSTATIC ANALYSIS: SSF WITHOUT MAST	20
Metacentric Height at 0° Heel	20
Calculation of Draught.....	20
Draught Calculation: Method 1	21
Draught Calculation: Method 2	23
Ballast Water Properties	25
Metacentric Radius	25
SSF Center of Gravity.....	26
Center of Buoyancy	26
Metacentric Height without IST Effect	27
IST Effect on Metacentric Height	27
Comparison: SSF and Non-SSF	28

	Geometric Variation: Section 4 Height	29
	Geometric Variation: Outer and Inner Diameter of Section 4.....	32
	Geometric Variation: Outer and Inner Diameter of All Sections....	36
6	MAST SIZING AND OPTIMIZATION.....	39
	The Kempf Factor Defined.....	39
	Mast Geometry Assumptions	40
	Input Parameters for Mast Study	41
	Mast Size Limits	42
	Mast Selection Criteria	44
7	HYDROSTATIC ANALYSIS: SSF WITH MAST	48
	SSF Properties with Mast	48
	Comparison: Non SSF and SSF	50
	Geometric Variations	51
8	RIGHTING MOMENT AND RIGHITNG LEVER ANALYSIS	54
	Righting Moment and Righting Lever: Baseline SSF	56
	Comparison: Non-SSF and SSF	62
	Righting Moment and Righting Lever For Varying Geometry	63
	Geometric Variation: Section 4 Height	64
	Geometric Variation: Section 4 Diameters	67
	Geometric Variation: All Section Diameters	71
	Comparison: All Geometric Variations.....	74
9	PARAMETRIC ROLL RESONANCE.....	78
	Parametric Roll with Damping	78

Defining the M_R and \overline{GZ} Curves	79
Susceptibility Criteria for Parametric Roll	81
Design Variables for Baseline SSF	81
Susceptibility Criteria	84
Numerical Simulation	85
10 WIND HEELING ARM ANALYSIS	91
Wind Heeling Arm Equation	92
Wind Heeling Arm Model	93
Wind Heeling Arm Evaluation	98
11 EXPERIMENTAL DATA	105
12 CONCLUSION AND FURTHER WORK	110
REFERENCES	113
APPENDIX	
A UMBRELLA USED AS MAST	A1

LIST OF TABLES

Table	Page
4.1. Density of SSF body and Submerging Fluid.....	16
4.2. Section Properties: Baseline SSF.....	17
4.3. Mass Properties: Baseline SSF	17
5.1. Comparison: Non-SSF and SSF	28
6.1. Mast Properties	42
6.2. Range of Mast Weights for Comfortable Float Motion	46
7.1. Hydrostatic Properties: SSF with Mast.....	49
7.2. Comparison: Hydrostatic Properties Non-SSF vs. SSF	50
8.1. Geometry Properties: Section 4 Height	65
8.2. Geometry Properties: Section 4 Diameters	68
8.3. Geometry Properties: All Section Diameters	72
8.4. Maximum Righting Moment Values	74
8.5. Maximum Righting Lever Values	75
8.6. Angles of Vanishing Stability and Air Entrance Angles	77
9.1. p and q Values for ABS Prescribed Values of μ	85
9.2. Inequality Values for ABS Prescribed Values of μ	85
10.1. Modeled Umbrella Properties	94
10.2. M_H for Various Wind Speeds	95
11.1. Calculated Properties for Experimental SSF.....	105
12.1. Comparison: All Geometric Variations	110

LIST OF FIGURES

Figure		Page
3.1.	General SSF	11
3.2.	Cross-Sectional View of General SSF	12
4.1.	Baseline SSF Geometry	15
4.2.	Cross-Section: Baseline SSF	16
4.3.	Definition of Coordinate System	18
5.1.	Section 4 Height Limits	29
5.2.	Draught vs. Section 4 Height	30
5.3.	Displaced Volume vs. Section 4 Height	31
5.4.	Hydrostatic Properties vs. Section 4 Height	32
5.5.	Section 4 Outer and Inner Diameter Limits	33
5.6.	Draught vs. Section 4 Diameters	33
5.7.	Displaced Volume vs. Section 4 Diameters	34
5.8.	Hydrostatic Properties vs. Section 4 Diameters	35
5.9.	All Outer and Inner Diameter Limits	36
5.10.	Draught vs. All Diameters	36
5.11.	Displaced Volume vs. All Diameters	37
5.12.	Hydrostatic Properties vs. All Diameters	38
6.1.	Pictorial Representation of Mast Geometry	41
6.2.	Draught vs. Mast Weight	42
6.3.	Metacentric Height vs. Mast Weight (up to 35lbs)	43
6.4.	Metacentric Height vs. Mast Weight (up to 33lbs)	44

6.5.	Kempf Factor vs. Mast Weight (up to 33lbs)	45
6.6.	Metacentric Height vs. Kempf Factor	46
7.1.	SSF with Mast at 0° Heel	48
7.2.	Hydrostatic Properties vs. Section 4 Height	51
7.3.	Hydrostatic Properties vs. Section 4 Diameters	52
7.4.	Hydrostatic Properties vs. All Diameters	53
8.1.	SSF with Mast at 0° Heel	54
8.2.	SSF with Mast at 31.5° Heel	55
8.3.	SSF with Mast at any Heel Angle, ϕ	56
8.4.	Righting Moment vs. Heel Angle: Baseline SSF	58
8.5.	Righting Lever Diagram	59
8.6.	Righting Lever vs. Heel Angle: Baseline SSF	59
8.7.	Water Plane Moment of Inertia vs. Heel Angle	60
8.8.	Comparison: Non-SSF and SSF Righting Moments	62
8.9.	Comparison: Non-SSF and SSF Righting Levers	63
8.10.	Section 4 Height Variations	64
8.11.	Righting Moment vs. Heel Angle: Section 4 Height	65
8.12.	Righting Lever vs. Heel Angle: Section 4 Height	66
8.13.	Section 4 Diameter Variations	67
8.14.	Righting Moment vs. Heel Angle: Section 4 Diameter	69
8.15.	Righting Lever vs. Heel Angle: Section 4 Diameter	70
8.16.	All Section Diameter Variations	70
8.17.	Righting Moment vs. Heel Angle: All Section Diameters	71

8.18.	Righting Lever vs. Heel Angle: All Section Diameters	73
8.19.	Righting Moment vs. Heel Angle: All Geometric Variations	75
8.20.	Righting Lever vs. Heel Angle: All Geometric Variations.....	76
9.1.	M_R Comparison: Empirical Data and Curve Fit	79
9.2.	\overline{GZ} Comparison: Empirical Data and Curve Fit	80
9.3.	Metacentric Height vs. Wave Crest Location.....	82
9.4.	Roll Amplitude for Free Roll, $\mu = 0.0$	86
9.5.	Roll Amplitude: $\mu = 0.03$	87
9.6.	Roll Amplitude: $\mu = 0.05$	87
9.7.	Roll Amplitude: $\mu = 0.075$	88
9.8.	Roll Amplitude: $\mu = 0.10$	88
9.9.	Roll Amplitude: $\phi_0 = 23.90^\circ$ & $\mu = 0.05$	89
9.10.	Roll Amplitude: $\phi_0 = 26.00^\circ$ & $\mu = 0.05$	90
10.1.	NREL (2011) Offshore Wind Data.....	91
10.2.	Projected Wind Area for Modeled Umbrella	93
10.3.	M_R Curve: Maximum Wind Heeling Moment	95
10.4.	M_R Curve: Various Wind Heeling Arms	96
10.5.	M_R Curve: Different ϕ_0 with common V_w	97
10.6.	$\phi_{01} = 0.00^\circ$, $\phi_{02} = 15.00^\circ$, $V_w = 315.00 \frac{in}{sec}$, & $\mu = 0.05$	99
10.7.	Wind Roll: $\phi_0 = 0.00^\circ$, $V_w = 315.00 \frac{in}{sec}$, & $\mu = 0.05$	100

10.8.	Wind Roll: $\phi_{01} = 15.00^\circ, V_w = 315.00 \frac{in}{sec}$, & $\mu = 0.05$	101
10.9.	Wind Heel Angles: $\phi_{01} = 0.00^\circ$ & $\phi_{02} = 15.00^\circ$	102
10.10.	Wind Heel Angles: $V_{w1} = 236.25 \frac{in}{sec}$ & $V_{w2} = 354.38 \frac{in}{sec}$	103
10.10.	$\phi_0 = 5.00^\circ, V_{w1} = 236.25 \frac{in}{sec}$, $V_{w2} = 354.38 \frac{in}{sec}$, & $\mu = 0.05$.	104
11.1.	Experimental SSF.....	106
11.2.	Actual Draught of Experimental SSF.....	106
11.3.	Heeled SSF	107
11.4.	Roll Amplitude: Baseline SSF Heeled to 22°	108
11.5.	Experimental SSF in Waves	109

Chapter 1

INTRODUCTION

Offshore wind power, available between 5 and 50 miles off the coast of the USA, is an untapped resource for renewable energy (Butterfield, et al, 2010, p. 1). A proposed method of harnessing this energy is by attaching a wind turbine to a floating platform. These platforms would float off the coast in wind rich locations. This requires that the platforms be stable in many conditions. They must be durable, able to support the weight of the wind turbine, and be able to withstand both wind and wave loads and the roll and pitch motions associated with them (Butterfield, et al, 2007, p. 1).

It is conventional for a floating platform to gain its buoyancy force by the direct displacement of water (Cheung, 2000, p. 1). Yet, there are other methods of stabilization and, in general, offshore platforms fall into one, or a combination, of three floating platform classifications: ballast, buoyancy, and mooring lines. All three of these classifications, when designed correctly, achieve a stable platform. However, all of them have disadvantages that should be weighed against their advantages (Butterfield, et al, 2007, p. 3-7).

The most common of the above stated methods of stabilization is the use of mooring lines, or Tension Leg Platforms (TLP). However, the richest wind resources are located in ocean areas where the depth is greater than 30m (Butterfield, et al, 2010, p. 1). This presents a problem when a floating platform is located in deep sea regions where the depth is great, because the cost increases with depth. Mooring lines are not economically feasible in deep water (Butterfield, et al, 2007, p. 3-7). Also, TLP's are complex and require significant onsite installation, unless significant design work is done to ensure it is

stable in shallow draught water, and that it has a self-deploying anchoring mechanism to allow for deployment from port (Butterfield, et al, 2007, p. 3-7).

The *Ballast Classification* includes floating platforms that uses ballast weight or a ballast tank to increase stability. An example is a spar-buoy, which has a large ballast weight suspended beneath the floating platform to resist roll motion (Butterfield, et al, 2011, p. 3-7). While the ballast classification, when compared to the other classifications, has increased wave resistance, does not have the same cost problems associated with a TLP, and requires little onsite installation and maintenance, it does have some drawbacks. The suspended ballast requires a certain depth for operation this renders float-out from port unfeasible unless, like the TLP, design work is done to ensure self-deployment of the suspended ballast weight once a proper depth is achieved. In addition, the ballast tank/weight is complex and costly (Butterfield, et al, 2007, p. 3-7).

The *Buoyancy Classification* includes floating platforms that use a weighted water plane area to increase stability. An example of such a platform is a barge (Butterfield, et al, 2007, p. 3-7). This allows for operation in all depths and allows for float-out from port. The simple shape of the barge allows for easier fabrication and it is less costly than both the TLP and spar-buoy. Its depth independence allows it to float freely without a specific location. To maintain a central location, the floating platform requires the use of catenary mooring and anchor lines (Butterfield, et al, 2007, p. 3-7).

There are additional “add-on” techniques that increase the stability of a floating platform (of any classification). These techniques include adding a bilge keel, adding a roll fin, integrating a passive roll tank, or using a pneumatic roll tank. However, not all of these are economically feasible and not all of them are compatible with the use of a wind

turbine. Therefore, the floating platform must be stable, compatible with a wind turbine, and economically feasible.

A Suction-Stabilized floating platform, or Suction-Stabilized Float (SSF), is an alternate option that may prove well suited for offshore wind applications. An SSF utilizes an internal void, or chamber, to trap water above the water plane. This trapped water acts as ballast that counters the roll or pitch motion of the floating platform. It does this by changing volume and weight with the roll or pitch motion of the float. As the float rolls or pitches, the center of gravity of the ballast water acts farther from the center of floatation, in the opposite direction of roll or pitch, to increase the restoring force. Its restoring effect increases with increased roll or pitch angle (Montgomery, 2012, p. 1), (Redkar, 2012, p. 2).

Currently, scale models constructed for use with an umbrella in a backyard pool application have proven stable in test trials. However, no rigorous mathematical models have been applied to these scale models to verify stability. These are necessary to expand upon the current model and to optimize the design without the time consuming process of trial and error associated with test trials.

This project aims to create a mathematical model for a suction stabilized float platform with the goal of defining the hydrostatic properties, determining the stability criteria, narrowing down the factors that increase or decrease stability, and suggesting methods to increase stability.

This report is organized as follows:

- Chapter 2 presents a literature review of current research pertaining to ship and floating platform hydrostatics and dynamic, deep-sea wind turbine floating platforms, and Suction-Stabilization.
- Chapter 3 presents background information as it relates to a Suction-Stabilized Float and gives a more detail definition of the SSF.
- Chapter 4 presents the baseline geometry of the SSF used for this report.
- Chapter 5 presents the basis for analysis of the baseline SSF without a mast and then expands that analysis to examine various geometries.
- Chapter 6 examines the ways in which adding a mast affects hydrostatic properties.
- Chapter 7 presents the analysis for the baseline SSF with a specific mast and then expands that analysis to examine various geometries.
- Chapter 8 presents that analysis for determining Righting Moment and Righting Lever of the SSF. Various Geometry changes are examined to examine how certain parameters affect the Righting Moment and Righting Lever.
- Chapter 9 presents the analysis for parametric roll resonance susceptibility of the baseline geometry.
- Chapter 10 presents the analysis for wind heeling moments of the baseline geometry at various wind speeds.
- Chapter 11 presents experimental data.
- Chapter 12 presents the conclusions drawn from chapters 1-11 and suggests areas of future work.

Chapter 2

LITERATURE REVIEW

In the textbook, *Ship Hydrostatics and Stability (2003)*, it fully describes the method of analyzing the stability of a ship. The most important metrics with respect to ship stability are the metacentric height, \overline{GM} and the righting lever, \overline{GZ} . The metacenter is the intersection of the line of action of the buoyancy force when the ship is upright and the line of action of the buoyancy force when the ship heels to an angle, ϕ (Biran, 2003, p. 37-40). A floating body is stable when the metacenter is vertically above the center of gravity. For large angle of heel, greater than 7° , metacentric height is not an accurate measure of stability. Beyond this angle, inclined waterlines no longer intersect the centerline and the metacenter moves away from its previous position (Vidac-Perunovic, 2011, p. 1, 2). Because of this, for heel and pitch angle above 7° , another metric must be used to determine stability.

The righting moment, as defined by Euler, is an alternate metric used to determine ship stability when the heel angle is large. This metric relates the couple of the gravitational force and the buoyancy force of the ship to the ship's stability. As long as the couple of these two forces causes a restoring, or righting, moment, which returns the ship to equilibrium, the ship remains stable (Kliava, 2010, p. 1).

Biran (2003) defines the righting moment as the product of the distance between the center of buoyancy and the ship center of gravity with the weight of the ship.

$$M_R = W_{ship} * \overline{GZ} \quad (2.1)$$

Where M_R is the righting moment, W_{ship} is the weight of the ship, and \overline{GZ} is the horizontal distance between the ship's center of gravity and the ship's center of buoyancy (Biran, 2003, p. 112).

The value \overline{GZ} characterizes the righting moment.

$$\overline{GZ} = \ell_k - \overline{KG} \sin \phi \quad (2.2)$$

Where ℓ_k is the value of stability cross-curves and is usually determined with the use of a computer, and \overline{KG} is the vertical distance between the bottom-most point on the ship and the ship's center of gravity. The relationship between value of stability cross-curves, ℓ_k , and the heel angle, ϕ , is not linear and, in general, cannot be defined explicitly. For small angles of heel, it is possible to calculate the righting lever using the metacentric height (Biran, 2003, p. 112-114).

$$\overline{GZ} = \overline{GM} \sin \phi \quad (2.3)$$

(2.3) is only valid for small angles, and the definition of a small angle is dependant on the specific ship (Biran, 2003, p. 113). In general, a small angle is one where the metacenter does not move visibly from its initial position in equilibrium.

The methods used in this text are the basis for the static analyses in this report. The equations defined in this text are for a ship and not a floating platform. The methods used in this text, while applicable, must be altered to account for the geometry of the float. In general, a float is a much simpler geometry than a ship. Where a ship is, usually, symmetric around one axis a float is symmetric around two.

Parametric roll resonance is defined as the amplification of roll motion in head or following seas. This occurs when the ship's wave encounter frequency is approximately

twice the natural roll frequency of the ship, and the damping is insufficient to dissipate parametric roll energy. The result is a resonant condition (ABS, 2008).

Roll motion is defined as follows in the ABS Guide (2008):

When the roll equilibrium is disturbed, the hydrostatic restoring moment acts to oppose the instantaneous roll angle and tends to return the ship back to the upright position. Because of inertia, the ship does not stop at the instant when the equilibrium angle is reached but continues to roll to at a progressively slower velocity until a maximum roll angle is reached. At this point, the excess roll restoring moment causes the ship to begin to right itself. Once upright, inertia causes the ship to continue to roll. As before, the restoring moment works against further motion and it stops at some roll angle. (ABS, 2004, p. 2)

The period of the above-described oscillations is the natural roll period of the ship.

The International Maritime Code (IMO) (1995) outlines the process for calculating wind loads. In the IMO code (1995), wind force, F_{wind} , is calculated by the following equation,

$$F_{wind} = \frac{1}{2} (C_S C_H \rho_{air} V^2 A) \quad (3.4)$$

Where C_S is the shape coefficient of the structural member exposed to the wind, C_H is the height coefficient which is dependent on the height above sea level of the structural member exposed to the wind, ρ_{air} is the air density ($1.222 \frac{kg}{m^3}$), V is the wind

velocity, and A is the projected area of all surfaces exposed to the wind. This is the equation used to calculate the wind heeling moment for this project.

The conference paper, *Engineering Challenges for Floating Offshore Wind Platforms* (2007), discusses the various issues and obstacles that offshore wind turbine platforms must overcome to become economically feasible. These include factors such as, water depth, topology, waves, sea ice, and seabed conditions.

There are no analytical methods presented in this paper. The focus is mainly on the big picture issues presented by the various classifications of floating platforms. It is applicable to this study because it defines several floating platform classifications and that it allows the reader to evaluate the issues that might arise from each.

The three classifications of offshore platforms are listed below:

1. **Ballast:** Platforms achieve stability by using ballast weights hung below a central buoyancy tank. These weights create a righting moment and provide a high resistance to roll and pitch. The draught on a ballast platform is generally high enough that it offsets heave motion (Butterfield, et al, 2007, p. 3).
2. **Mooring Lines:** Platforms achieve stability through mooring line tension, which creates a righting moment. A platform that utilizes a mooring line is called a Tension Leg Platform (TLP) (Butterfield, et al, 2007, p. 3).
3. **Buoyancy:** Platforms that use distributed buoyancy to achieve stability. The use of a weighted water plane serves to create a righting moment (Butterfield, et al, 2007, p. 3).

Other methods of roll stabilization that are used in shipbuilding, but are not applicable to this report, are listed below. These roll stabilization methods create a

moment that adds to the righting moment of the ship and increases the ships ability to restore itself to an equilibrium position (Biran, 2003, p. 286).

- **Bilge Keel:** A bilge keel is an appendage that protrudes from the longitudinal bottom edge of a ship or float platform. The bilge keel creates additional friction by increasing the wetted surface to resist roll motion. (Bangun, 2010). It does this by creating a hydrodynamic resistance force to oppose roll motion and by creating vortices that increase the viscous damping of the roll motion (Biran, 2003, p. 286).
- **Roll Fins:** Roll fins are wing shaped bodies that extend transversely from the body of a ship. Roll fins create hydrodynamic forces that oppose roll motion. The efficiency of a roll fin is reliant on the ship's velocity, so at low speeds, or – as in the case of platform – in the absence of forward velocity, it provides little to no additional roll resistance (Biran, 2003, p. 286).
- **Anti –Roll Tank:** An anti-roll tank operates by using a water mass as ballast. There are several different ways of creating an anti-roll tank, but the common method of operation is the same for all. It operates by allowing the center of gravity of the water ballast to change position in such a way that it adds to the righting moment. For example, if the ship heels towards port, the water volume increases on the starboard side and decreases on the port side. This increases the ballast mass on the starboard side and thus, increases the righting moment and aides in roll resistance (Biran, 2003, p. 287-288).
- **Pneumatic Floating Platform:** A pneumatic floating platform utilizes indirect displacement, in which the platform has an open bottom trapping pressurized air that displaces water. This trapped air is used as the virtual spring and damper

system that helps the dynamic characteristics of the float platform (Cheung, 2000, p. 1)

None of the above listed roll stabilization methods, except a modified version of the anti-roll tank, are analyzed in this report. They are mentioned to inform the reader of other methods available and how they differ from the method of Suction-Stabilization.

Patent application number 13/242,489 describes the embodiments of a Suction-Stabilized Float (SSF). The SSF is a float that has a buoyant portion and an internal chamber portion, which is open at the bottom and holds a volume of liquid above the interface, or waterline, of the surrounding fluid (Montgomery, 2012, p. 1). The fluid trapped above the waterline creates a downward force that adds to the restoring moment of the SSF. It acts in the same manner as an anti-roll tank, only the volume is open to the submerging fluid rather than the atmosphere (Montgomery, 2012, p. 1). The SSF used for this report is one of the many embodiments described in the patent application. This patent application is a general description of a SSF and does not discuss analysis techniques.

Exhaustive searches for analyses and reports applicable to the method of Suction-Stabilization as described in Patent application number 13/242,489 have resulted in few pertinent references. Therefore, this project will adapt the existing theories of ship stability and apply them to the SSF platform described in Montgomery (2012).

Chapter 3

BACKGROUND INFORMATION

A suction-stabilized float (SSF) is a float platform that can, but does not require the use of devices such as mooring lines, bilge keels, and passive roll tanks to increase stability. Instead, the SSF utilizes an internal volume that is closed to the atmosphere and opens to the fluid in which it floats (Montgomery, 2012, p. 1), (Redkar, 2012, p. 2).

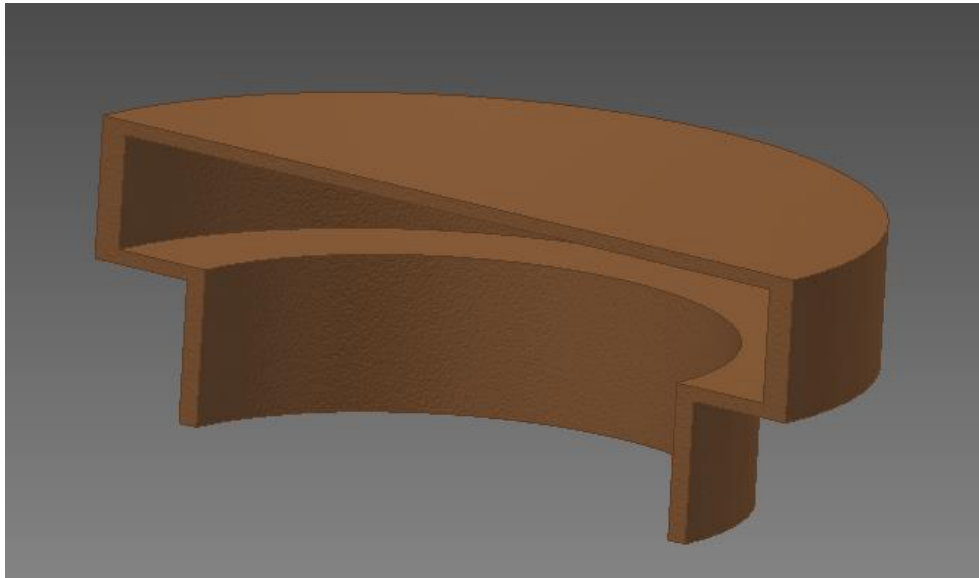


Figure 3.1: General SSF

Figure 3.1 shows an example of SSF geometry. In general, it is a float platform with more than one diameter: a smaller diameter lower section and a larger diameter upper section. The internal volume is hollow so that fluid can fill it completely. The SSF is sealed to the atmosphere and open to fluid. The geometry of the SSF is such that the waterline lies within the lower and upper limits of the larger volume. The effect of this is to “trap” fluid above the water line. The trapped water is in contact with the walls of the SSF on all sides except the bottom, where it is open to the fluid. The interface between the trapped ballast water and the submerging fluid is a closed surface, which forces the

internal fluid obey Pascal's Principle. Pascal's Principle states that pressure in a static fluid in a closed system is the same in all directions (Baumeister, et al, 1978, 3-37).

The body construction uses a material with a density much lower than that of the fluid in which it is submerged. This allows the fluid trapped inside the SSF to act as ballast. However, the effect of the trapped water does more than simply act as ballast. It also adds to the overall stability of the SSF by raising the effective metacentric height (Montgomery, 2012, p. 1), (Redkar, 2012, p. 2-5).

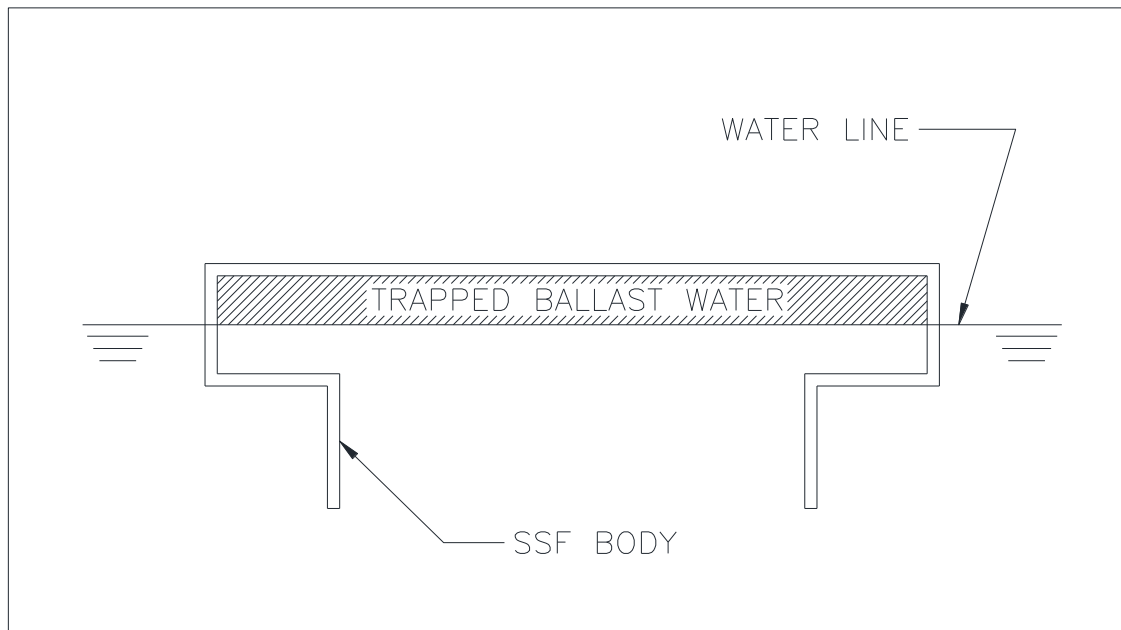


Figure 3.2: Cross-Sectional View of General SSF

When a floating platform, or ship, has an internal volume that is not enclosed on all four sides, it is called a *slack-tank*. The effect of this *slack-tank* is to lower the metacentric height through a phenomenon known as the “free surface effect” (Biran, 2003, p. 137-142). However, in the case of the SSF, the internal tank does not open to air but rather opens to the submerging fluid. The result of this is that the internal volume acts

as an inverse slack tank (IST) and raises the metacentric height rather than lower it (Redkar, 2012, p. 2-5).

In the case of a slack tank, when the ship or platform rotates away from equilibrium to any heel angle, the surface remains horizontal while the fluid in the tank conforms to the angle of heel. This results in an added wedge of fluid in the direction of heel and a subtracted wedge of fluid, of the same volume, on the side opposite of heel. This acts as a moving mass from one side of the ship or platform in the direction of heel and increases the heeling moment, which decreases stability (Unknown Author, 1987, p. 47).

For the SSF, the IST acts in an opposite manner. The ballast fluid trapped inside the internal volume shifts when the float undergoes either a roll or a pitch motion. When the SSF is subjected to a roll or pitch motion, the shape of trapped water along the waterline changes. For example, in the case of a small heel angle, when the SSF heels towards port (left) in a stable waterline the volume on the left side of the SSF is reduced while the volume starboard is increased. For small heel angles, these volumes are equivalent and the mass of the trapped fluid does not change. Therefore, the volume that is subtracted from the port side is added to the starboard side. This results in a shift of the center of gravity of the trapped fluid towards starboard. The net result is an additional righting moment that brings the SSF back to its equilibrium position, which is the opposite of free surface effect. For larger angles of heel, however, the mass of the trapped water increases to account for volumetric changes and increases the IST effect of the trapped water and increases the righting moment.

The SSF is used as a platform to hold a mast, either an umbrella or wind turbine, that is, in general, of similar weight to the SSF. Problems arise from the high center of gravity of the mast when attached to the SSF. Without the ballast mass of the “inverse slack tank,” the center of gravity falls above, or close to, the metacenter and the float becomes unstable. The IST acts to both raise this metacenter and increase stability (Redkar, 2012, p. 2-5).

For the SSF to function in its intended manner, it is necessary for the SSF to act as a closed system with the atmosphere, and that no air enters the internal volume. Referring to Pascal’s Principle, once the internal volume of the SSF is open to the atmosphere it is no longer a closed system and the pressure is no longer constant within the boundaries of the internal volume. This negates the IST effect and causes the trapped water to act a standard slack tank and lowers the effective metacentric height rather than increases it.

This extreme value of roll or pitch is defined as the *Air Entrance Angle*, α . This is not to be confused with the *Angle of Vanishing Stability*, ϕ_{VS} , which is the angle at which the righting moment becomes negative. However, both of these angles are significant in that they signify when the SSF is no longer stable. As a general statement of stability: *the SSF becomes unstable at the lesser of the two angles ϕ_{VS} and α .*

This report analyzes a specific case of a SSF. The stability of this SSF is analyzed in both static and dynamic situations. This specific case of the SSF serves as the baseline geometry. The baseline geometry is then expanded to explore how changing certain metrics affect the performance of the SSF.

Chapter 4

BASELINE GEOMETRY

Chapter 4 introduces the baseline float used for all analysis in this report. This geometry is used for the basis of comparison when other geometries are examined. If not explicitly stated, the baseline geometry is the basis for the analysis.

Baseline Geometry of SSF.

The platform analyzed in this project is a scaled model of one intended for use in a deep-sea wind turbine application. The intention and purpose of this platform is to serve as the floating base for an umbrella used in a backyard pool. However, the physics and analysis of this model are applicable to that of a larger model and can be adapted to an SSF used in a wind turbine application.

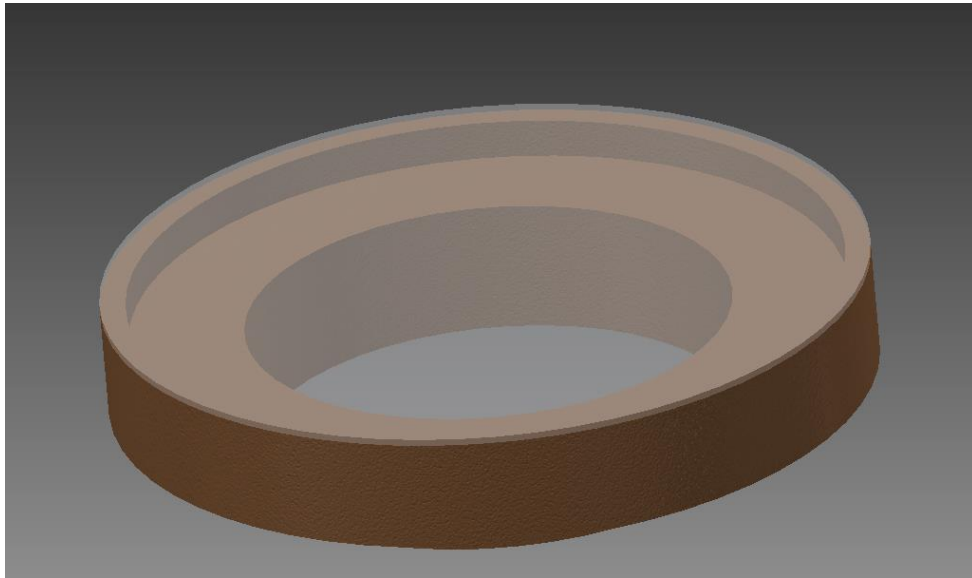


Figure 4.1: Baseline SSF Geometry

The SSF is a circular float with an empty internal volume. The baseline geometry used for this analysis is shown in Figure 4.1.

The materials used in this analysis are listed below (*Note: this does not imply the materials must be what are listed below*):

- **SSF body:** Polyurethane foam,
- **Top Plate:** Acrylic/Plexiglas
- **Submerging Fluid:** Salt water.

Table 4.1

Density of SSF and Submerging Fluid.

Density of Salt Water	0.0370 lbs/in ³
Density of SSF Body	0.0017 lbs/in ³
Density of SSF Top Plate	0.0425 lbs/in ³

Table 4.1 lists the given densities used for the analyses in this paper. All masses are calculated using the values in Table 4.1.

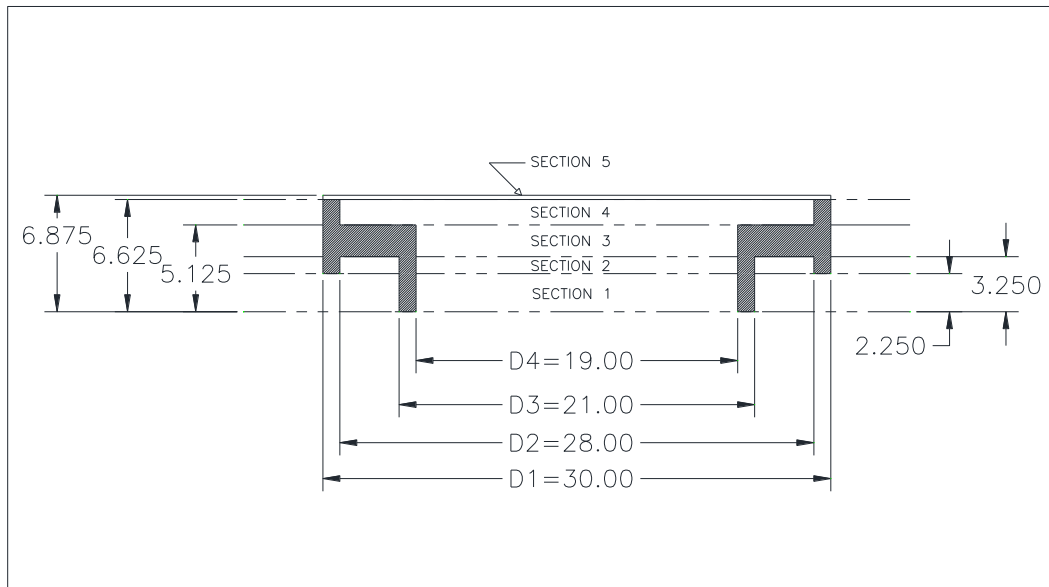


Figure 4.2: Cross-Section: Baseline SSF

Figure 4.2 defines the cross-section for the baseline SSF geometry. This geometry is the initial geometry used for analysis. Special cases are analyzed and compared to this baseline in the following sections when a comparison is necessary. Unless specified, any analysis in this paper refers to the baseline geometry.

Table 4.2

Section Properties: Baseline SSF.

	Height (in)	Ab(in²)	Aw(in²)	Vb (in³)	Vw (in³)	Vtot (in³)	Ib (in³)	Iw (in³)	Itot (in³)
Section 1	2.250	62.800	283.500	141.30	637.88	779.18	3,149.00	6,398.00	9,547.00
Section 2	1.000	154.000	552.900	154.00	552.90	706.90	12,738.00	27,024.00	39,762.00
Section 3	1.875	423.300	283.500	793.69	531.56	1,325.25	33,364.00	6,348.00	39,762.00
Section 4	1.500	91.100	615.800	136.65	923.70	1,060.35	9,589.00	30,172.00	39,762.00
Section 5	0.250	706.900	N/A	176.73	N/A	176.73	39,762.00	N/A	39,762.00
TOTAL	6.875	N/A	N/A	1402.363	2646.038	4048.400	N/A	N/A	N/A

Table 4.2 lists all pertinent properties of the baseline geometry. When a variation of the baseline is analyzed, the properties listed in Table 4.2 are not explicitly shown, but are calculated using the same methods.

Table 4.3

Mass Properties: Baseline SSF.

	mb (lbf)	mw (lbf)	mtot (lbf)
Section 1	0.240	23.601	23.842
Section 2	0.262	20.457	20.719
Section 3	1.349	19.668	21.017
Section 4	0.232	34.177	34.409
Section 5	7.511	N/A	7.511
TOTAL	9.594	97.903	107.498

Table 4.3 lists all masses needed to calculate the hydrostatic properties of the baseline SSF in calm water at 0° heel.

Coordinate System.

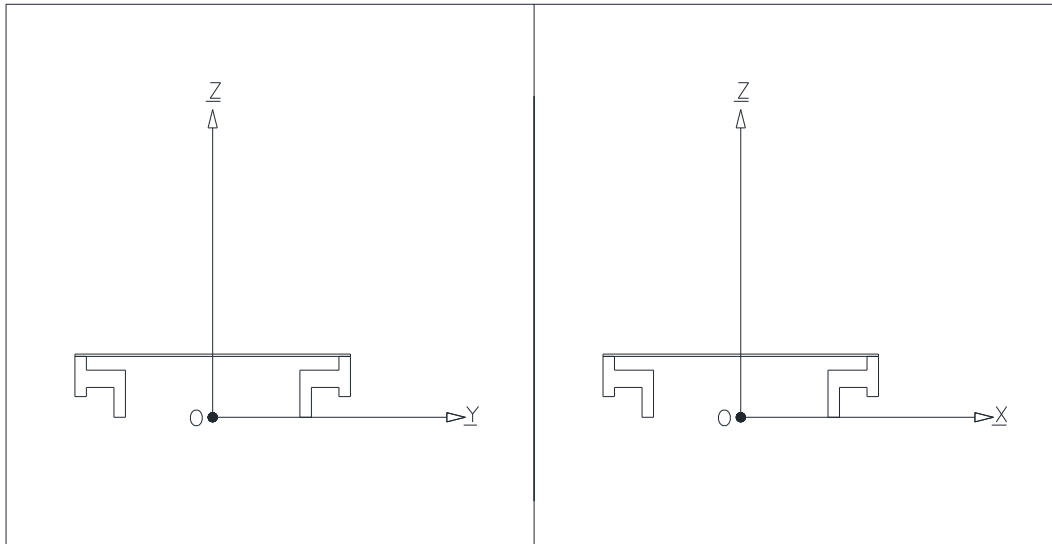


Figure 4.3 Definition of Coordinate System

It is important to note the coordinate system used. The standard ship coordinate system and nomenclature, as defined by Biran, is used for this study (Biran, 2003, p. 277).

- Translation in the X-Direction is referred to as Surge.
- Translation in the Y-Direction is referred to as Sway.
- Translation in the Z-Direction is referred to as Heave.
- Rotation about the X-Axis is referred to as Roll.
- Rotation about the Y-Axis is referred to as Pitch.
- Rotation about the Z- Axis is referred to as Yaw.

It is apparent from Figure 4.3 that the baseline SSF is symmetric around both the xOz axis and the yOz axis and that these cross-sections are identical to one another. This results in equivalent Surge and Sway translations and pitch and the roll rotations. Or,

when any incident force is applied at any location perpendicular to the Z-axis that incident direction can be defined as either the X-axis or the Y-axis.

Chapter 5

HYDROSTATIC ANALYSIS: SSF WITHOUT MAST

Chapter 5 presents the calculation method used in this report for determining the Hydrostatic properties of the baseline SSF without a mast attached. In future chapters, hydrostatic properties are not explicitly shown and they use the same methodology outline in this chapter. All calculations in this chapter are based on the analysis presented in Biran (2003).

Metacentric Height at 0° Heel.

Metacentric height, \overline{GM} , is calculated by the following equation (Biran, 2003, p. 39),

$$\overline{GM} = \overline{BM} + \overline{KB} - \overline{KG} \quad (5.1)$$

Where, \overline{BM} , is the metacentric radius, \overline{KB} , is the distance from the base point K to the center of buoyancy, and \overline{KG} is the distance from the base point K to the center of gravity of the float.

Calculation of Draught.

To calculate the metacentric height of the SSF, is necessary to first determine the draught, T . There are two methods to determine the draught for the SSF.

The first method assumes that the water line lies in Section 4 and then equates the mass of the body and the water above the waterline to the buoyancy force.

The second method assumes the displacement volume is determined by the total mass of the SSF body and the total mass water it would take to completely fill the internal volume of the SSF. This method validates the SSF design and ensures that the water line lies in the intended location.

Both methods are described in the following sections.

Draught Calculation: Method 1. The SSF is designed in such a way that the waterline lays in Section 4 (between the top of Section 3 and the bottom of Section 5). This determines the range of heights of the waterline, or the draught, of the SSF.

For equilibrium of the SSF the buoyancy force must balance with the weight of the SSF, including the trapped ballast water.

$$W_{SSF} + W_{bw} = F_{buoy} \quad (5.2)$$

Where W_{SSF} is the total weight of the SSF, W_{bw} is the weight of the ballast water above the waterline, and F_{buoy} is the buoyancy force. Some simplification yields,

$$m_{SSF} + m_{bw} = \rho_{SW} * V_{dis} \quad (5.3)$$

Where m_{SSF} is the total mass of the SSF, m_{bw} is the mass of the ballast water above the waterline, and V_{dis} is the total displacement volume of the SSF. In (5.3) m_{SSF} and ρ_{SW} are both known, and m_{bw} and V_{dis} are unknown. However, m_{bw} and V_{dis} can be defined in terms of the draught, T , because T is dependant on V_{dis} and m_{bw} is dependent on T .

The equation for draught when the waterline lies in section 4 is as follows,

$$T = \left[\frac{V_{dis} - \eta}{A_{bS4}} \right] + \xi \quad (5.4)$$

Where A_{bS4} is the Section 4 Area of the body, and η is the sum of the volumes of the body section below Section 4, and ξ is the total height of the body up to Section 4.

$$\eta = \sum_1^{i=3} V_{bSi} = 141.3in^3 + 154.00in^3 + 793.70in^3 = 1089.00in^3$$

$$\xi = \sum_1^{i=3} H_{Si} = 2.25in + 1.00in + 1.875in = 5.125in$$

Solving for V_{dis} and using the values for η and ξ yields the following equation,

$$\begin{aligned} V_{dis} &= [(T - \xi) * A_{bS4}] + \eta \\ V_{dis} &= [(T - 5.125in) * 91.10in^2] + 1089.00in^3 \\ V_{dis} &= (91.10in^2)T - 466.89in^3 + 1089.00in^3 \\ V_{dis} &= (91.10in^2)T + 622.10in^3 \end{aligned} \quad (5.5)$$

The mass of the ballast water is found by multiplying the density of water by volume above the water plane.

$$m_{ballast} = V_{WaWP} * \rho_{SW} \quad (5.6)$$

Where V_{WaWP} is the volume of water above the water line and is calculated by multiplying the area of the trapped water in Section 4, A_{wS4} , by the height from top of the waterline to the bottom of Section 5. Since, the height from top of the waterline to the bottom of Section 5 is dependent on T .

$$V_{WaWP} = A_{wS4} * (\zeta - T) \quad (5.7)$$

Where,

$$\zeta = \sum_1^{i=5} H_{Si} = 6.625in \quad (5.8)$$

Using this value and solving the equation for m_{bw} in terms of T yields the following equation,

$$\begin{aligned}
 V_{WaWP} &= A_{wS4} * (\zeta - T) \\
 V_{WaWP} &= (615.8in^2) * (6.625in - T) \\
 V_{WaWP} &= 4079.68in^3 - (615.8in^2) * T \tag{5.9}
 \end{aligned}$$

Inserting (5.8) into (5.5),

$$\begin{aligned}
 m_{ballast} &= [4079.68in^3 - (615.8in^2) * T] * \rho_{water} \\
 m_{ballast} &= [4079.68in^3 - (615.8in^2) * T] * (.037 \frac{lbs}{in^3}) \\
 m_{ballast} &= 150.95lbs - (22.78 \frac{lbs}{in}) * T \tag{5.10}
 \end{aligned}$$

Inserting (5.9) and (5.4) into (5.2) and solving for T gives the value for the draught.

$$\begin{aligned}
 m_{body} + [150.95lbs - (22.78 \frac{lbs}{in}) * T] &= \rho_{water} * [(91.10in^2)T + 622.10in^3] \\
 9.59lbs + [150.95lbs - (22.78 \frac{lbs}{in}) * T] &= (.037 \frac{lbs}{in^3}) * [(91.10in^2)T + 622.10in^3] \\
 160.54lbs - (22.78 \frac{lbs}{in}) * T &= (3.37 \frac{lbs}{in}) * T + 23.02lbs \\
 \Rightarrow T = \frac{137.51lbs}{26.15 \frac{lbs}{in}} &= 5.26in \tag{5.11}
 \end{aligned}$$

Draught Calculation: Method 2. This method assumes the SSF is completely filled with water prior to submersion and that the mass to determine T is that of the SSF and the total mass of water contained the internal void when completely filled.

$$\sum_1^{i=5} (m_{bi} + m_{wi}) = m_{total} = 107.90lbs \quad (5.12)$$

As in 5.2.1, displacement volume is calculated by equating the buoyancy force to the mass of the body and the total weight of water inside the float when completely filled.

$$V_{Tdis} * \rho_{SW} = m_{total} \quad (5.13)$$

Where V_{Tdis} is the volume displacement due to the total mass of the float and the total mass of water inside the internal volume.

Solving (5.12) for V_{Tdis} ,

$$V_{Tdis} = \frac{m_{total}}{\rho_{SW}} = \frac{107.90lbs}{.0370 \frac{lbs}{in^3}} = 2,916.21in^3 \quad (5.14)$$

Referring to Table 5.1 and comparing volumes, the waterline is found to lie within the vertical boundaries of Section 4.

To determine T , the total volume of the sections below Section 4 are subtracted from the displacement volume, V_{Tdis} . This quantity is then divided by the total area of the water plane when the waterline lies in Section 4. The total height of the sections below Section 4 must then be added to this value.

$$\eta_2 = \sum_1^{i=3} (V_{bi} + V_{wi}) = 2814.33in^3 \quad (5.15)$$

$$T = \left[\frac{V_{Tdis} - \eta_2}{(A_{WS4} + A_{BS4})} \right] + \xi \quad (5.16)$$

$$T = \left[\frac{2916.21in^3 - 2814.33}{(615.80in^2 + 91.10in^2)} \right] + 5.125in \quad (5.17)$$

$$T = 5.27in$$

This result is almost identical to the value found in section 5.1.

Ballast Water Properties.

The mass of the ballast water is determined using (5.6) and (5.9).

$$V_{waWP} = 4079.68in^3 - (615.8in^2) * 5.26in = 840.57in^3 \quad (5.17)$$

$$m_{bw} = V_{waWP} * \rho_{sw} = (.037 \frac{lbs}{in^3}) * 840.57in^3 = 31.13lbs \quad (5.18)$$

The center of gravity of this water ballast is determined using (5.8) and (5.10).

$$KG_{bw} = \left[\frac{\zeta - T}{2} \right] + T = \frac{\zeta + T}{2} = \frac{6.625in + 5.26in}{2} = 5.94in \quad (5.19)$$

Metacentric Radius.

Metacentric radius, \overline{BM} , is calculated by (5.20). The volume displaced is that found using method one in 5.2.1.

$$\overline{BM} = \frac{I_{wp}}{V_{dis}} \quad (5.20)$$

Where I_{wp} is the Area Moment of Inertia of the water plane and V_{dis} is the total volume displaced. I_{wp} is found in Table 5.1.

$$I_{wp} = I_{bs4} + I_{ws4} = 39,762in^4$$

V_{dis} is calculated by using the value of T found in (5.11) and inserting it in (5.5).

$$V_{dis} = (91.10in^2)(5.26in) + 622.10in^3 = 1101.29in^3$$

The water plane area moment of inertia used, since the waterline lies in Section 4, is that of Section 4, found in Table 4.3.

$$\begin{aligned}\overline{BM} &= \frac{I_{wp}}{V_{dis}} = \frac{39,762in^4}{1101.29in^3} \\ \overline{BM} &= 36.105in\end{aligned}\quad (5.21)$$

SSF Center of Gravity.

The center of gravity, \overline{KG}_t , is calculated by a mass balance of the float mass and the ballast water mass.

$$\begin{aligned}\overline{KG}_t &= \frac{(\overline{KG}_b * m_b) + (\overline{KG}_{ballast} * m_{ballast})}{(m_b + m_{ballast})} \\ \overline{KG}_t &= \frac{(6.12in * 9.59lbs) + (5.94in * 31.13lbs)}{(9.59lbs + 31.13lbs)} = 5.98in\end{aligned}\quad (5.22)$$

Center of Buoyancy.

The center of buoyancy, \overline{KB} , is calculated by a mass balance of the SSF mass below the waterline.

$$\begin{aligned}\overline{KB} &= \dots \\ \overline{KB} &= \frac{\left[\frac{H_{S1}}{2} * m_{bS1} \right] + \left[\left(\frac{H_{S2}}{2} + H_{S1} \right) * m_{bS2} \right] + \left[\left(\xi - \frac{H_{S3}}{2} \right) * m_{bS3} \right] + \left[\left(\xi + \frac{T - \xi}{2} \right) * m_{bbWP} \right]}{\sum_1^{i=3} m_{bSi} + m_{bbWP}}\end{aligned}\quad (5.23)$$

Where m_{bbWP} is the mass of the SSF below the water line and above the start of Section 4, H_{bbWP} is the height of the SSF below the water line and above the start of Section 4.

$$\begin{aligned}m_{bbWP} &= (T - \xi)(A_{bS4}) * \rho_b \\ m_{bbWP} &= (5.26in - 5.125in)(91.10in^3) \left(.0017 \frac{lbs}{in^3} \right) = .02lbs\end{aligned}\quad (5.24)$$

The center of buoyancy is calculated using the values calculated in (5.24) into (5.23).

$$\overline{KB} = \frac{[1.13in * .24lbs] + [2.75in * .26] + [4.19in * 1.35lbs] + [5.19in * .02lbs]}{1.87lbs} \quad (5.25)$$

$$\overline{KB} = 3.60in$$

Metacentric Height without IST Effect.

Metacentric Height is calculated using (5.1) with the values found in (5.21), (5.22), and (5.23).

$$\overline{GM} = 36.11in + 3.60in - 5.98in$$

$$\overline{GM} = 33.73in$$

IST Effect on Metacentric Height.

The water in this region acts like an inverted tank with the free surface open to the water beneath. With this in mind, the IST is treated in the opposite fashion as that of a free surface slack tank open to the atmosphere (Redkar, 2012, p. 2-3). Whereas the free surface tank results in an effective metacentric height that is lower than the metacentric height of the body alone, the inverted tank will raise metacentric height.

$$l_F = \frac{I_{w4}}{V_{dis}} \quad (5.26)$$

$$l_F = \frac{30,172in^4}{1101.29in^3} = 27.40in$$

$$\overline{GM}_{eff} = \overline{GM} + l_F \quad (5.27)$$

$$\overline{GM}_{eff} = 33.73in + 27.40in$$

$$\overline{GM}_{eff} = 61.13in$$

Comparison: Non-SSF and SSF.

It is important to compare the baseline SSF to that of a float with the same geometry that does not utilize suction stabilization. This requires the internal volume of the float to operate as an open system with the outside atmosphere. When the internal volume is not a closed system there is no ballast water trapped above the waterline and the draught is dependent only on the mass of the float.

Table 5.2

Comparison: Non-SSF and SSF

	Baseline SSF	Baseline Without SSF
Total Weight	40.74 lbf	9.59 lbf
Draught, in	5.26 in	3.02 in
Displacement Volume	1101.90 in ³	259.30 in ³
KB, in	3.69 in	1.81 in
KG, in	5.98 in	6.12 in
BM, in	36.11 in	49.13 in
GM, in	33.73 in	44.82 in
lf, in	27.40 in	N/A
GM_{eff}, in	61.13 in	N/A

From Table 5.2, a float with Suction-Stabilization compared to a float without Suction-Stabilization has a higher effective metacentric height. Note that the draught is much lower and lies in Section 2, which will leave more than half of the float body above the waterline.

$$\Delta \overline{GM} = \overline{GM}_{SSF_{eff}} - \overline{GM}_{NSSF} = 61.13in - 44.82in = 16.31in$$

The Suction-Stabilization increases the \overline{GM}_{eff} of the baseline geometry when compared to a float that does not utilize Suction-Stabilization.

Geometric Variation: Section 4 Height.

The height of Section 4 is important in that it can drastically change the allowed volume of trapped water ballast. It is important to examine this parameter and its effects on the hydrostatic properties of the SSF.

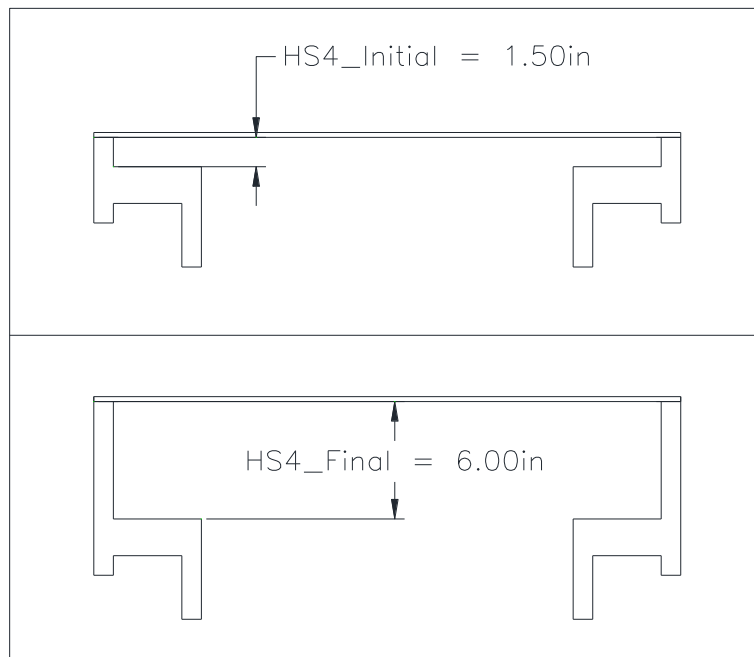


Figure 5.1: Section 4 Height Limits

Figure 5.1 defines the initial and final heights used. Note the baseline height was used as the initial case. When the height of Section 4 is less than that of the baseline the waterline of the SSF no longer falls within the vertical limits of Section 4, which may lead to an unstable condition.

The methods used to determine the metacentric height is the same as used in sections 5.1 – 5.8.

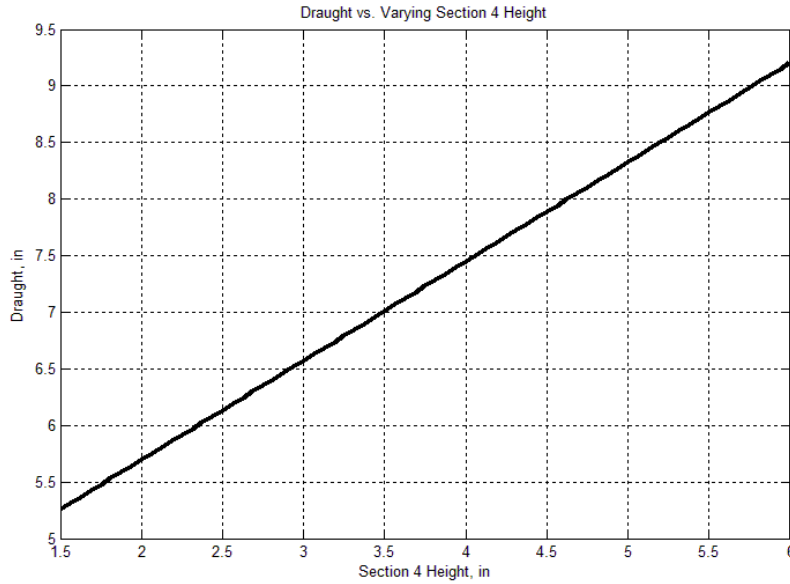


Figure 5.2: Draught vs. Section 4 Height

Figure 5.2 plots the draught against the height of section 4. The draught increases linearly with the height of Section 4. Using the (5.3) – (5.7) yields the following equation,

$$\sum_1^{i=5} (A_{bi} H_{bi}) + A_{wS4} \left(\sum_1^{i=5} H_{Si} - T \right) \rho_{SW} = \rho_{SW} \left[T - \left(\sum_1^{i=3} H_{Si} \right) \right] A_{bS4} + \left(\sum_1^{i=3} V_{bSi} \right) \quad (5.28)$$

$$\Rightarrow T = \frac{\left[\left(\frac{\sum_1^{i=5} (A_{bi} H_{bi})}{\rho_{SW}} \right) + A_{wS4} \left(\sum_1^{i=5} H_{Si} \right) + \left(\sum_1^{i=3} H_{Si} \right) A_{bS4} - \left(\sum_1^{i=3} V_{bSi} \right) \right]}{(A_{wS4} + A_{bS4})} \quad (5.29)$$

From (5.29), it is seen that as the Section 4 increases so does the draught. This is

because the following quantities, $\left(\frac{\sum_{i=1}^{i=5} (A_{bi} H_{bi})}{\rho_{sw}} \right)$ and $A_{wS4} \left(\sum_{i=1}^{i=5} H_{Si} \right)$, are in the numerator

and increase with the height of Section 4 while the remaining variables remain constant.

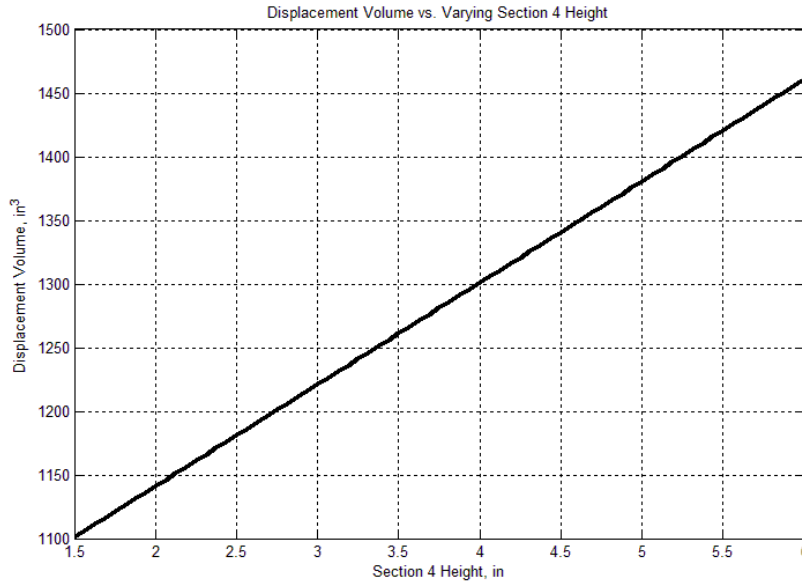


Figure 5.3: Displaced Volume vs. Section 4 Height

Using (5.29) in (5.5), the only term that changes value is T , and since T increases with the increase in Section 4 height, the displaced volume also increases. This results in a lower metacentric radius, and thus a lower metacentric height, because the Area Moment of Inertia of the water plane remains constant while the displaced volume increases.

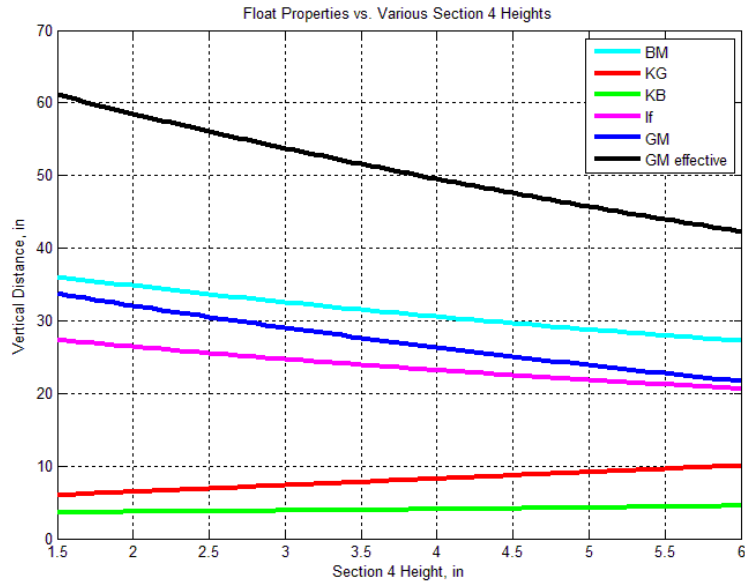


Figure 5.4: Hydrostatic Properties vs. Section 4 Height

Figure 5.4 plots the properties used to determine metacentric height against the height of Section 4. As predicted by (5.29), the height of Section 4 increases the effective metacentric height decreases.

Geometric Variation: Outer and Inner Diameters of Section 4.

The second geometric variation explored was increasing the outer diameter of the SSF and the inner diameter of Section 4 & 5 while keeping the outer and inner diameters of Section 1, 2, & 3 constant and how this affects the draught and metacentric height of the SSF.

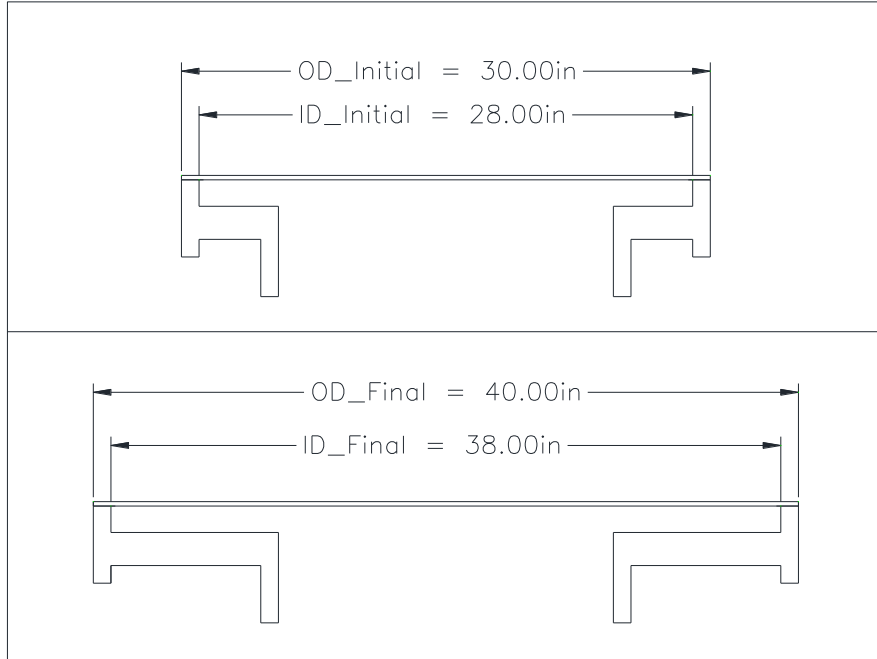


Figure 5.5: Section 4 Outer and Inner Diameter Limits

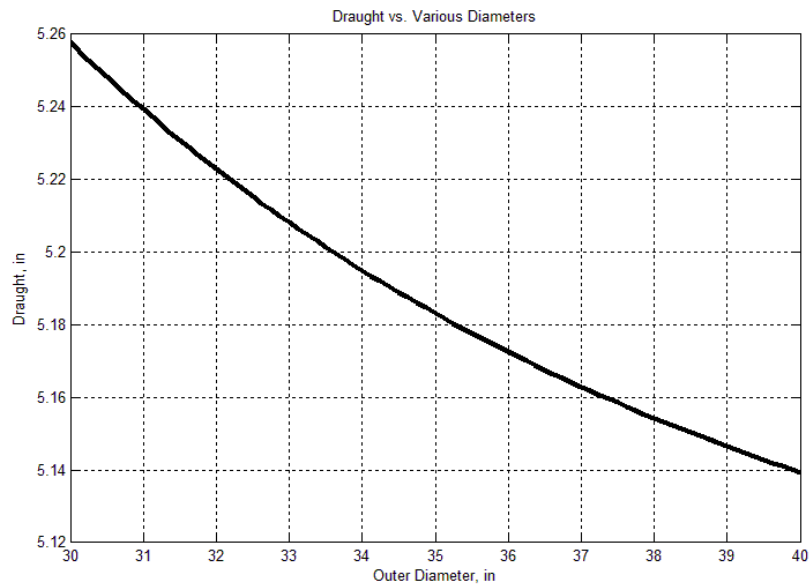


Figure 5.6: Draught vs. Section 4 Diameters

Figure 5.6 plots the draught against the increasing outer and inner diameters of Section 4 & Section 5. As these diameters increase the draught decreases.

Using (5.29) ,

$$T = \frac{\left[\left(\frac{\sum_1^{i=5} (A_{bi} H_{bi})}{\rho_{SW}} \right) + A_{wS4} \left(\sum_1^{i=5} H_{Si} \right) + \left(\sum_1^{i=3} H_{Si} \right) A_{bS4} - \left(\sum_1^{i=3} V_{bSi} \right) \right]}{(A_{wS4} + A_{bS4})}$$

All terms, in both the numerator and denominator, on the right hand side of (5.29) increase with the increase of the outer and inner diameters of Section 4 & Section 5. From Figure 5.6, it is seen that the denominator increases at a faster rate than the numerator, which results in a decreased draught.

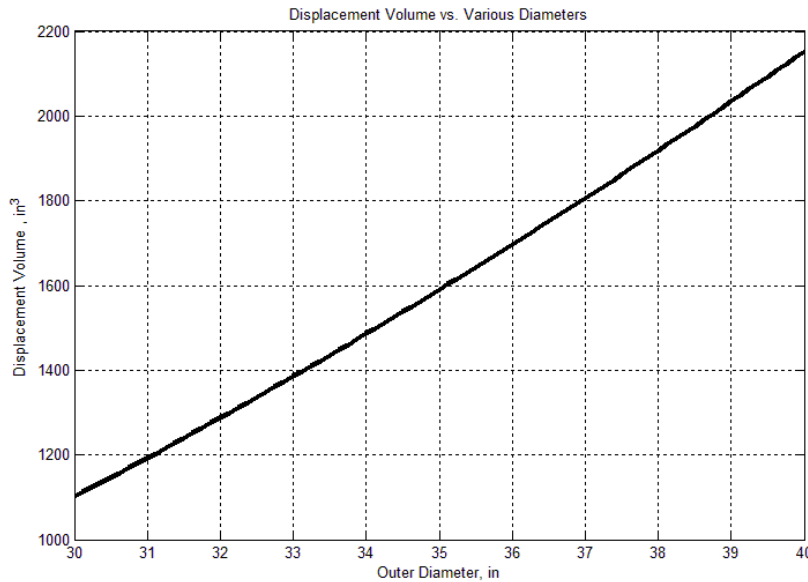


Figure 5.7: Displaced Volume vs. Section 4 Diameters

However, it is necessary to state that a decreased draught does not result in a decreased displacement volume. Figure 5.7 shows that the displacement volume increases as the outer diameter increases. Since the density of the SSF is significantly less than that of the water, a larger submerged volume does not equate to a large displacement mass.

Rewriting (5.5),

$$V_{dis} = \left[\left(T - \left(\sum_1^{i=3} H_{Si} \right) \right) * A_{bS4} \right] + \left(\sum_1^{i=3} V_{bSi} \right) \quad (5.30)$$

In (5.30) A_{bS4} and $\sum_1^{i=3} V_{bSi}$ increase with the outer and inner diameters of Section 4 & Section 5, which is much greater than the decrease in T . This results in an increased displacement volume.

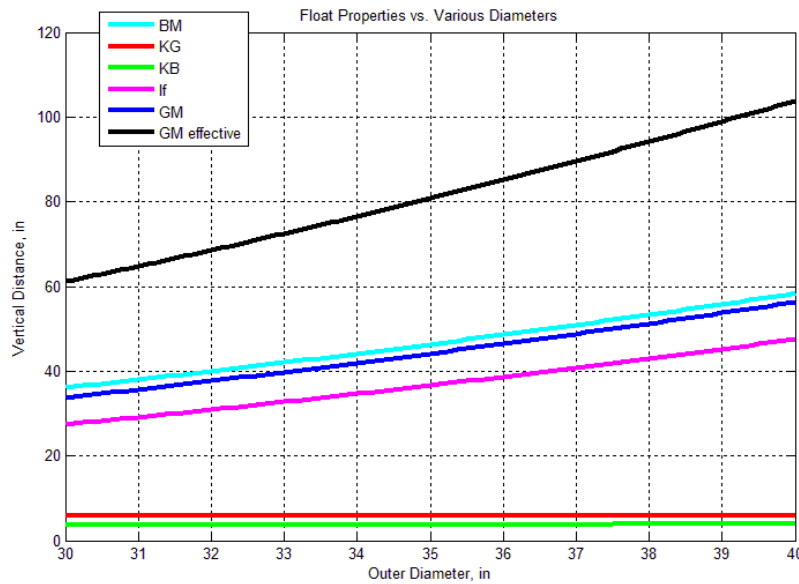


Figure 5.8: Hydrostatic Properties vs. Section 4 Diameters

Figure 5.8 plots the properties used to determine metacentric height against the increasing outer diameter. As the outer diameter increases the effective metacentric height increases. The increase in metacentric height is a direct effect of the offset increase in the displaced volume with the much greater increase in both the SSF total water plane area moment of inertia and the ballast waters area moments of inertia.

Geometric Variation: Outer and Inner Diameters of All Sections.

The third geometric variation explored was increasing all diameters of the SSF by the same amount and how this affects the draught and metacentric height of the SSF.

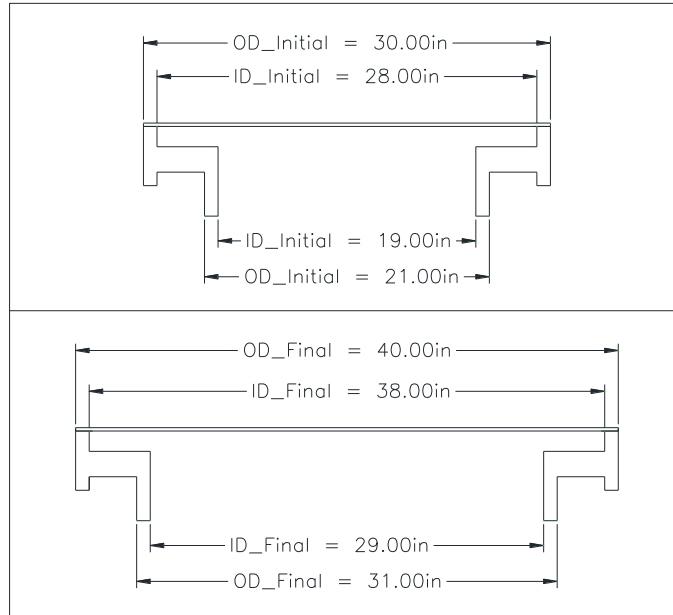


Figure 5.9: All Outer and Inner Diameter Limits

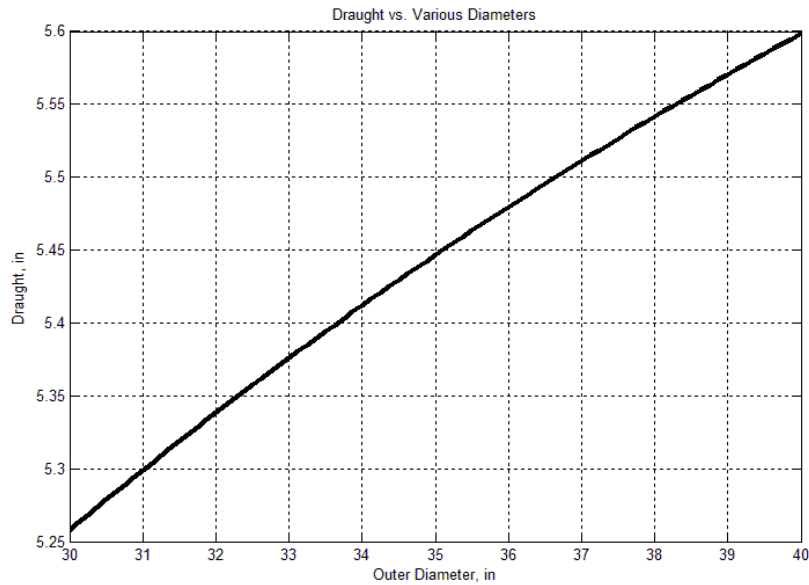


Figure 5.10: Draught vs. All Diameters

Figure 5.10 plots the draught against the increasing inner and outer diameters. As all diameters increase uniformly, the draught also increases.

Using (5.29),

$$T = \frac{\left[\left(\frac{\sum_{i=1}^{i=5} (A_{bi} H_{bi})}{\rho_{SW}} \right) + A_{wS4} \left(\sum_{i=1}^{i=5} H_{Si} \right) + \left(\sum_{i=1}^{i=3} H_{Si} \right) A_{bS4} - \left(\sum_{i=1}^{i=3} V_{bSi} \right) \right]}{(A_{wS4} + A_{bS4})}$$

All terms, in both the numerator and denominator, on the right hand side of (5.29) increase with the increase of the outer and inner diameters of Section 4 & Section 5. From Figure 5.10, it is seen that the denominator increases at a slower rate than the numerator, which results in an increase in draught.

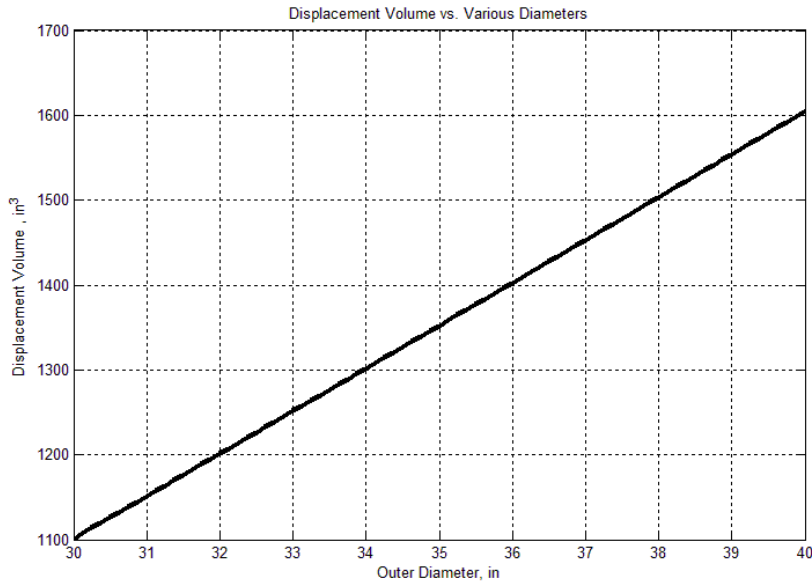


Figure 5.11: Displacement Volume vs. All Diameters

Figure 5.11 plots the displaced volume against the increasing diameter. Comparing this to Figure 5.7, it is seen that while the displaced volume increases it does

not increase as much as the geometry changes in 5.8. This result stems from the fact that Section 3 of SSF, while it does see a volume increase, it does not have the same volume and mass increase as when the inner and outer diameters of Section 1 are held constant.

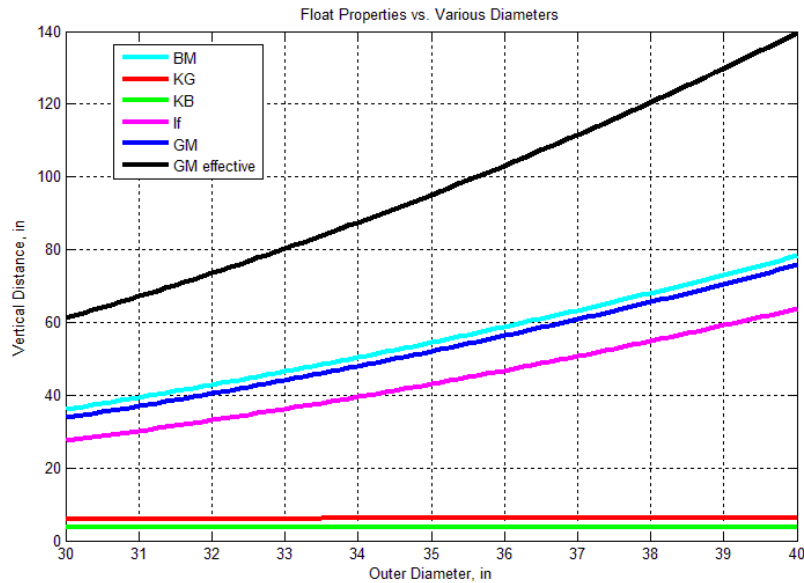


Figure 5.12: Hydrostatic Properties vs. All Diameters

Figure 5.12 plots the properties used to determine metacentric height against the increasing inner and outer diameter. As both the inner and outer diameter, increase the effective metacentric height increases. It is noted that the increase in metacentric height is greater when all diameters of the SSF are increased in unison. This is due to the lower displacement volume and an increased area moment of inertia.

Chapter 6

MAST SIZING AND OPTIMIZATION

The SSF is designed to specifically hold either an umbrella, in the case of backyard pool application, or, in the case of deep-sea application, a wind turbine. Both have relatively similar physical properties: a tall cylindrical shaft that rises vertically from the SSF and a mass of some sort mounted to the top of that shaft. It is fairly easy to infer that this will both increase the mass of the SSF and raise the Center of Gravity. Both metrics are important in determining stability. This chapter evaluates mast height and weight and how it affects the hydrostatic properties of the Baseline SSF.

Two metrics will determine the ideal mast size: *metacentric height*, which was defined in Chapter 5, and *the Kempf factor*, which is described in this chapter.

Kempf Factor Defined.

The Kempf factor is a non-dimensional number used to evaluate the free roll characteristics of a ship or floating platform. It is used to determine where a ship or floating platform's motions are *tender*, *comfortable*, or *stiff*. Tender motions result from a large roll period and are associated with low metacentric heights. Comfortable motions signify that the roll period is balanced for the ship or floating body. Stiff motion results in short rolls periods that may become too violent (Biran, 2003, p. 133-135).

The SSF is symmetric about both the X and Y-axes, it is assumed that roll and a pitch are equivalent and therefore the Kempf factor is applicable to both of these motions.

$$KEMPF = P_{roll} \sqrt{\frac{g}{D_o}} \quad (6.1)$$

Where g is the gravitational constant in $\frac{in}{s^2}$, D_o is the outer diameter of the float, and P_{roll} is the natural roll period of the float.

$$\omega_{roll} = \sqrt{\frac{g \overline{GM}}{i_m^2}} \quad (6.2)$$

$$P_{roll} = \frac{2\pi}{\omega_{roll}} \quad (6.3)$$

Where ω_{roll} is the natural angular frequency of free roll of the SSF, i_m is the mass radius of gyration, and \overline{GM} is the metacentric height as defined in section 5.1. The value of the Kempf factor determines the floats motions (Biran, 2003, p. 133-135).

- For Kempf factor values **below 8**, the float motion is STIFF.
- For Kempf factor values **between 8 and 14**, the float motion is COMFORTABLE.
- For Kempf factor values **above 14**, the float motion is TENDER.

The purpose of using this metric is to determine which mast height and weight results in a roll period that does not cause a motion that is too stiff or too tender.

Mast Geometry Assumptions.

For the following analysis, a mast is defined as a vertical, thin cylindrical rod with a spherical mass at its highest point. This geometry simulates either an umbrella or a wind turbine and will be used to determine the mast used for the remainder of this paper. The assumptions used to define mast geometry are listed below:

1. The mast body is a cylinder with a concentrated mass with its center at the highest point of the body cylinder. The mast attaches to the suction-stabilized platform at its center.
2. The concentrated mass is half of the mass of the body cylinder.
3. The mast has a uniform density.
4. The mast's center of gravity is found by the following equation,

$$KG_{mast} = \frac{2H_{mast}}{3} + H_{body} \quad (6.4)$$

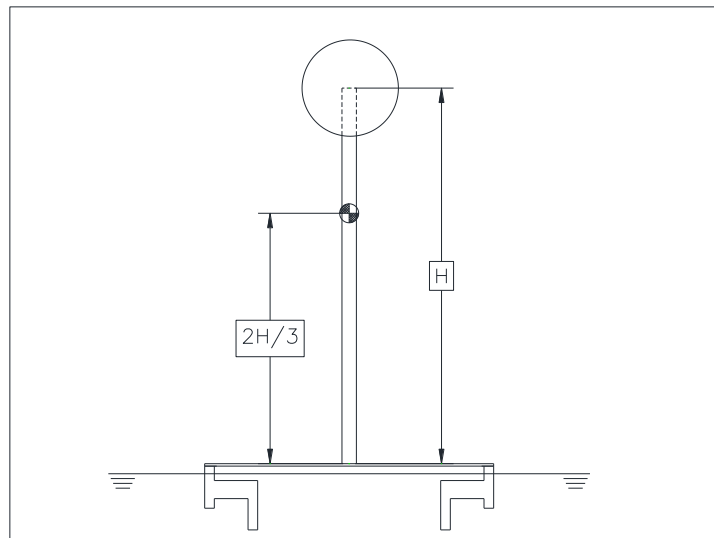


Figure 6.1: Pictorial Representation of Mast Geometry

Input Parameters for Mast Study

Using the initial geometry, as defined in Chapter 4, for the Baseline SSF, seven different mast heights were used to analyze the mast effect on the SSF.

Table 6.1

Mast Properties

Mast Height, in	Mast Cylinder KG, in	Concentrated Mass KG, in	Total KG, in
15.00	14.38	21.88	16.63
30.00	21.88	36.88	26.63
45.00	29.38	51.88	36.63
60.00	36.88	66.88	46.63
75.00	44.38	81.88	56.63
90.00	51.88	96.88	66.63
105.00	59.38	111.88	76.63

Mast Size Limits.

First, it is important to determine the mast weight at which the water line rises above the limits of Section 4 as defined in figure 4.1. For proper function, the waterline must lie in Section 4 for the Baseline SSF.

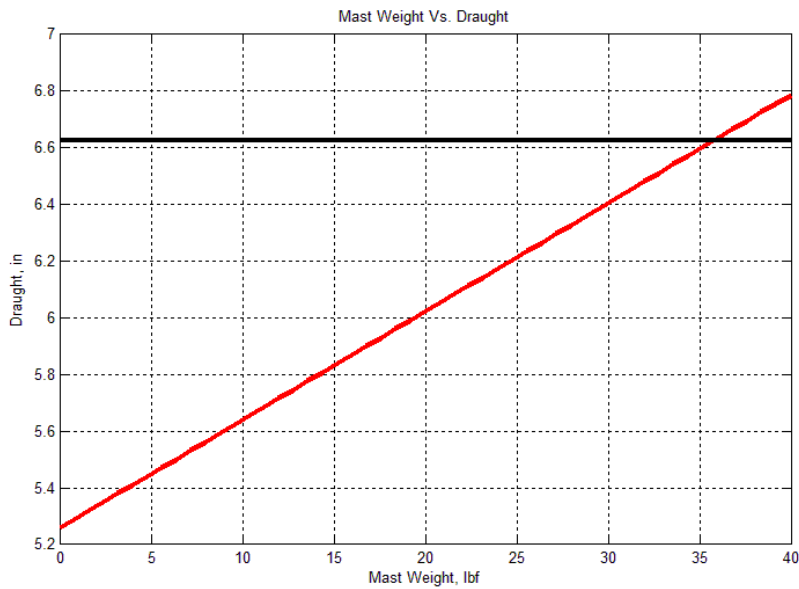


Figure 6.2: Draught vs. Mast Weight

Figure 6.2 show the draught change based solely on the added weight of the mast. The black line illustrates the maximum draught allowable for the waterline to remain

within the upper and lower bounds of Section 4. The red line illustrates the increasing draught as the mast weight increases. From figure 6.2 it is seen that when the mast weight exceeds 36lbs, the waterline falls above the limit of Section 4.

Next, it is imperative that the metacentric height remain positive. A negative metacentric height, in most cases, leads to instability (Biran, 2003, p. 147-151).

To ensure a positive metacentric height, the weight of the mast is limited by the upper extreme value of 35 pounds and the metacentric height is calculated for a range of mast weights between 0-35lbs.

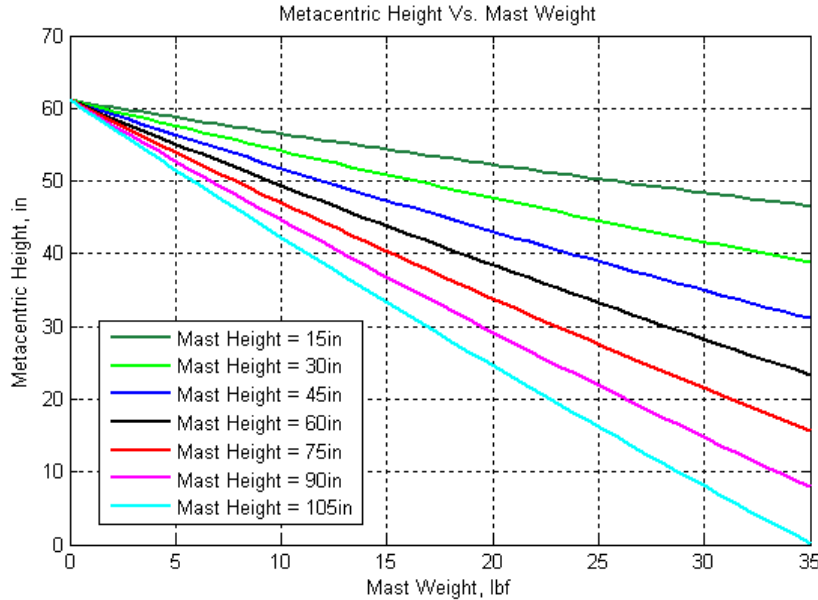


Figure 6.3: Metacentric Height vs. Mast Weight (up to 35lbs).

Figure 6.3 shows that metacentric height becomes negative for a mast height of 105in at 35lbs. To insure against a negative metacentric height, the mast weight is limited to an upper extreme of 33lbs.

Mast Selection Criteria.

Each of the seven mast geometries shown in Table 6.1 were analyzed by iterating the mast weight from 0lbs to 33lbs.

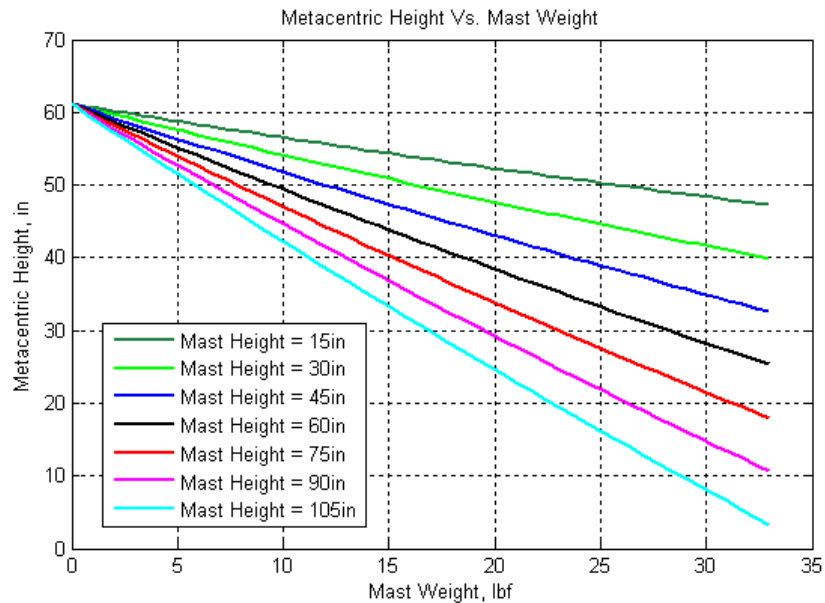


Figure 6.4: Metacentric Height vs. Mast Weight (up to 33lbs).

Figure 6.4, shows that for all mast heights, as the weight of the mast increases the metacenter decreases. The taller the mast, the higher its center of gravity and the more massive the mast, the more that center of gravity location plays a role in determining the metacentric height. Referring to (5.1), $\overline{GM} = \overline{BM} + \overline{KB} - \overline{KG}$, a higher \overline{KG} will reduce the metacentric height as will the larger V_{dis} that is a result of the added weight of the mast.

Stability decreases with both increasing mast height and increasing mast weight.

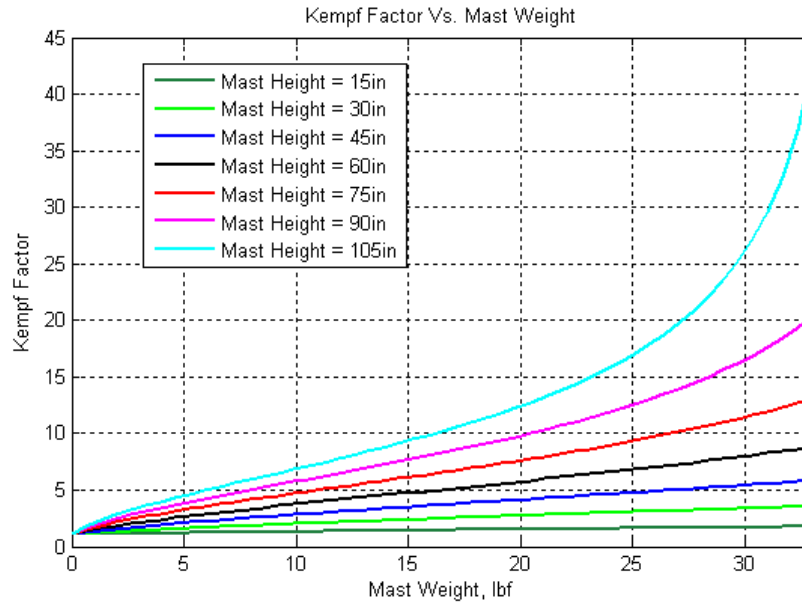


Figure 6.5: Kempf Factor vs. Mast Weight (up to 33lbs).

Figure 6.5 shows that, for all mast heights, as the weight of the mast increases the Kempf factor also increases. This results in a larger roll period for masts with higher centers of gravity and higher weight. A low mast center of gravity results in a *stiffer* float motion and a high center of gravity results in a *more tender* motion. It is desirable to use a mast that will result in a *comfortable* roll motion or a *moderately stiff* motion.

Using these criteria, i.e. a Kempf factor between 8 and 14, and the mast heights between 15in and 105in a range for *comfortable* float motion is found.

Table 6.2:

Range of Mast Weights for Comfortable Float Motion.

Mast Height, in	Weight when Kempf's Factor = 8, lbf	Weight when Kempf's Factor = 14, lbf
15.00	N/A	N/A
30.00	N/A	N/A
45.00	N/A	N/A
60.00	N/A	N/A
75.00	28.30	N/A
90.00	22.40	33.00
105.00	17.80	27.00

Table 6.2 gives the appropriate mast weight for a certain mast height that will result in a *comfortable* float motion.

It is also interesting to note the correlation between the Kempf factor and the metacentric height of the SSF.

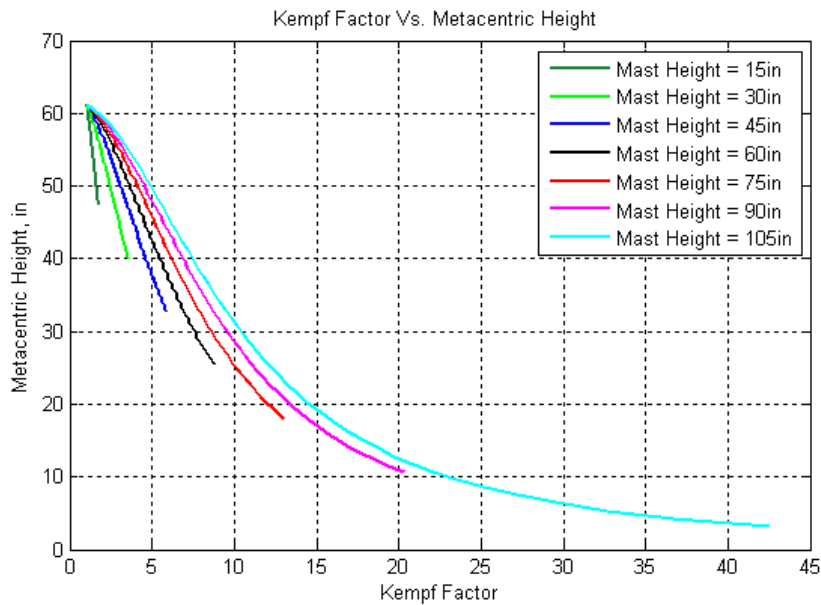


Figure 6.6: Metacentric Height vs. Kempf Factor.

Figure 6.6 plots the correlation between the Kempf factor and the metacentric height. The lower values of mast height have a smaller variation in metacentric height and therefore the Kempf factor does not vary as it does with taller masts. The Kempf factor increases as the metacentric height approaches zero. This implies that the lower the metacentric height the larger the roll period of the SSF.

Adding the mast to the SSF increases the center of gravity, displaced volume, center of buoyancy, and the draught. It decreases the metacentric radius, the metacentric height, the inverse free surface effect, and the effective metacentric height. The most important of these factors being the effective metacentric height, which is determined by the metacentric radius, the center of buoyancy, and the center of gravity. The taller and more massive the mast, the more adversely it will affect the metacentric height.

Chapter 7

HYDROSTATIC ANALYSIS: SSF WITH MAST

This chapter presents the hydrostatic properties of the baseline SSF with a mast. The SSF is then compared to a float with the same basic geometry that does not utilize Suction-Stabilization. It then expands the analysis to the same geometries examined in chapter 5.

SSF Properties with Mast.

The mast chosen was based on a nine-foot round patio umbrella, exact specifications can be found in appendix A.

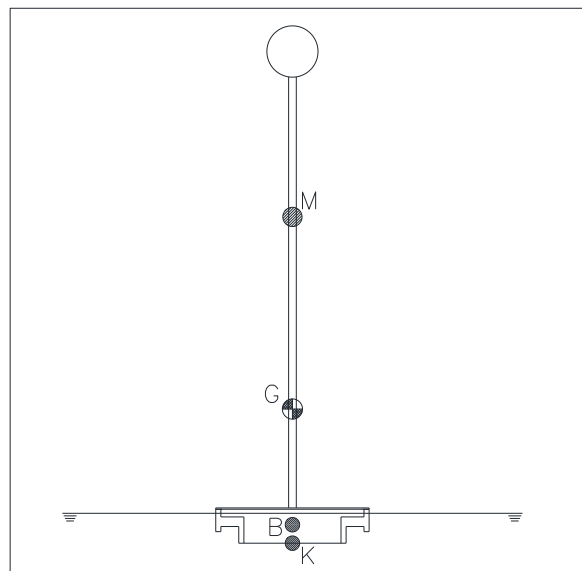


Figure 7.1: SSF with Mast at 0° Heel.

The hydrostatic properties were calculated using the methods shown in Chapter 5, method 1. The SSF weight and center of gravity was adjusted for the added mast weight, which lowers the metacentric height, the trapped water ballast volume and mass, and increases the draught, the SSF center of gravity, and the displaced volume.

Table 7.1

Hydrostatic Properties: SSF with Mast.

	Baseline
Mast Weight	15.00 lbf
Mast Height	92.00 in
Mast KG	65.00 in
Ballast Water Weight	18.08 lbf
Ballast Water Volume	488.70 in ³
Ballast Water KG	6.23 in
Total Weight	42.68 lbf
Draught, in	5.83 in
Displacement Volume	1153.40 in ³
KB, in	3.69 in
KG, in	26.86 in
BM, in	34.47 in
GM, in	11.30 in
lf, in	26.16 in
GMeff, in	37.46 in

Roll period and the Kempf factor are calculated using the values in Table 7.1.

$$\omega_{roll} = 2\pi \sqrt{\frac{g \overline{GM}}{i_m^2}} = 2.908 \frac{rad}{sec} \quad (7.1)$$

$$P_{roll} = \frac{2\pi}{\omega_{roll}} = 2.16 \text{ sec} \quad (7.2)$$

$$KEMPF = P_{roll} \sqrt{\frac{g}{D_o}} = 7.75 \quad (7.3)$$

Comparison: Non-SSF and SSF.

Table 7.2

Comparison: Hydrostatic Properties Non-SSF and SSF.

	Baseline SSF	Baseline Without SSF
Total Weight	42.68 lbf	24.59 lbf
Draught, in	5.83 in	4.12 in
Displacement Volume	1153.40 in ³	664.70 in ³
KB, in	3.69 in	2.93 in
KG, in	26.86 in	42.03 in
BM, in	34.47 in	50.19 in
GM, in	11.30 in	11.09 in
lf, in	26.16 in	N/A
GM_{eff}, in	37.46 in	N/A

Once again, the inverse slack tank effect of the ballast water serves to increase the metacentric height significantly when compared to a float platform that does not utilize Suction-Stabilization.

$$\Delta \overline{GM} = \overline{GM}_{SSF_{eff}} - \overline{GM}_{NSSF} = 37.46in - 11.09in = 26.37in$$

Suction-Stabilization increases the \overline{GM}_{eff} of the baseline geometry when compared to a float that does not utilize Suction-Stabilization.

Geometry Variations.

The same three geometric variation examined in 5.9-5.11 were examined again with the added weight of the mast and the resulting increase in center of gravity and draught.

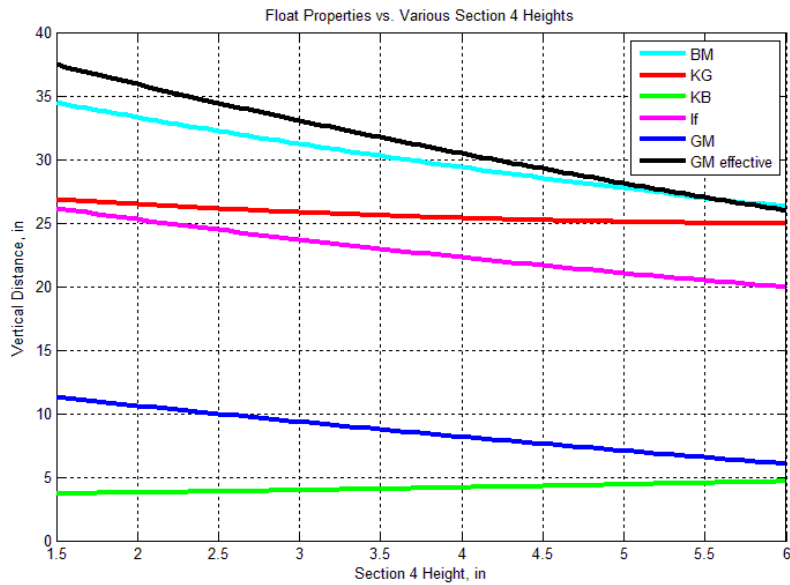


Figure 7.2: Hydrostatic Properties vs. Section 4 Heights.

Figure 7.2 plots the various properties of the SSF against an increasing Section 4 height. The trends seen with the mast included are the same as when there is no mast attached. However, the metacentric height and the effective metacentric height are much lower. This is due to the added weight of the mast and the higher center of gravity of the SSF with the attached mast.

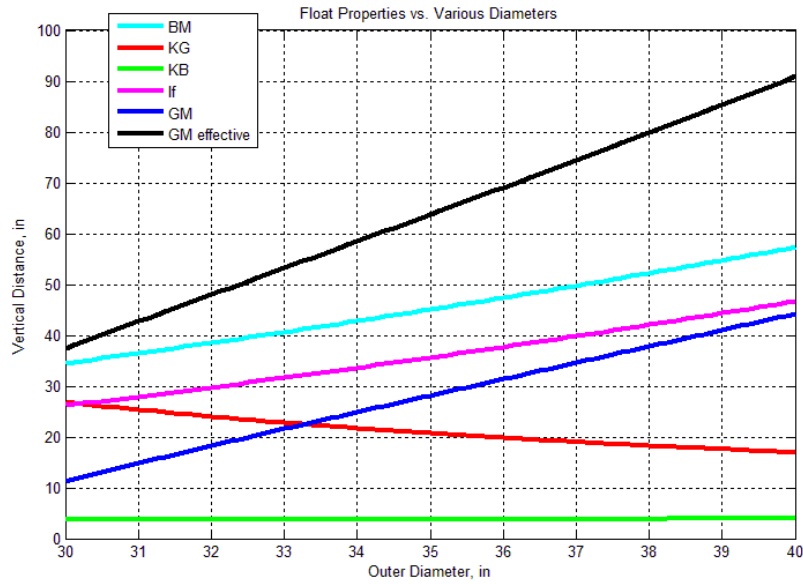


Figure 7.3: Hydrostatic Properties vs. Section 4 Diameters.

Figure 7.3 plots the various properties of the SSF against an increasing Outer Diameter. The trends seen with the mast included are the same as when there is no mast attached. However, the metacentric height and the effective metacentric height are much lower. It is interesting to note that the overall \overline{KG} decreases from around 29in to around 18in. From this result, it is seen that the mast effect of lowering the effective metacentric height decreases as the outer and inner diameters of Section 4 increase.

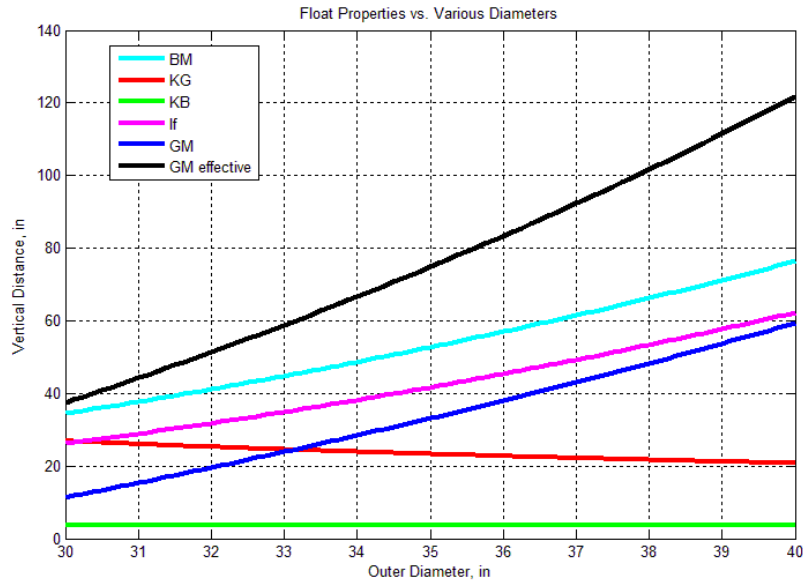


Figure 7.4: Hydrostatic Properties vs. All Diameters

Figure 7.4 plots the various properties of the SSF against a uniform increasing of all Diameters. The trends seen with the mast included are the same as when there is no mast attached. However, the metacentric height and the effective metacentric height are much lower. It is interesting to note that the overall \overline{KG} decreases from around 29in to around 20in. From this result, it is seen that the mast effect of lowering the effective metacentric height decreases as all diameters increase in a uniform manner.

Chapter 8

RIGHTING MOMENT AND RIGHTING LEVER ANALYSIS

This chapter presents the method for calculating both the righting moment and righting arm for the baseline SSF with a mast. It then expands that analysis to include select cases of the geometric variations presented in chapter 7.

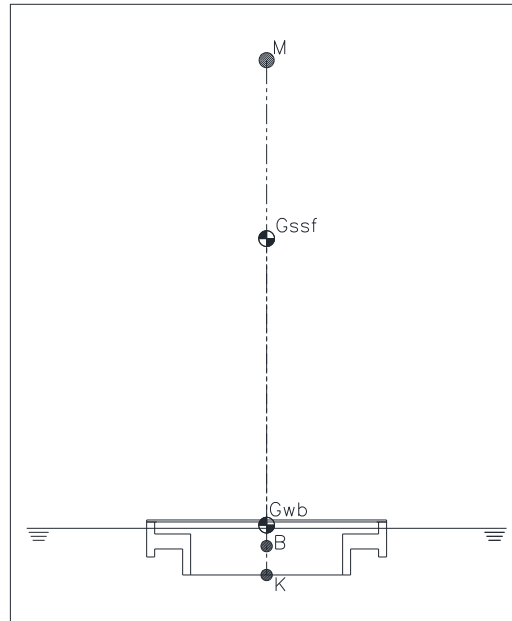


Figure 8.1: SSF with Mast at 0° Heel.

Figure 8.1 shows the water ballast CG and the CG of the float in their respective locations rather than combined. This will illustrate the water ballast effect at more pronounced angles of heel.

All properties in this section were calculated using data obtained from the solid model of the SSF. A plane was oriented parallel to the xOy plane at a vertical height equal to the calculated draught. This plane was then rotated and the mass, volume, and location properties above and below the plane were taken. From this, the centers of gravity and buoyancy were found with respect to the fixed-SSF frame.

It is assumed that the added mass below the waterline does not significantly affect draught. This allows the center of rotation to remain at O and also serve as the center of flotation.

A full range of heel angles were analyzed, from level to the air entrance angle, because of this the small angle assumptions are not valid and therefore the metacentric height is not used as a measure of stability. Instead, the righting moment and the righting lever are used to determine stability.

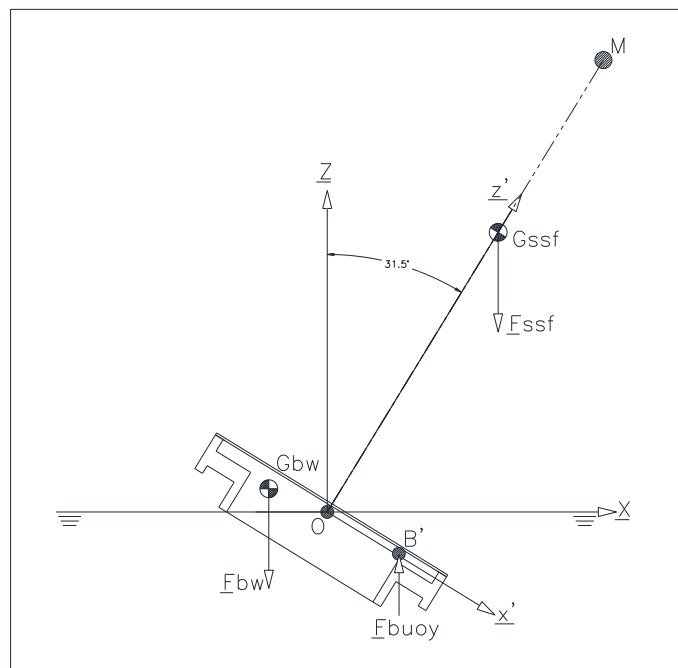


Figure 8.2: SSF with Mast at 31.5° Heel.

Figure 8.2 shows the maximum heel angle allowable for the baseline geometry. At 31.5° heel the inner corner of Section 1 breaches the water lines and the internal volume is no longer air tight. This nullifies the effect of the ballast water by rendering it ineffective. Because of this, the extreme value for heel angle is 31.5° for the following analysis.

Righting Moment and Righting Lever: Baseline SSF.

To simplify the equations, all calculations are performed in the earth-fixed frame.

This requires that some of the data taken be rotated by the rotation matrix, \underline{R} .

$$\underline{R} = \begin{bmatrix} \cos\phi & 0 & -\sin\phi \\ 0 & 1 & 0 \\ \sin\phi & 0 & \cos\phi \end{bmatrix} \quad (8.1)$$

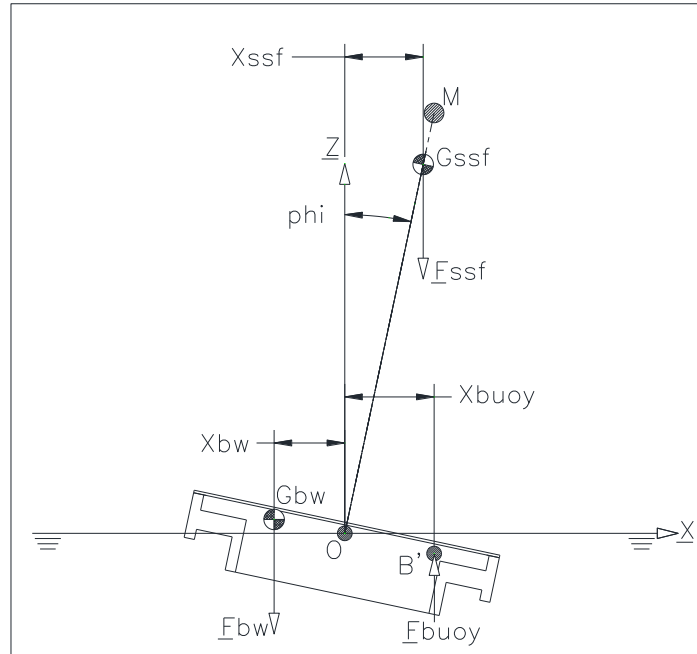


Figure 8.3: Suction-Stabilized Float with Mast at any Heel Angle, ϕ .

Figure 8.3 is a free-body diagram of the baseline float heeled to an angle ϕ . The righting moment is calculated by summing the moments around the center of flotation, O.

$$\sum M_o = (X_{ssf} * F_{ssf}) + (X_{buoy} * F_{buoy}) + (X_{bw} * F_{bw}) \quad (8.2)$$

Where F_{buoy} is the buoyancy force, X_{buoy} is the horizontal distance from O to the SSF center of buoyancy, F_{bw} is the gravitational force of the ballast water, X_{bw} is the horizontal distance from O to the ballast water center of gravity, F_{SSF} is the gravitational

force of the SSF without the weight of the ballast water, and X_{SSF} is the horizontal distance from O to the center of gravity of the SSF without the weight of the ballast water.

Where,

$$F_{ssf} = -W_{ssf} \quad (8.3)$$

and,

$$F_{bw} = -W_{bw} \quad (8.4)$$

and.

$$\begin{aligned} F_{buoy} &= -F_{ssf} + -F_{bw} \\ \Rightarrow F_{buoy} &= -(-W_{ssf} + -W_{bw}) = W_{ssf} + W_{bw} \end{aligned} \quad (8.5)$$

Where W_{ssf} is the weight of the SSF without the ballast water, and W_{bw} is the weight of the ballast water.

Inserting (8.3), (8.4), and (8.5) into (8.2),

$$\sum M_o = (X_{ssf} * -W_{ssf}) + [X_{buoy} * (W_{ssf} + W_{bw})] + (X_{bw} * -W_{bw}) \quad (8.6)$$

$$\Rightarrow \sum M_o = W_{ssf} (X_{buoy} - X_{ssf}) + W_{bw} (X_{buoy} - X_{bw}) \quad (8.7)$$

Looking at (8.7) conclusions about the heeling moment become evident. It is known that X_{bw} always lies in the negative X-direction. Likewise, X_{ssf} and X_{buoy} always lie in the positive X-direction. The quantity $W_{ssf} (X_{buoy} - X_{ssf})$ remains positive for the following condition: $X_{buoy} > X_{ssf}$. Also, the quantity $W_{bw} (X_{buoy} - X_{bw})$ remains positive for all values of X_{buoy} and X_{bw} .

The righting moment will increase until $X_{buoy} > X_{ssf}$ and then it will decrease.

Once the righting moment begins to decrease it will remain positive while the following condition is true:

$$W_{bw}(X_{buoy} - X_{bw}) > W_{ssf}(X_{buoy} - X_{ssf}) \quad (8.8)$$

If the left hand side of (8.8) becomes greater than the right hand side before air is allowed to enter into the internal volume, the righting moment becomes negative and the SSF capsizes.

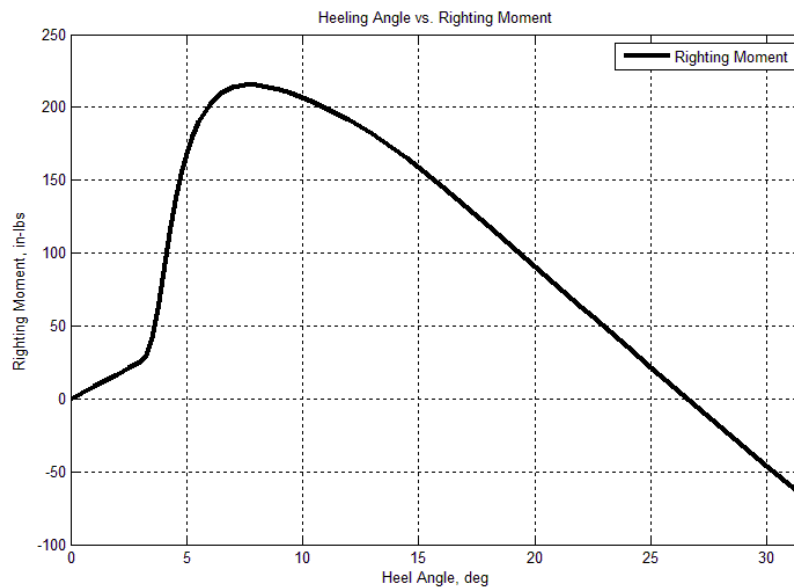


Figure 8.4: Righting Moment vs. Heel Angle: Baseline SSF.

Figure 8.4 plots the righting moment against the heel angle. The maximum heeling moment of 215.30in-lbs occurs at a heel angle of 8°. Beyond this heel angle, the SSF will lose its power to return to equilibrium. It is interesting to note that the value of the righting moment becomes negative at 26.5°, which means the angle of vanishing stability occurs at a lower angle of heel than the entrance of air into the internal volume.

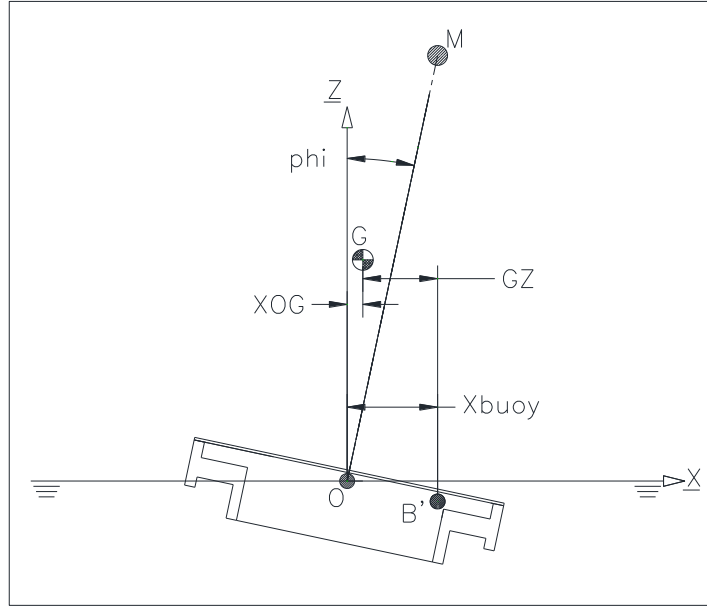


Figure 8.5: Righting Lever Diagram.

The righting lever, \overline{GZ} , as shown in Figure 8.5, is the horizontal distance between the total center of gravity of the SSF and the center of buoyancy, B' . As long as the value of \overline{GZ} is positive the righting moment remains positive.

$$\overline{GZ} = X_{buoy} - X_{OG} \quad (8.10)$$

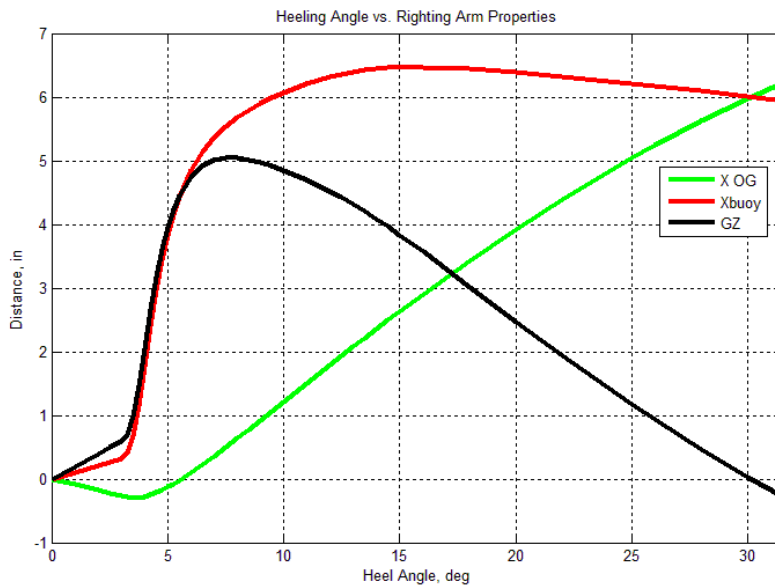


Figure 8.6: Righting Lever vs. Heel Angle: Baseline SSF.

Figure 8.6 plots X_{buoy} , X_{OG} , and \overline{GZ} against the heel angle. Note that the shape of the righting lever curve follows the same trend as that of the righting moment curve. The water ballast mass changes with every angle of heel, so its effect is to increase the righting moment. This added ballast weight increases the righting effect of the ballast water as the heel angle increases.

In Figures 8.4 and 8.6, the curves for the righting moment and the righting lever have similar trends. Between 3° and 5° , there is a linear ramp up where the righting moment and lever are relatively small in comparison to the maximum values. Between these angles the value of \overline{GM} stays relatively constant. On a ship, in general, this range has an upper limit between 10° and 12° . For a SSF the range where the value of \overline{GM} can be used as a measure of stability is decreased. The reason for this lies in the materials used in the construction of the SSF.

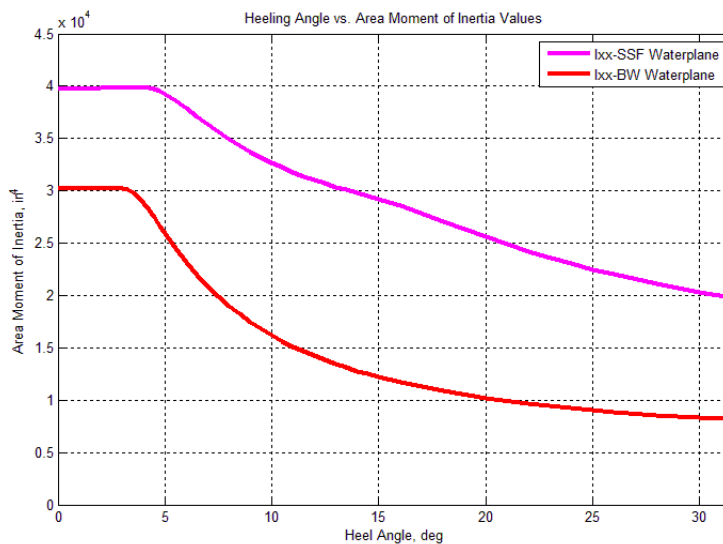


Figure 8.7: Water plane Moment of Inertia vs. Heel Angle

As seen in Figure 8.7, between 3° and 5° the moments of inertia of both the SSF and the ballast water remain constant. This is because the only portion of the SSF below the waterline is the float body, which is constructed of the low-density polyurethane foam. This keeps the center of buoyancy relatively close to the centerline of the SSF and the effect of the heeling angle small. In this range, the metacentric height doesn't change significantly.

Next, there is a sharp rise between 3° and 5° where the righting moment and lever increases sharply. This increase is an effect of the higher density acrylic top plate of the SSF falling below the waterline, which submerges a higher density component further from the center of flotation. This shifts the center of buoyancy, X_{buoy} , further in the positive X-direction and increases the righting moment. When correlated to Figure 8.7, it is seen that in this range of heel angles the moment of inertia for the ballast water begins to decrease sharply, while the SSF moment of inertia remains constant.

Following the sharp rise, there is a non-linear section between 5° and 15° where the righting moment reaches its maximum value and begins to decrease. In Figure 8.6 the curve for X_{OG} transitions from a negative value to a positive value between 6° and 7° . Referring to (8.7), this results in a decreasing value of \overline{GZ} , which also means a decrease in the righting moment.

In the last section of the curve, from 15° to 31.5° , the righting moment decreases until it reaches a negative value at 26.5° . In this range, the values for X_{OG} increase at an almost linear rate, while the values of X_{buoy} decrease non-linearly at a much less pronounced rate than the value of X_{OG} increases, which means the center of buoyancy is

not changing as fast as the SSF center of gravity. It also shows that the heeling moment of the center of gravity of the SSF, not including the ballast water, has more of an effect than the righting moment of the ballast water and the buoyancy force. Referring to (8.7) shows that this offset will result in a decreasing value of \overline{GZ} decreasing.

Comparison: Non-SSF and SSF. Once again, it is important to compare the result of the float with suction-stabilization to that of a float that does not utilize suction-stabilization. The analysis of the Non-SSF is the same as outlined in 8.1.1, only without the added effects of the ballast water.

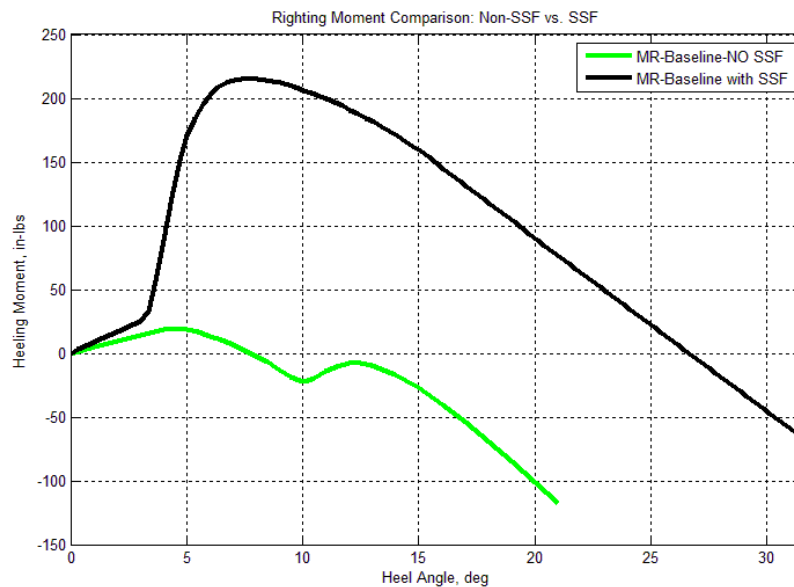


Figure 8.8: Comparison: Non-SSF and SSF Righting Moment.

Figure 8.10, shows a marked increase in the righting moment of the SSF versus the Non-SSF. The Non-SSF reaches a maximum righting moment of 19.63in-lbs at a heel angle of 4.5°. This is 90.9% lower than that of the SSF.

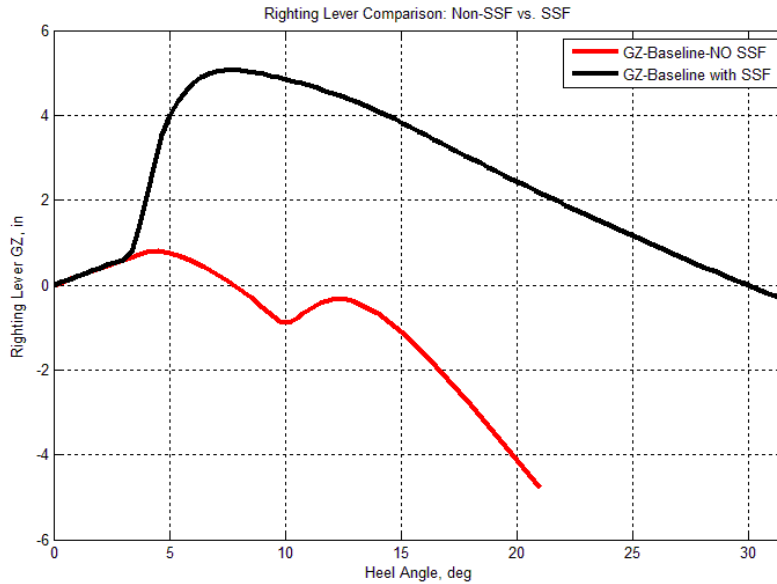


Figure 8.9: Comparison: Non-SSF and SSF Righting Lever.

Figure 8.11, shows a marked increase in the righting lever of the SSF versus the Non-SSF. The Non-SSF has a maximum righting lever of .798in at a heel angle of 4.5°. This is 84.2% lower than that of the SSF.

At 10° for the NSSF, as shown in both Figure 8.8 and 8.9, there is a slight increase in the righting moment, not enough to make it stable, but enough to stand out on the plot. This increase is due to the higher density top plate of the Non-SSF being submerged below the waterline and increasing the value of X_{buoy} .

Figures 8.10 and 8.11 clearly show that Suction-Stabilization dramatically increases the stability of the float.

Righting Moment and Righting Lever: Varying Geometries.

Geometry and design influence the hydrostatic and hydrodynamic characteristics of the SSF. To understand the exact ways that geometry effect the stability of the SSF, six

geometric variations were analyzed in the same manner as the baseline SSF and then compared to the baseline SSF by their respective Righting Arms and Righting Levers.

Geometry Variation: Section 4 Height.

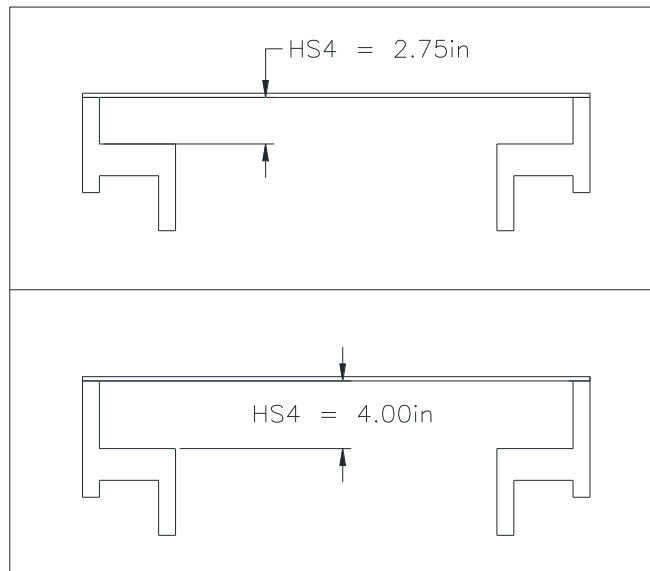


Figure 8.10: Section 4 Height Variations.

Figure 8.10 gives a pictorial representation of the two Section 4 heights used to compare the effect of Section 4 height on both the righting moment and the righting lever.

Table 8.1

Geometric Properties: Section 4 Height.

	Baseline	Height S4 = 2.75in	Height S4 = 4.00in
Mast Weight	15.00 lbf	15.00 lbf	15.00 lbf
Mast Height	92.00 in	92.00 in	92.00 in
Mast KG	65.00 in	65.00 in	65.00 in
Ballast Water Weight	18.08 lbf	21.58 lbf	25.09 lbf
Ballast Water Volume	488.70 in ³	583.35 in ³	677.99 in ³
Ballast Water KG	6.23 in	7.40 in	8.58 in
Total Weight	42.68 lbf	46.37 lbf	50.07 lbf
Draught, in	5.83 in	6.926 in	8.024 in
Displacement Volume	1153.40 in ³	1253.30 in ³	1353.20 in ³
KB, in	3.69 in	3.91 in	4.17 in
KG, in	26.86 in	25.97 in	25.38 in
BM, in	34.47 in	31.73 in	29.38 in
GM, in	11.30 in	9.66 in	8.18 in
If, in	26.16 in	27.07 in	22.30 in
GMeff, in	37.46 in	33.74 in	30.47 in
Kempf's Factor	7.75	7.86	7.98

Table 8.1 gives a comparison of the various properties of the two Section Four heights against the baseline geometry.

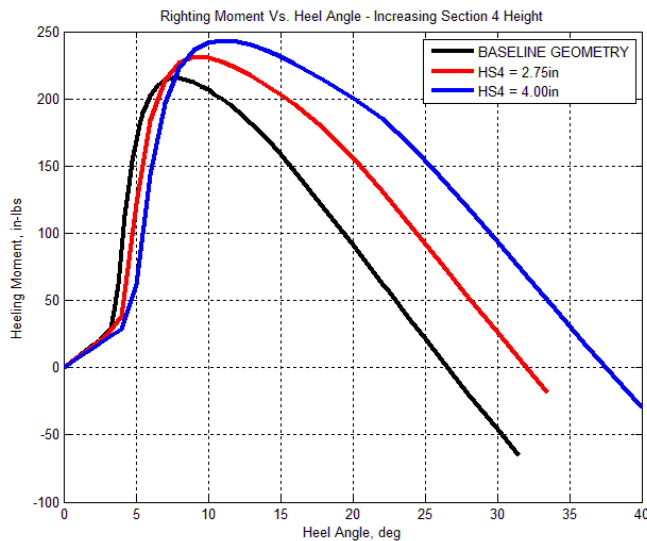


Figure 8.11: Righting Moment vs. Heel Angle: Section 4 Heights.

Figure 8.11 plots the righting moment for the two Section 4 Heights against the heel angle. The righting moment for the baseline SSF is plotted in black for comparison. The righting lever reaches a maximum value of 215.30in-lbs at 8° when Section 4 height is 1.50in, a value of 231.32in-lbs at 10° when Section 4 height is 2.75in, and a value of 243.52in-lbs at 12° when Section 4 height is 4.00in. Increasing the height of Section 4, appears to keep the righting moment at a higher value for more degrees of heel.

The righting moment is greater than 150in-lbs for a range of at $4.5^\circ - 15.5^\circ$ when Section 4 height is 1.50in, for a range of at $5^\circ - 16^\circ$ when Section 4 height is 2.75in, and for a range of at $6.5^\circ - 25.5^\circ$ when Section 4 height is 4.00in. From this, it is apparent the greater the height of section 4, the larger the range of heel angles that will have a large heeling moment. This means that the float will have an increased tendency to return to equilibrium. However, this must be weighed against the lowered metacentric height and increased roll period.

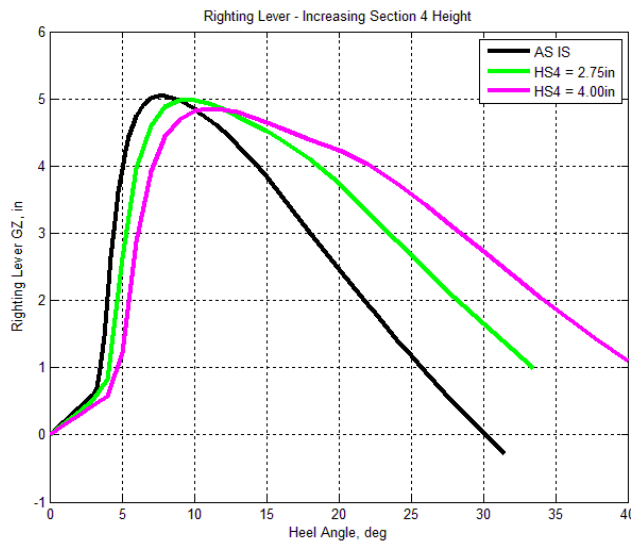


Figure 8.12: Righting Lever vs. Heel Angle: Section 4 Heights.

Figure 8.12 plots the righting lever for the two Section 4 Heights against the heel angle. The righting lever for the baseline SSF is plotted in black for comparison. Where the peak values of the righting moment were all similar, the maximum values for the righting lever were not. The righting lever reaches a maximum value of 5.044in at 8° when Section 4 height is 1.50in, a value of 4.984in at 11° when Section 4 height is 2.75in, and a value of 4.849 at 12° when Section 4 height is 4.00in.

Geometry Variation: Section 4 Diameters.

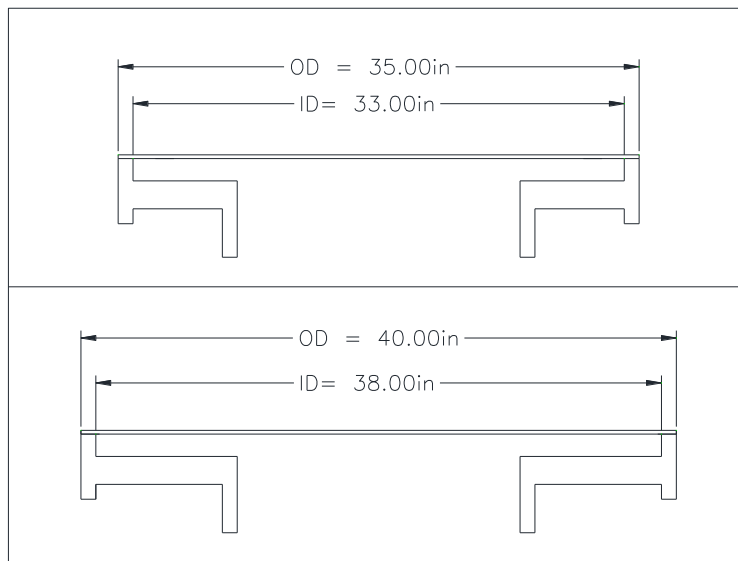


Figure 8.13: Section 4 Diameter Variations.

Figure 8.13 gives a pictorial representation of the two outer diameter variations used to compare the effect of outer diameter on both the righting moment and the righting lever.

Table 8.2

Geometric Properties: Section 4 Diameters.

	Baseline	OD = 35in, ID = 19in	OD = 40in, ID = 19in
Mast Weight	15.00 lbf	15.00 lbf	15.00 lbf
Mast Height	92.00 in	92.00 in	92.00 in
Mast KG	65.00 in	65.00 in	65.00 in
Ballast Water Weight	18.08 lbf	32.30 lbf	48.81 lbf
Ballast Water Volume	488.70 in ³	872.79 in ³	1319.00 in ³
Ballast Water KG	6.23 in	6.12 in	6.04 in
Total Weight	42.68 lbf	60.48 lbf	81.13 lbf
Draught, in	5.83 in	5.605 in	5.462 in
Displacement Volume	1153.40 in ³	1634.60 in ³	2192.60 in ³
KB, in	3.69 in	3.81 in	3.89 in
KG, in	26.86 in	20.72 in	16.96 in
BM, in	34.47 in	45.07 in	57.31 in
GM, in	11.30 in	28.15 in	44.24 in
lf, in	26.16 in	35.61 in	46.68 in
GMeff, in	37.46 in	63.77 in	90.92 in
Kempf's Factor	7.75	4.69	3.23

Table 8.2 gives a comparison of the various properties of the two outer diameter geometries against the baseline geometry.

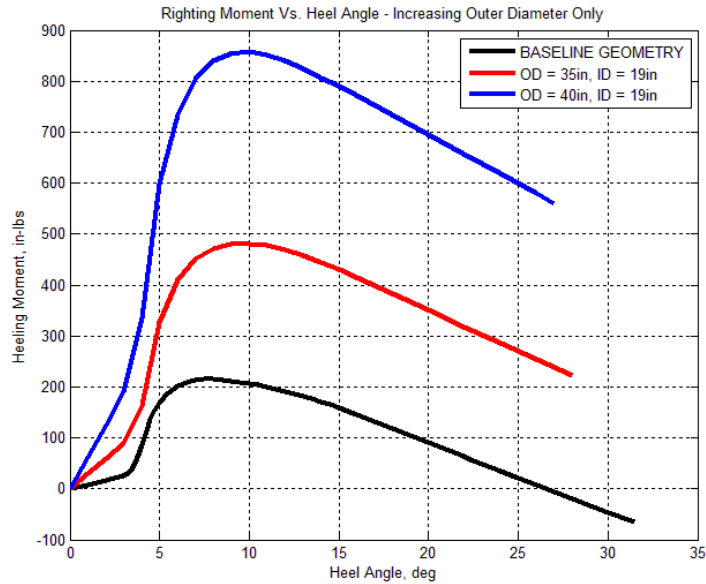


Figure 8.14: Righting Moment vs. Heel Angle: Section 4 Diameters.

Figure 8.14 plots the righting moment for the two Section 4 diameters against the heel angle. The righting moment for the baseline SSF is plotted in black for comparison. There is a large disparity between the curves. The righting moment peaks at a value of 215.30in-lbs at 8° when the outer diameter of Section 4 is 30in and the inner diameter of Sections 1 & 2 is 19in, at a value of 481.36in-lbs at 11° when the outer diameter of Section 4 is 35in and the inner diameter of Sections 1 & 2 is 19in, and at a value of 857.58in-lbs at 11° when the outer diameter of Section 4 is 40in and the inner diameter of Sections 1 & 2 is 19in.

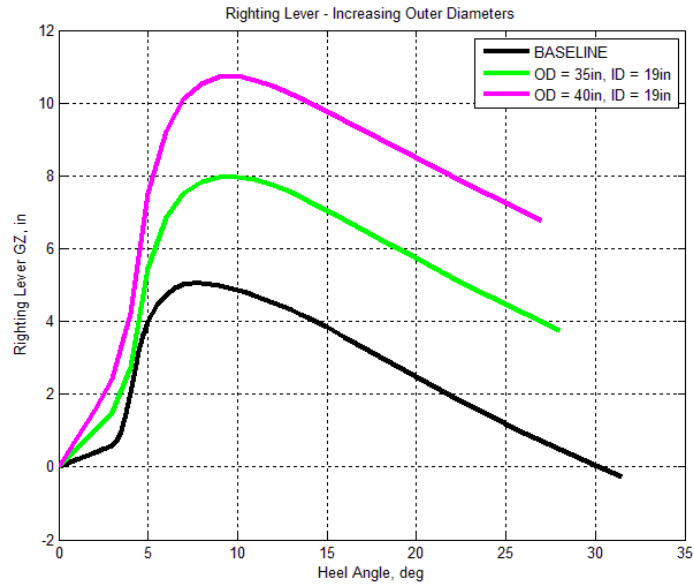


Figure 8.15: Righting Lever vs. Heel Angle: Section 4 Diameters.

Figure 8.15 plots the righting lever for the two outer diameter variations against the heel angle. The baseline geometry is plotted for a comparison. The righting lever reaches a maximum at a value of 5.044in at 8° when the outer diameter of Section 4 is 30in and the inner diameter Sections 1 & 2 is 19in, at a value of 7.971in at 12° when the outer diameter of Section 4 is 35in and the inner diameter Sections 1 & 2 is 19in, and at a value of 10.735in at 10° when the outer diameter of Section 4 is 40in and the inner diameter Sections 1 & 2 is 19in.

The righting moment and lever curves end abruptly at 28° when the outer diameter of Section 4 is 35in and the inner diameter Sections 1 & 2 is 19in, and at 27° when the outer diameter of Section 4 is 40in and the inner diameter of Sections 1 & 2 is 19in. At these angles air is allowed to enter the internal volume.

So, while the righting moment is larger than the baseline geometry increasing the diameter to gain stability limits the range of allowable heeling angles.

Geometry Variation: All Section Diameters.

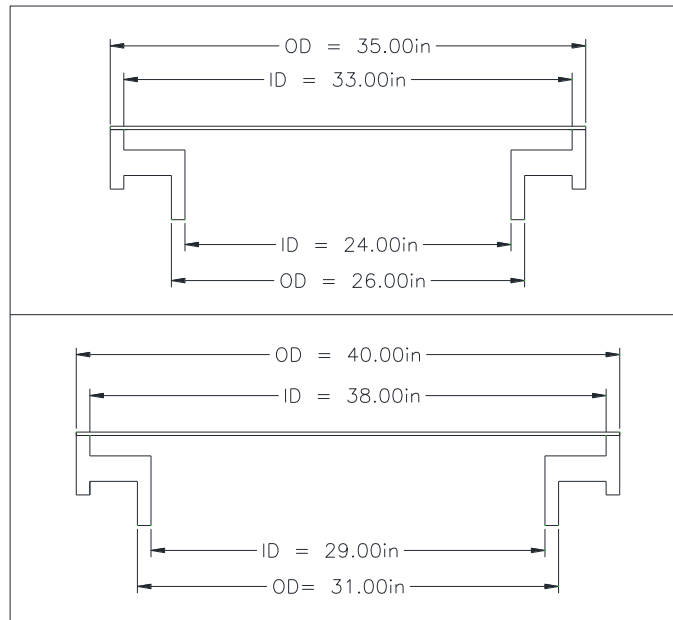


Figure 8.16: All Section Diameter Variations

Figure 8.16 gives a pictorial representation of the two diameter variations used to compare the effect of diameter on both the righting moment and the righting lever.

Table 8.3

Geometric Properties: All Section Diameters.

	Baseline	OD = 35in, ID = 24in	OD = 40in, ID = 29in
Mast Weight	15.00 lbf	15.00 lbf	15.00 lbf
Mast Height	92.00 in	92.00 in	92.00 in
Mast KG	65.00 in	65.00 in	65.00 in
Ballast Water Weight	18.08 lbf	23.96 lbf	29.54 lbf
Ballast Water Volume	488.70 in ³	647.55 in ³	798.32 in ³
Ballast Water KG	6.23 in	6.25 in	6.27 in
Total Weight	42.68 lbf	51.70 lbf	60.83 lbf
Draught, in	5.83 in	5.868 in	5.921 in
Displacement Volume	1153.40 in ³	1397.20 in ³	1644.10 in ³
KB, in	3.69 in	3.68 in	3.68 in
KG, in	26.86 in	23.28 in	20.74 in
BM, in	34.47 in	55.72 in	76.43 in
GM, in	11.30 in	33.13 in	59.38 in
lf, in	26.16 in	41.67 in	62.26 in
GMeff, in	37.46 in	74.80 in	121.63 in
Kempf's Factor	7.75	4.65	3.18

Table 8.3 gives a comparison of the various properties of the two diameter geometries against the baseline geometry.

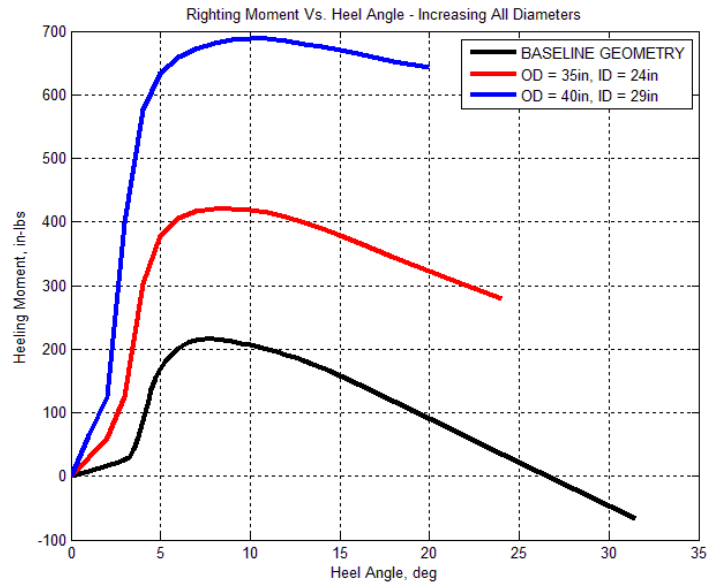


Figure 8.17: Righting Moment vs. Heel Angle: All Section Diameters.

Figure 8.17 plots the righting moment for the two diameter variations against the heel angle. The baseline geometry is plotted for a comparison. There is a large disparity between the curves. The righting moment peaks at a value of 215.30in-lbs at 8° when the outer diameter of Section 4 is 30in and the inner diameter of Sections 1 & 2 is 19in, at a value of 420.64in-lbs at 10° when the outer diameter of Section 4 is 35in and the inner diameter of Sections 1 & 2 is 24in, and at a value of 689.02in-lbs at 11° when the outer diameter of Section 4 is 40in and the inner diameter of Sections 1 & 2 is 29in.

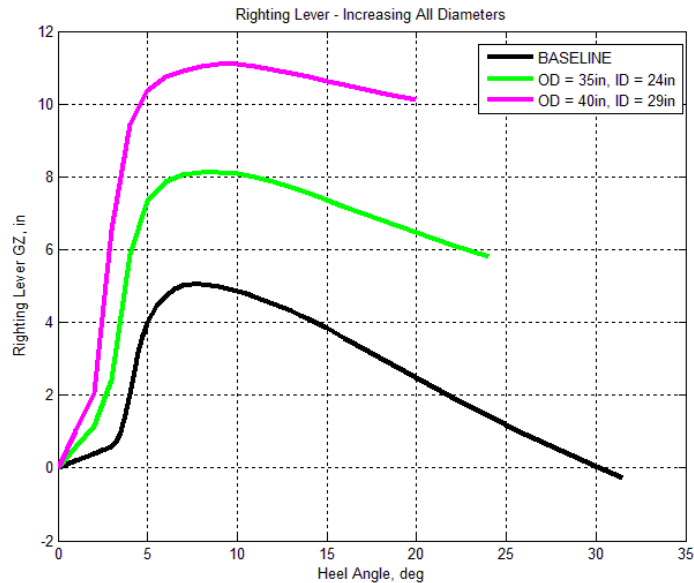


Figure 8.18: Righting Lever vs. Heel Angle: All Section Diameters.

Figure 8.18 plots the righting lever for the two diameter variations against the heel angle. The baseline geometry is plotted for a comparison. The righting lever reaches a maximum at a value of 5.044in at 8° when the outer diameter of Section 4 is 30in and the inner diameter of Sections 1 & 2 is 19in, at a value of 8.111in at 10° when the outer diameter of Section 4 is 35in and the inner diameter of Sections 1 & 2 is 24in, and at a

value of 11.087in at 10° when the outer diameter of Section 4 is 40in and the inner diameter of Sections 1 & 2 is 29in.

The righting moment and lever curves end abruptly at 24° when the outer diameter of Section 4 is 35in and the inner diameter of Sections 1 & 2 is 24in, and at 20° when the outer diameter of Section 4 is 40in and the inner diameter of Sections 1 & 2 is 29in. At these angles air is allowed to enter the internal volume. So, while the righting moment is larger than the baseline geometry increasing the diameter to gain stability limits the range of allowable heeling angles.

Comparison: all Geometric Variations.

Table 8.4

Maximum Righting Moment Values.

	Heel Angle (Deg)	Maximum Righting Moment (in-lbs)
Baseline	8	215.3
HS4 = 2.75in	10	231.32
HS4 = 4.00in	12	243.52
OD = 35in, ID = 24in	10	420.64
OD = 35in, ID = 19in	11	481.26
OD = 40in, ID = 29in	11	689.02
OD = 40in, ID = 19in	11	857.58

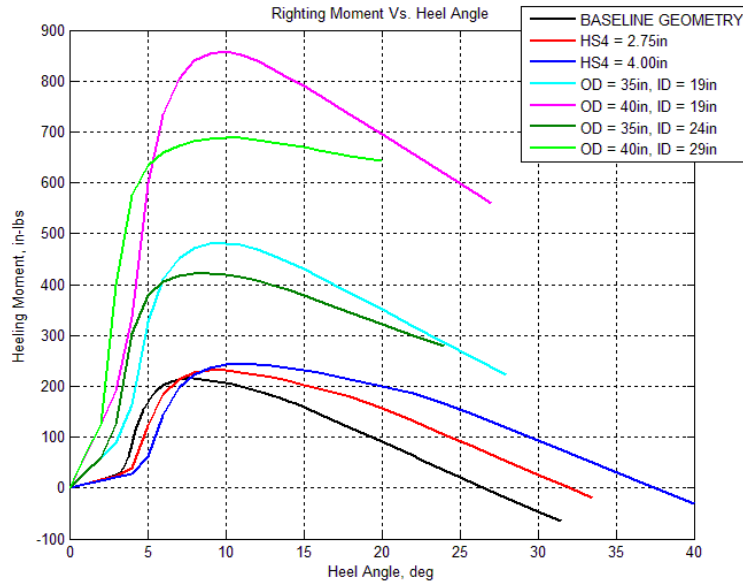


Figure 8.19: Righting Moment vs. Heel Angle: All Geometric Variations.

Figure 8.19 plots the righting lever for all geometries present in 8.2.1-8.2.3. Table 8.4 lists the maximum righting moments of the various geometries in ascending order.

Table 8.5

Maximum Righting Lever Values.

	Heel Angle (Deg)	Maximum Righting Lever (in)
HS4 = 4.00in	12	4.849
HS4 = 2.75in	10	4.984
Baseline	8	5.044
OD = 35in, ID = 19in	11	7.9711
OD = 35in, ID = 24in	10	8.111
OD = 40in, ID = 19in	11	10.735
OD = 40in, ID = 29in	11	11.087

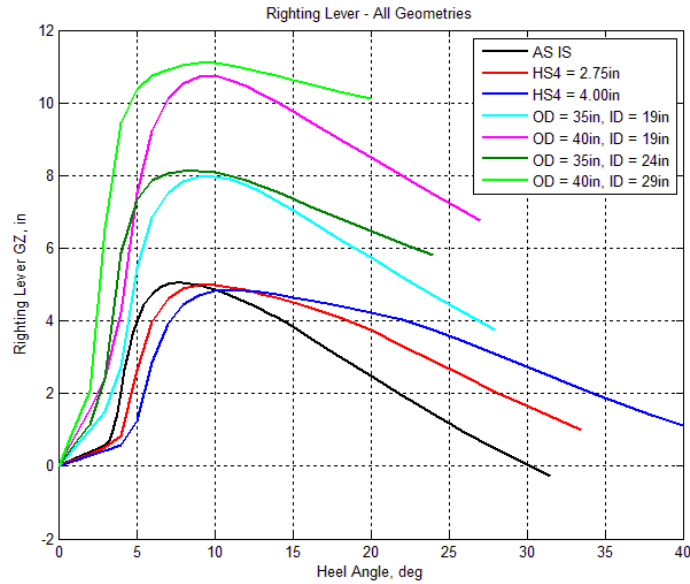


Figure 8.20: Righting Lever vs. Heel Angle: All Geometric Variations.

Figure 8.20 plots the righting lever against the heel angle for all geometries presented in 8.2.1-8.2.3. Table 8.5 lists the maximum righting levers of the various geometries in ascending order. It is interesting to note that the length of the righting arm is not an exact indicator of the righting moment. For example, the righting lever is 5.044in for the baseline geometry, while the length of the righting lever is 4.849in when the height of Section 4 is 4.00in.

This, however, does not imply that the righting moment follows a similar trend. Looking at Table 8.4, the value of the righting moment is 215.30in-lbs for the baseline geometry, while the value of the righting moment is 243.52in-lbs when the height of Section 4 is 4.00in. This is a result of the increased height of Section 4, which increases the weight of the trapped water and creates a larger righting moment for a shorter righting lever length.

Table 8.6

Angles of Vanishing Stability and Air Entrance Angles.

	Angle of Vanishing Stability (deg)	Air Entrance Angle (deg)
Baseline	26.5	31.5
HS4 = 2.75in	32	33.5
HS4 = 4.00in	37	40
OD = 35in, ID = 19in	N/A	28
OD = 40in, ID = 19in	N/A	27
OD = 35in, ID = 24in	N/A	24
OD = 40in, ID = 29in	N/A	20

Table 8.6 lists the angles of vanishing stability and the air entrance angles for the seven SSF Geometries. The baseline geometry and the geometries with increased Section 4 heights have an angle of vanishing stability that is less than the air entrance angle. Increasing the diameters, both the Section 4 diameters alone and all diameters equally, eliminates the angle of vanishing stability, because it significantly decreases the air entrance angle. At first glance, this may appear as a negative, however when the increased righting moment is taken into account it is more beneficial to decrease the air entrance angle in order to increase the righting moment and stability.

Chapter 9

PARAMETRIC ROLL RESONANCE

This chapter presents a parametric roll resonance analysis for the baseline SSF. Wave input is an important factor in overall stability of semi-submersibles such as the SSF. Normally, parametric roll resonance occurs when vessel is moving at a forward velocity. However, the SSF is floating platform with no forward velocity. Therefore, for the analysis presented in this chapter, it is assumed that all waves are incident upon a stationary body with its center of rotation located at the center of flotation. It is also important to note that this analysis assumes the SSF is not tethered to the ocean, or pool floor.

The guidelines set up by the ABS guide (2004) are the basis for the calculations in this chapter. Some equations were modified to more correctly model the SSF.

Parametric Roll with Damping.

The governing ODE for roll motion with damping, as defined by the ABS Guide (2005), is:

$$\ddot{\phi} + 2\mu\omega_o\dot{\phi} + \omega_o^2 f(\phi, t) = 0 \quad (9.1)$$

Where ϕ is the heel angle at a given time, $\ddot{\phi}$ is the second derivative of the heel angle with respect to time, $\dot{\phi}$ is the first derivative of the heel angle with respect to time, μ is the roll damping coefficient, ω_o is the natural roll frequency of the SSF, and $f(\phi, t)$ is a restoring function based on the righting arm \overline{GZ} .

$$f(\phi, t) = \frac{\text{sign}(\phi)}{\overline{GM}_o} \overline{GZ}(|\phi|, t) \quad (9.2)$$

Where $\text{sign}(\phi)$ equals (-1) for negative values of heel and (+1) for positive values of heel, $|\phi|$ is the absolute values of the heel angle, \overline{GM}_o is the metacentric height at level in calm water, and $\overline{GZ}(|\phi|, t)$ is the righting arm function defined either explicitly through experimental data or through an appropriate approximation.

Inserting (9.2) into (9.1),

$$\ddot{\phi} + 2\mu\omega_o \dot{\phi} + \frac{\omega_o^2 \text{sign}(\phi)}{\overline{GM}_o} \overline{GZ}(|\phi|, t) = 0 \quad (9.3)$$

Defining the M_R and \overline{GZ} Curves. To solve (9.3) and determine the roll characteristics of the SSF it is necessary to define the \overline{GZ} curve. To do this, a curve was fit to the data tabulated in Chapter 8.

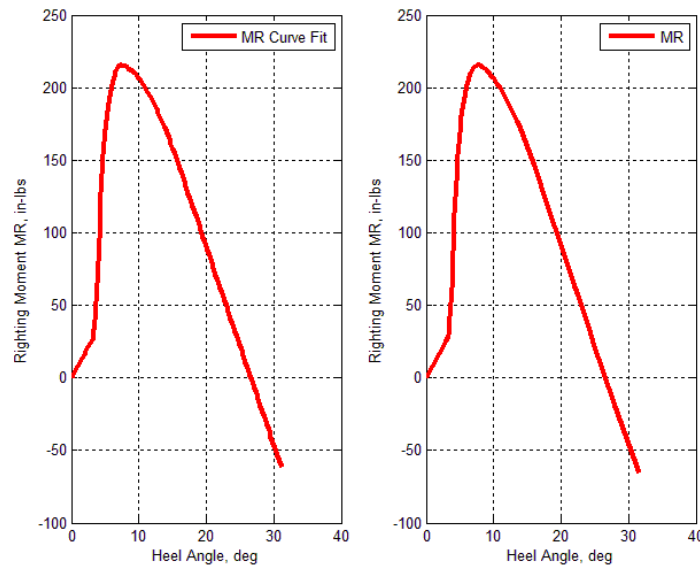


Figure 9.1: Righting Moment Comparison: Empirical Data Curve and Curve Fit

$$M_R = \begin{cases} 8.4489\phi - 0.0122 : & 0^\circ < \phi \leq 3^\circ \\ -29.161\phi^3 + 359.81\phi^2 - 1378.3\phi + 1706.1 : & 3^\circ < \phi \leq 5^\circ \\ 1.4486\phi^3 - 36.243\phi^2 + 299.42\phi - 602.6 : & 5^\circ < \phi \leq 9^\circ \\ -0.6574\phi^2 + 6.8626\phi + 203.61 : & 9^\circ < \phi \leq 15^\circ \\ 0.0124\phi^2 + 14.254\phi + 370.47 : & 15^\circ < \phi \leq 31.5^\circ \end{cases} \quad (9.4)$$

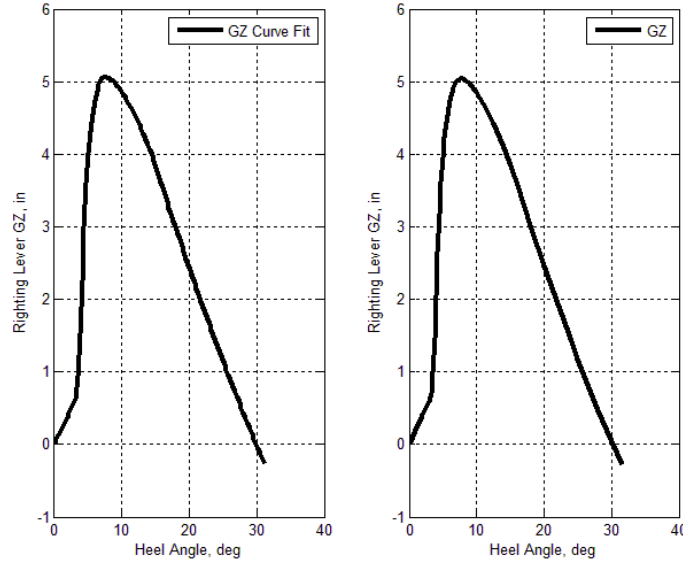


Figure 9.2: Righting Lever Comparison: Empirical Data Curve and Curve Fit

$$\overline{GZ} = \begin{cases} 0.198\phi - 0.0003 : & 0^\circ < \phi \leq 3^\circ \\ -0.6837\phi^3 + 8.4354\phi^2 - 32.31\phi + 40.064 : & 3^\circ < \phi \leq 5^\circ \\ 0.0342\phi^3 - 0.853\phi^2 + 7.0359\phi - 14.152 : & 5^\circ < \phi \leq 9^\circ \\ -0.0131\phi^2 + 0.1252\phi + 4.9122 : & 9^\circ < \phi \leq 15^\circ \\ 0.0024\phi^2 - 0.3647\phi + 8.7691 : & 15^\circ < \phi \leq 31.5^\circ \end{cases} \quad (9.5)$$

(9.4) and (9.5) defines the curves for the righting moment, M_R , and the righting lever, \overline{GZ} .

Susceptibility Criteria for Parametric Roll

Before the roll characteristics can be evaluated, the SSF design must be checked for susceptibility to parametric roll resonance. Since it was the worst case, the baseline SSF is used for this analysis.

Design Variables for Baseline SSF. The length of the design wave is equal to the length between perpendiculars. In the case of the SSF this is the outer diameter of Section 4.

$$\lambda = L_{pp} = OD_{S4} \quad (9.6)$$

$$\lambda = 30in$$

Where λ is the design wave length, L_{pp} is the length between perpendiculars, and OD_{S4} is the outer diameter of Section 4.

According to ABS guide (2004), the wave height need not exceed $2(D_m - T)$.

$$\begin{aligned} H_w &= 2(D_m - T) \\ H_w &= 2(6.875in - 5.8313in) = 2.09in \end{aligned} \quad (9.7)$$

Where H_w is the wave height, D_m is the moulded depth, and T is the moulded draught. These values are found in Table 7.1.

The wave period and frequency corresponding to the wavelength are calculated as follows:

$$P_w = \sqrt{\frac{2\pi\lambda}{g}} \quad (9.8)$$

$$P_w = \sqrt{\frac{2\pi(30in)}{386.4 \frac{in}{sec^2}}} = .698 \text{ sec}$$

$$\omega_w = \frac{2\pi}{P_w} \quad (9.9)$$

$$\omega_w = \frac{2\pi}{.698 \text{ sec}} = 9.00 \frac{rad}{sec}$$

Where P_w is the wave period, ω_w is the wave frequency, and g is gravitational constant in $\left(\frac{in}{sec^2}\right)$.

Next, the above-defined wave is moved from the center of the SSF to the outermost edge. The metacentric height, \overline{GM} , is calculated for different wave crest locations along the body. These locations occur in increments of $.1L_{pp} = .1OD = 3in$.

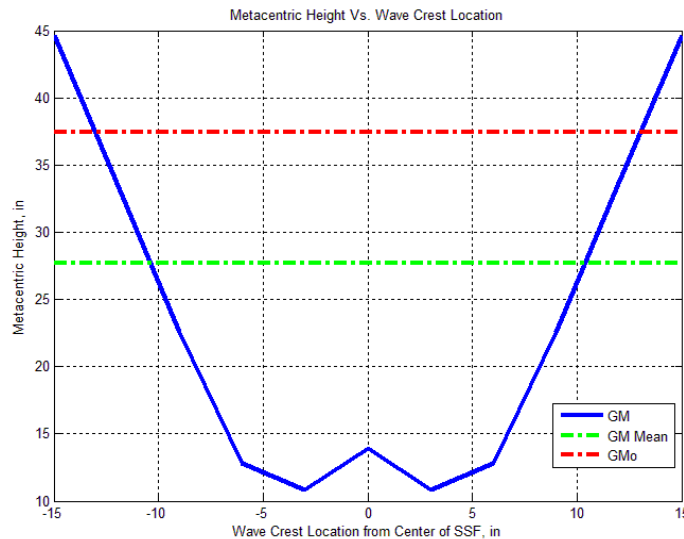


Figure 9.3: Metacentric Height vs. Wave Crest Location

Figure 9.3 shows the values of \overline{GM} as the wave crest moves from one edge of the SSF to the other. From this plot, it is seen that the maximum value of \overline{GM} occurs when the wave crest is located 15in from the center of the SSF and the minimum value occurs when the wave crest is located at 3in from the center of the SSF. Note that the minimum value of \overline{GM} does not occur when the wave crest is at the centerline of the SSF. This is an effect of the increased IST effect at this wave crest location.

The following equations define all the parameters needed to determine whether the SSF is susceptible to parametric roll.

$$\begin{aligned}\overline{GM}_{\min} &= 10.80in \\ \overline{GM}_{\max} &= 44.62in \\ \overline{GM}_m &= .5(\overline{GM}_{\max} + \overline{GM}_{\min}) = 27.71in\end{aligned}\tag{9.10}$$

The amplitude of parametric excitation, \overline{GM}_a , is defined as,

$$\overline{GM}_a = .5(\overline{GM}_{\max} - \overline{GM}_{\min}) = 16.91in\tag{9.11}$$

The amplitude of stability change in longitudinal waves expressed in terms of frequency, ω_a , is defined as,

$$\omega_a = \sqrt{\frac{g\overline{GM}_a}{i_m^2}} = 1.954 \frac{rad}{sec}\tag{9.12}$$

The mean value of stability change in longitudinal waves expressed in terms of frequency, ω_m , is defined as,

$$\omega_m = \sqrt{\frac{g\overline{GM}_m}{i_m^2}} = 2.502 \frac{rad}{sec}\tag{9.13}$$

Since the SSF has no forward velocity, the frequency of encounter, ω_E , is equivalent to the wave frequency.

$$\omega_E = \omega_W = 9.00 \frac{rad}{sec} \quad (9.14)$$

Parametric roll resonance, if it is to occur, will happen when ω_E is twice the natural frequency of the float, ω_o . From (9.9) it is seen that the wave encounter frequency is three times the value of $\omega_o = 2.908 \frac{rad}{sec}$ calculated in Chapter 7, (7.1).

Susceptibility Criteria. The ABS guide (2004) defines that the following criteria must be met for the SSF to be susceptible to parametric roll. Once again, the equations in the ABS guide (2004) account for a forward speed. Since the SSF is a stationary platform, there is no forward speed and the following equations have been modified to account for this.

$$0.25 - 0.5q - 0.125q^2 + 0.03125q^3 \leq p \leq 0.25 + 0.5q \quad (9.15)$$

Where,

$$p = \frac{\omega_m^2 - (\mu\omega_o)^2}{\omega_E^2} \quad (9.16)$$

$$q = \frac{\omega_a^2}{\omega_E^2} \quad (9.17)$$

Table 9.1

p and q Values for ABS Prescribed Values of μ .

Damping Coefficient	q	p
0.030	0.047	0.077
0.050	0.047	0.077
0.075	0.047	0.077
0.100	0.047	0.076

Table 9.1 lists the values of *p* and *q* for the various values of μ . These values are then used in (9.15) as a check for susceptibility.

Table 9.2

Inequality Values for ABS Prescribed Values of μ .

Damping Coefficient	LHS	p	RHS	Susceptibility Outcome
0.030	0.226	0.077	0.274	Negative
0.050	0.226	0.077	0.274	Negative
0.075	0.226	0.077	0.274	Negative
0.100	0.226	0.076	0.274	Negative

From Table 9.2, it is seen that, according to ABS Susceptibility criteria, the SSF is not susceptible to parametric resonance. This, however, will be verified in 9.3.

Numerical Simulation.

To verify the result of the ABS susceptibility criteria (9.1) will be solved numerically using the ODE45 algorithm contained in MATLAB.

To solve (9.3), the following substitution was made,

$$\begin{aligned}\phi_1 &= \phi \\ \phi_2 &= \dot{\phi}\end{aligned}$$

Which, when applied to (9.3), yields,

$$\dot{\phi}_2 + 2\mu\omega_o\phi_2 + \frac{\omega_o^2 \text{sign}(\phi_1)}{GM_o} \overline{GZ}(|\phi_1|, t) = 0 \quad (9.18)$$

The input for the numerical simulation is then,

$$D(\phi, t) = \begin{cases} \phi_2 \\ -2\mu\omega_o\phi_2 - \frac{\omega_o^2 \text{sign}(\phi_1)}{GM_o} \overline{GZ}(|\phi_1|, t) \end{cases} \quad (9.19)$$

The ABS guide (2004) requires that the following values of damping coefficient be used in the analysis of parametric roll, $\mu = 0.03, 0.05, 0.075$, and 0.10 . It also suggests and initial heel angle of 5° to ensure an adequate righting moment to check for parametric roll.

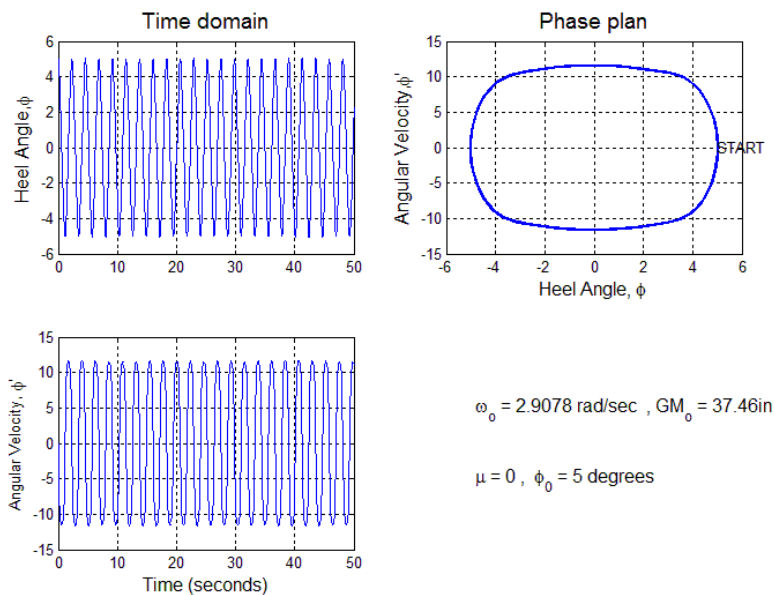


Figure 9.4: Roll Amplitude for Free Roll, $\mu = 0.0$

Figure 9.4 plot the case for free roll, the case when there is no damping effect by the water. In this case, the SSF rolls from 5° to -5° without cease. The roll is stable and does not increase or decrease.

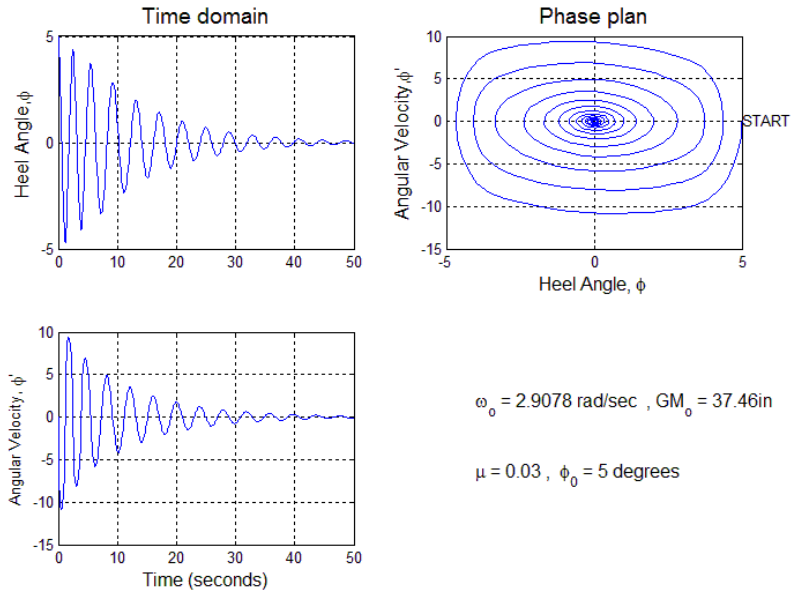


Figure 9.5: Roll Amplitude: $\mu = 0.03$

Figure 9.5 plots the case where $\mu = 0.03$. In this case, the SSF rolls from 5° to -4.9° and damps out to 0° in ~ 40 seconds.

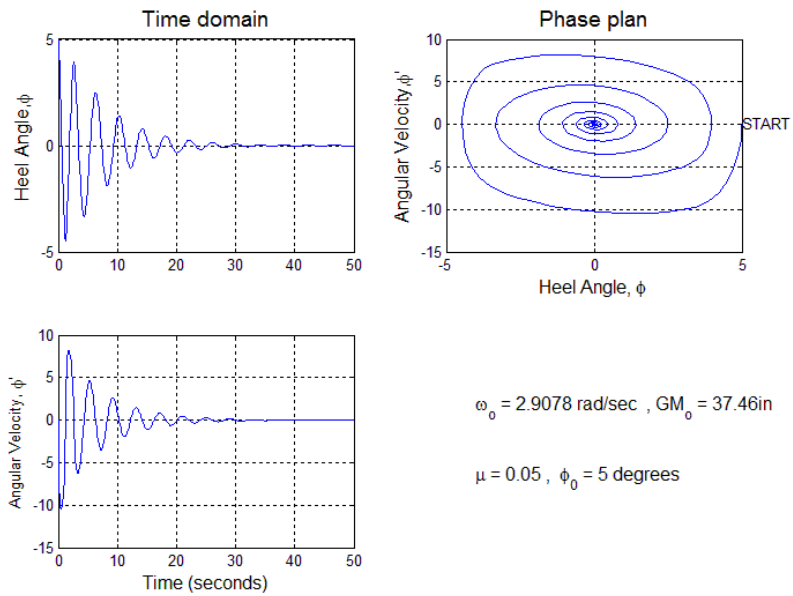


Figure 9.6: Roll Amplitude: $\mu = 0.05$

Figure 9.6 plots the case where $\mu = 0.05$. In this case, the SSF rolls from 5° to -4.8° and damps out to 0° in ~ 25 seconds.

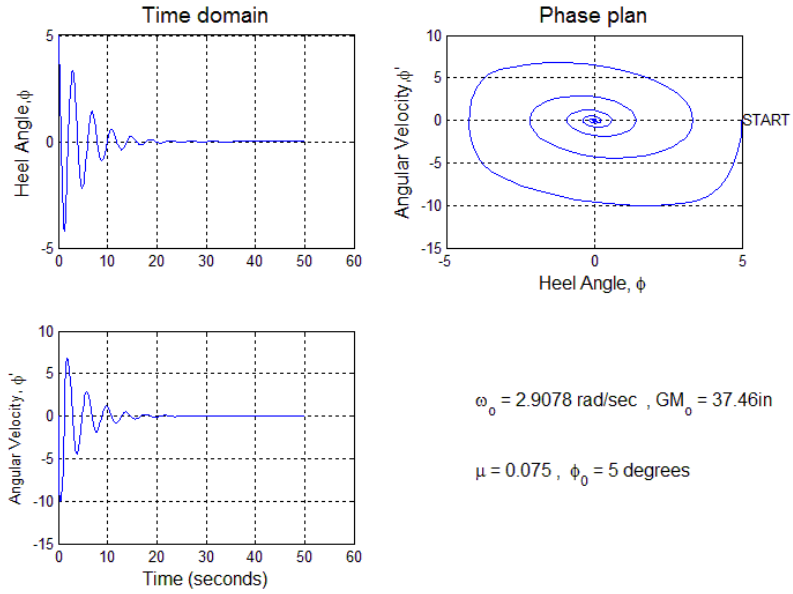


Figure 9.7: Roll Amplitude: $\mu = 0.075$

Figure 9.7 plots the case where $\mu = 0.075$. In this case, the SSF rolls from 5° to -4.5° and damps out to 0° in ~ 18 seconds.

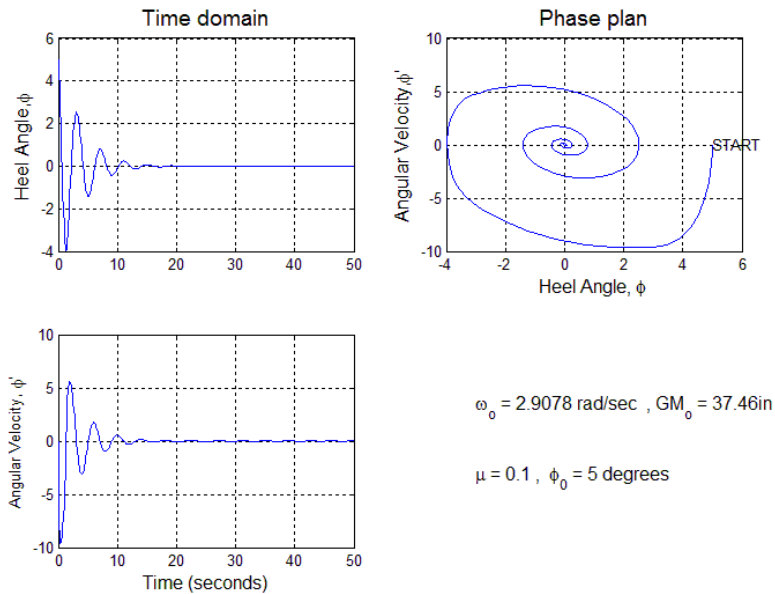


Figure 9.8: Roll Amplitude: $\mu = 0.10$

Figure 9.8 plots the case where $\mu = 0.10$. In this case, the SSF rolls from 5° to -4° and damps out to 0° in ~ 12 seconds.

Figures 9.4-9.8 plot the roll characteristics for the Baseline SSF with varying damping coefficients. Not one case, even when $\mu = 0.00$, displays parametric resonance, which confirms the prediction made with the susceptibility criteria in 9.2.

To verify this, an extreme heel angle of 23.90° is used for the undamped, $\mu = 0.00$, case and 26° for a damped case, $\mu = 0.05$. These values are just below the angle of vanishing stability: $\phi_{VS} = 26.50^\circ$ and any greater initial angle causes the SSF to capsize.

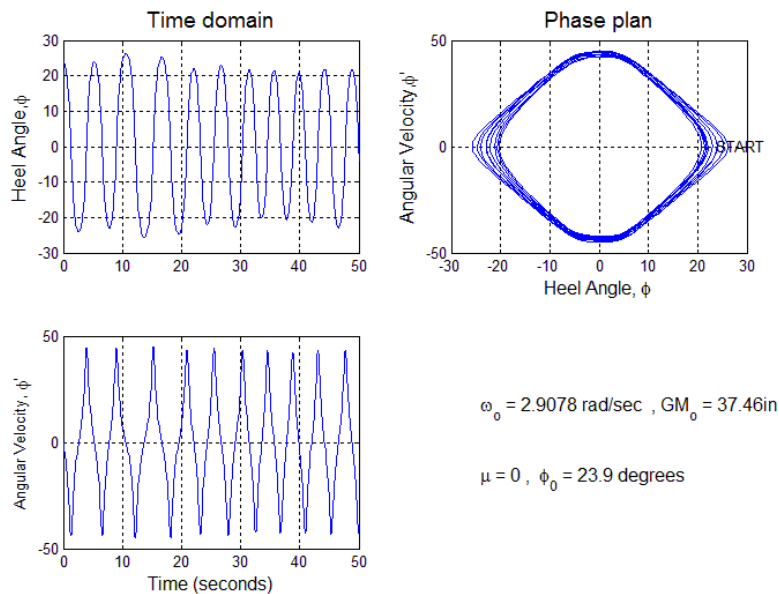


Figure 9.9: Roll Amplitude: $\phi_0 = 23.90^\circ$ & $\mu = 0.00$

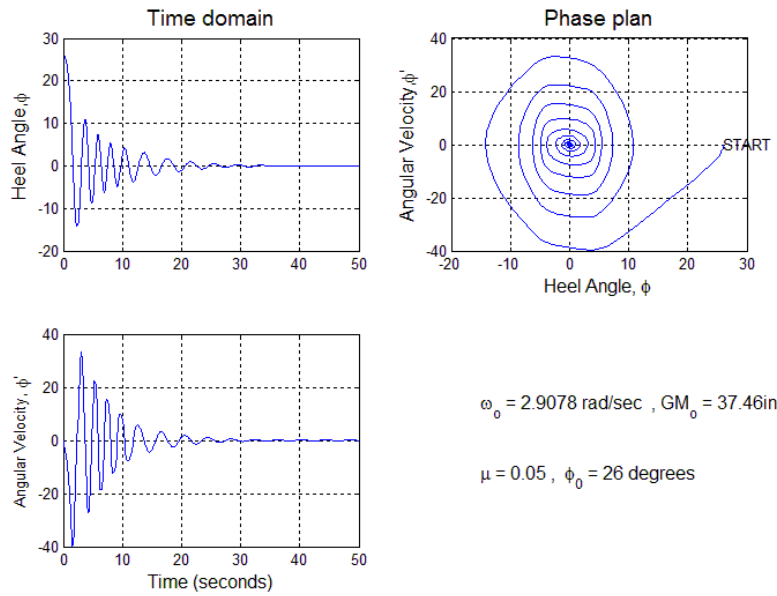


Figure 9.10: Roll Amplitude: $\phi_0 = 26.00^\circ$ & $\mu = 0.05$

As evidenced by Figures 9.9 and 9.10, even in extreme cases of initial heel angle the baseline SSF does not display parametric roll resonance.

Chapter 10

WIND HEELING ARM ANALYSIS

An important factor in the design of the SSF is its ability to withstand wind loads. The SSF used in this report is intended for use in a backyard pool where wind speeds are relatively low in comparison to offshore wind speeds. However, the intention of the SSF is for future use as an offshore wind turbine platform, so the wind speeds used in this chapter are the same as those found off the shores of the USA.

Offshore wind data presented by the National Renewable Energy Laboratory (NREL), displays the wind speeds off the coast of the United States of America (NREL, 2011).

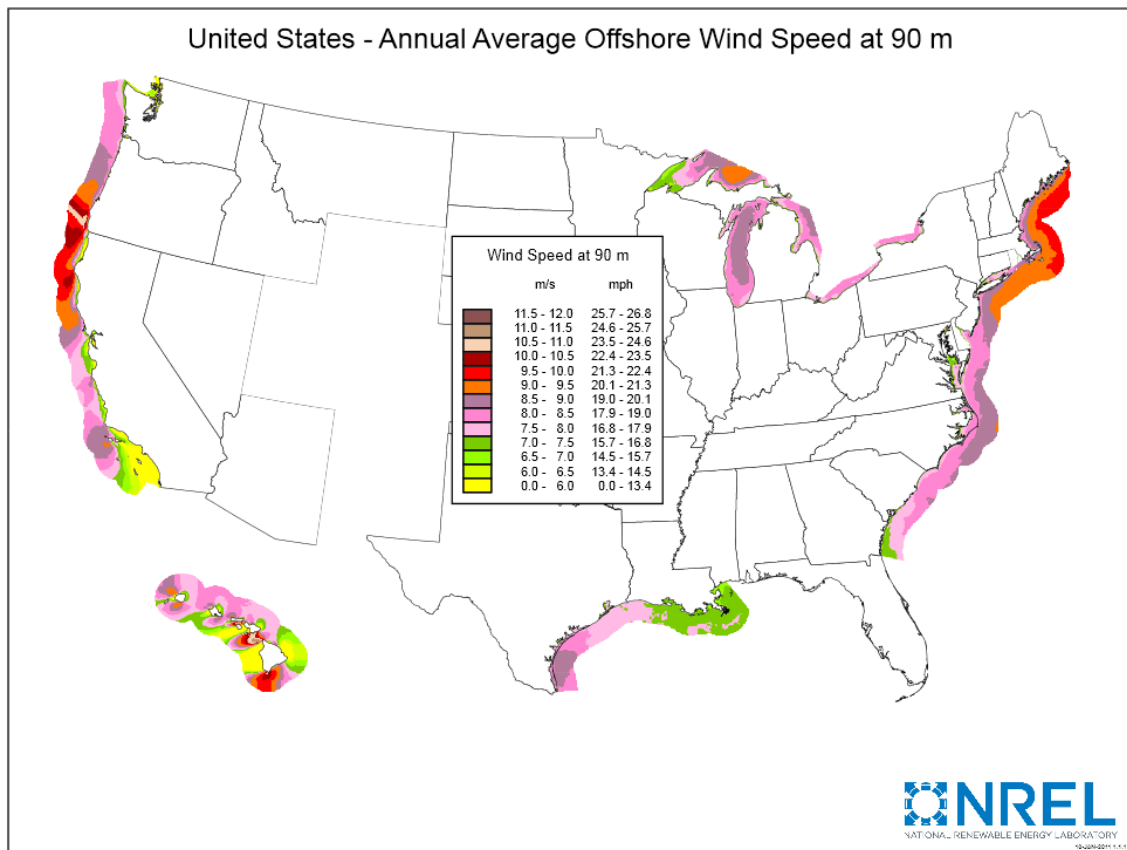


Figure 10.1: NREL (2011) Offshore Wind Data

Wind speeds vary from $0 \frac{m}{sec}$ to $12 \frac{m}{sec}$. The wind velocities values presented in

Figure 10.1 will serve to determine the wind velocities used in this project.

Wind Heeling Arm Equation.

The wind heeling arm equation is a modified version of the roll equation (9.3).

$$\ddot{\phi} + 2\mu\omega_o \dot{\phi} + \frac{\omega_o^2 \text{sign}(\phi)}{GM_o} \overline{GZ}(|\phi|, t) = \frac{M_w}{i_m^2 m_{SSF}} \quad (10.1)$$

Where M_w is the heeling moment induced by a constant wind force, i_m is the mass radius of gyration of the SSF, and m_{SSF} is the mass of the SSF including ballast water.

$$M_w = F_w Z_w \quad (10.2)$$

Where F_w is the wind force, and Z_w is the wind heeling arm.

$$F_w = \frac{1}{2} (C_s C_H \rho_{air} V_w^2 A_p) \quad (10.3)$$

Where C_s is coefficient based on the shape, C_H is coefficient based on the height of the projected area above the waterline, ρ_{air} is the density of air ($1.222 \frac{kg}{m^3}$), V_w is the wind velocity, and A_p is the projected area of the SSF exposed to wind above the waterline. It is assumed that the reaction of the wind moment acts at a depth equal to half the draught.

$$Z_w = H_{WCA} + \frac{T}{2} \quad (10.4)$$

Where H_{WCA} is the height of the center of the projected area of the SSF that is exposed to wind and T is the draught.

Inserting (10.3) and (10.4) into (10.2),

$$M_w = \frac{1}{2} C_S C_H \rho_{air} V_w^2 A_p \left(H_{WCA} + \frac{T}{2} \right) \quad (10.5)$$

When the SSF rolls to a certain heel angle, both A_p and Z_w will change. This change can be approximated as follows (Biran, 2003, p. 124-126), (IMO, 1995, p. 280-281),

$$M_w(\phi) = \frac{1}{2} C_S C_H \rho_{air} V_w^2 A_p \left(H_{WCA} + \frac{T}{2} \right) \cos^2(\phi) \quad (10.6)$$

Inserting (10.6) into (10.1) yields the following equation,

$$\ddot{\phi} + 2\mu\omega_o \dot{\phi} + \frac{\omega_o^2 \text{sign}(\phi)}{GM_o} \overline{GZ}(|\phi|, t) = \frac{\frac{1}{2} C_S C_H \rho_{air} V_w^2 A_p \left(H_{WCA} + \frac{T}{2} \right) \cos^2(\phi)}{i_m^2 m_{SSF}} \quad (10.7)$$

To simplify (10.7), the following variable is defined,

$$\beta = \frac{\frac{1}{2} C_S C_H \rho_{air} V_w^2 A_p \left(H_{WCA} + \frac{T}{2} \right)}{i_m^2 m_{SSF}} \quad (10.8)$$

Inserting (10.8) into (10.7) yields the following equation,

$$\ddot{\phi} + 2\mu\omega_o \dot{\phi} + \frac{\omega_o^2 \text{sign}(\phi)}{GM_o} \overline{GZ}(|\phi|, t) = \beta \cos^2(\phi) \quad (10.9)$$

Using the same substitution technique as done in Chapter 9 yields the following,

$$D(\phi, t) = \left\{ \begin{array}{l} \beta \cos^2(\phi) - 2\mu\omega_o \phi_2 - \frac{\omega_o^2 \text{sign}(\phi_1)}{GM_o} \overline{GZ}(|\phi_1|, t) \end{array} \right. \quad (10.10)$$

Wind Heeling Arm Model.

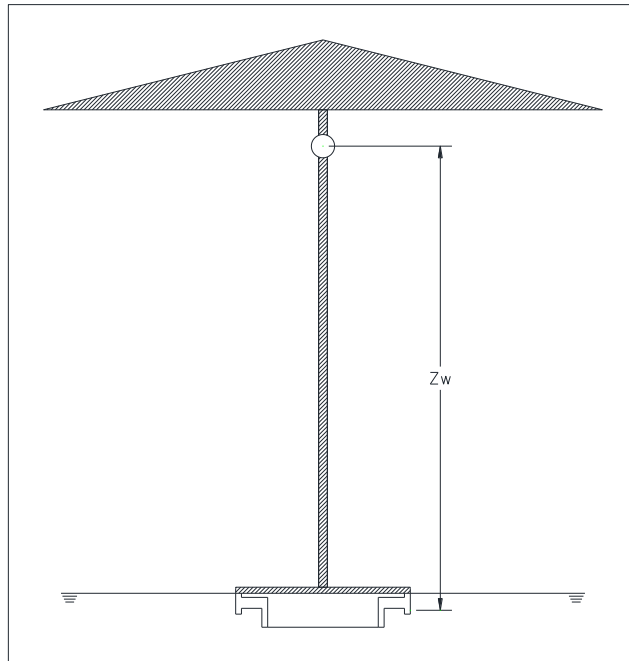


Figure 10.2: Projected Wind Area for Modeled Umbrella.

Figure 10.1 is pictorial representation of the umbrella used in the analysis of the wind-heeling arm. The hatched area is the projected area above the waterline exposed to the wind. This umbrella represents the mast used in Chapter 7-9. The projected area is depicted by the hatched area. The center of exposed area is the center of circle located ~7/8 of the total height above the waterline. The SSF is free-floating and not tethered to the pool, or ocean, floor.

Table 10.1

Modeled Umbrella Properties

Projected Area, A_p	730.35 in ²
Distance to Center of Area, Z_w	78.67 in
CS	0.5
CH	1

The values in Table 10.1 were taken from the following: C_S is found in Table 4.6.3.3.1 of the IMO Code and C_H is found in Table 4.6.3.3.2 of the IMO Code (1995).

Table 10.2

M_H for Various Speeds.

Wind Speed, m/sec	Wind Speed, in/sec	Wind Heeling Moment, lbs-in
1.00	39.37	2.55
2.00	78.74	10.18
3.00	118.11	22.91
4.00	157.48	40.73
5.00	196.85	63.65
6.00	236.22	91.65
7.00	275.59	124.75
8.00	314.96	162.93
9.00	354.33	206.21
10.00	393.70	254.58
11.00	433.07	308.05
12.00	472.44	366.60

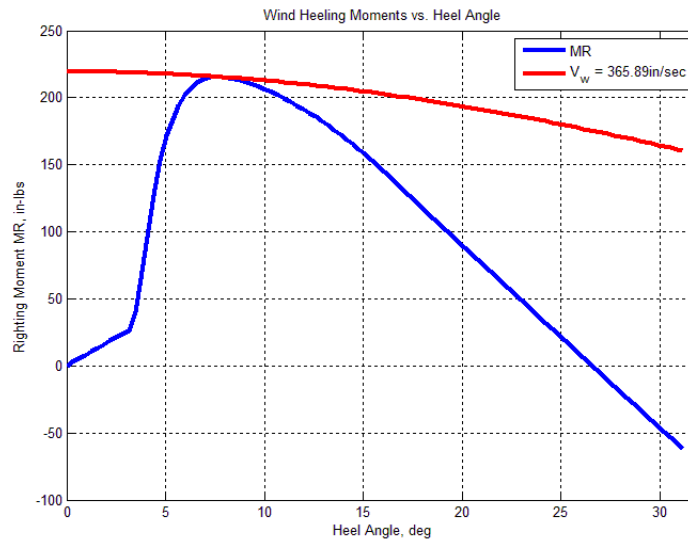


Figure 10.3: M_R Curve: Maximum Wind Heeling Arm.

Table 10.2 lists the max heeling moment for various wind speeds. The highlighted values create M_W that will capsize the SSF. The limiting wind speed is $V_W = 365.89 \frac{in}{sec}$

(for comparison: $V_w = 20.79\text{mph}$ & $V_w = 18.07\text{knots}$). Figure 10.3 illustrates

the M_w curve when $V_w = 365.89 \frac{\text{in}}{\text{sec}}$. It is apparent that any value of wind arm above this

value will capsize the float. Therefore, the analysis will limit V_w to a maximum value

of $354.38 \frac{\text{in}}{\text{sec}}$.

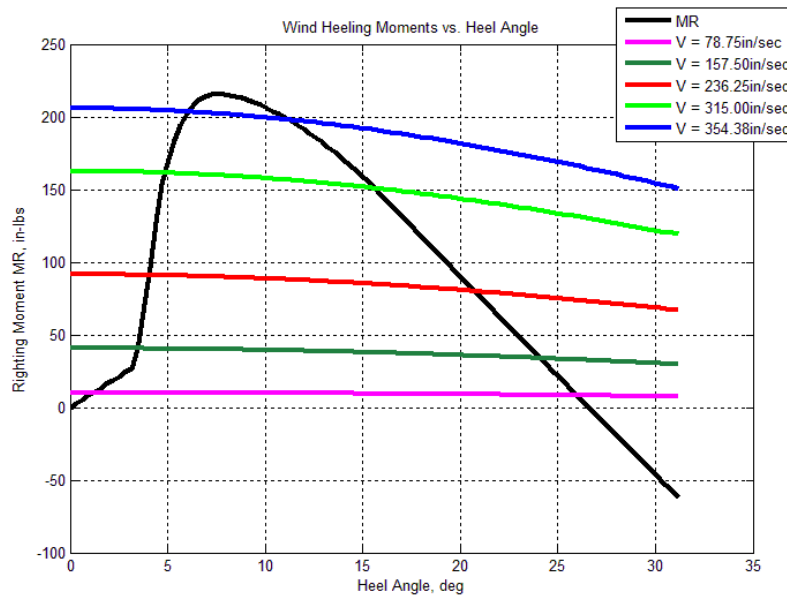


Figure 10.4: M_R Curve: Various Wind Heeling Arms

Figure 10.4 plots the wind heeling arm, M_w , over the M_R Curve. The varying M_w for the wind speeds intersects the M_R Curve in two places as illustrated below in Figure 10.5.

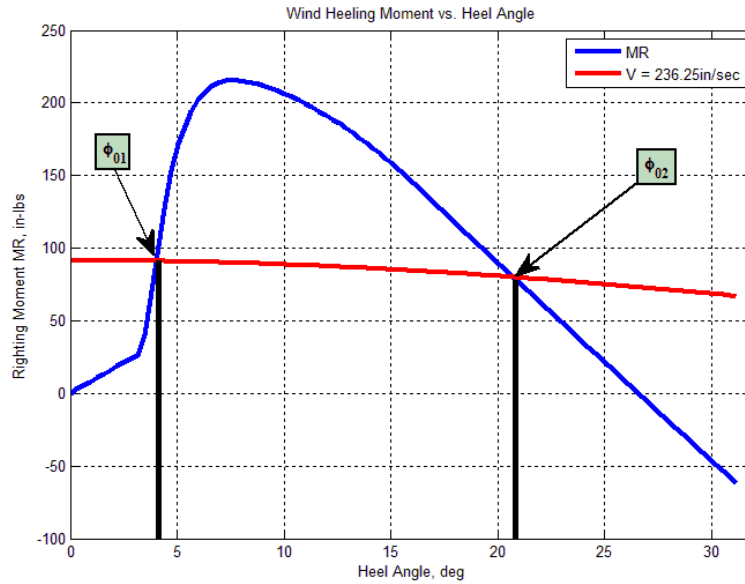


Figure 10.5: M_R Curve: Different ϕ_0 with common V_w

The first intersection, ϕ_{01} , indicates the angle at which $M_w > M_R$ for $\phi < \phi_{01}$ and $M_w < M_R$ for $\phi > \phi_{01}$. The second intersection, ϕ_{02} , indicates the angle at which $M_w < M_R$ for $\phi < \phi_{02}$ and $M_w > M_R$ for $\phi > \phi_{02}$.

Three cases of dynamic phenomena occur when a wind load is incident on the SSF. These are described below:

1. $\phi_0 < \phi_{01}$: Initially, $M_w > M_R$. The SSF will heel in the direction of the wind until M_R is sufficient to overcome M_w and then the SSF will roll in the opposite direction of the wind until M_w is sufficient to overcome M_R . The angles at which this occurs is greater than ϕ_0 . When the SSF rolls back in the direction of the wind the angle at which M_R overcomes M_w is less than the

first time this occurred. This process repeats, achieving angles that are closer in values, until an equilibrium angle is achieved.

2. $\phi_{01} < \phi_0 < \phi_{02}$: Initially, $M_W < M_R$. The SSF will heel in the opposite direction of the wind until M_W is sufficient to overcome M_R and then the SSF will roll in the direction of the wind until M_R is sufficient to overcome M_W . The angle at which this occurs is less than ϕ_0 . When the SSF rolls back in the opposite direction of the wind, the angle at which M_W overcomes M_R is greater than the first time this occurred. This process repeats, achieving angles that are closer in values, until an equilibrium angle is achieved.
3. $\phi > \phi_{02}$: Initially, $M_W > M_R$. The SSF never has a chance to recover because $M_W > M_R$ until the SSF reaches either the Angle of Vanishing Stability, ϕ_{VS} , or the Air Entrance Angle, α . This case will always result in the capsizing of the SSF.

Wind Heeling Arm Evaluation.

To make a comparison between the first and second cases, a specific example of each were evaluated. For this evaluation the wind speed, $V_W = 315.00 \frac{in}{sec}$, and damping coefficient, $\mu = 0.05$, were constant while two different initial heel angles, $\phi_{01} = 0.00^\circ$ and $\phi_{02} = 15.00^\circ$, were used.

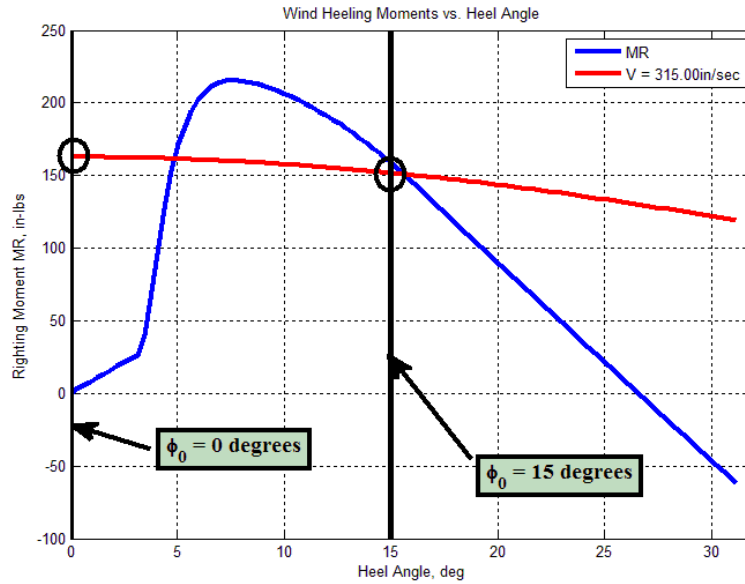


Figure 10.6: $\phi_{01} = 0.00^\circ$, $\phi_{02} = 15.00^\circ$, $V_w = 315.00 \frac{\text{in}}{\text{sec}}$, & $\mu = 0.05$

Figure 10.3 plots the wind heeling moments over the righting moment curve. The red line is the wind heeling moment. The initial heel angle $\phi_{01} = 0.00^\circ$ was chosen at the initial point of the wind heeling moment and the second heel angle $\phi_{02} = 15.00^\circ$ was chosen close to the point where M_w is almost greater than M_R .

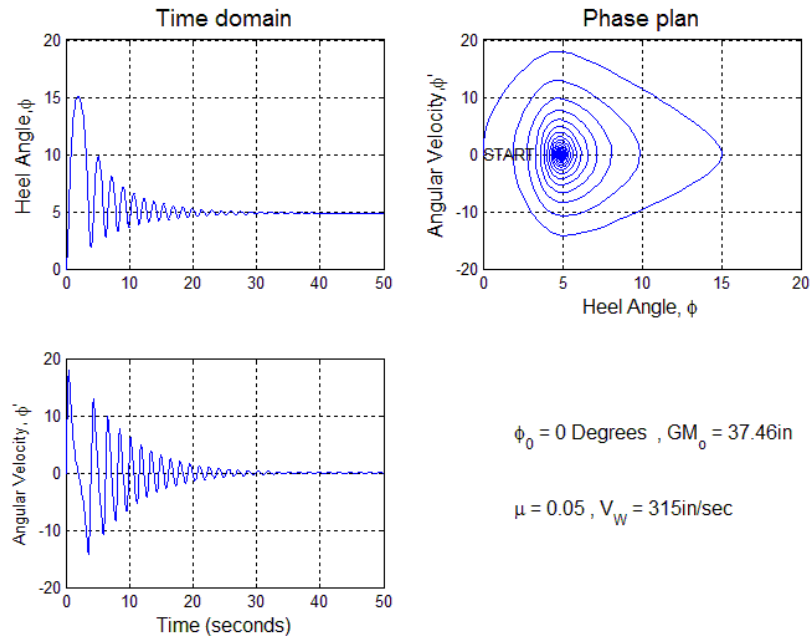


Figure 10.7: Wind Roll: $\phi_0 = 0.00^\circ$, $V_w = 315.00 \frac{in}{sec}$, & $\mu = 0.05$

Figure 10.4 illustrates the first case when $\phi < \phi_{01}$. The plots for the heel angle versus time, the angular frequency versus time, and the phase plane demonstrate the described behavior. The phase plane plot shows the starting angle, $\phi_0 = 0.00^\circ$, and that, in the first roll period, the SSF roll to an extreme angle, $\phi \approx 15^\circ$, and then it rolls back to angle above 0° , $\phi \approx 2.5^\circ$. The SSF float equalizes slightly under 5° .

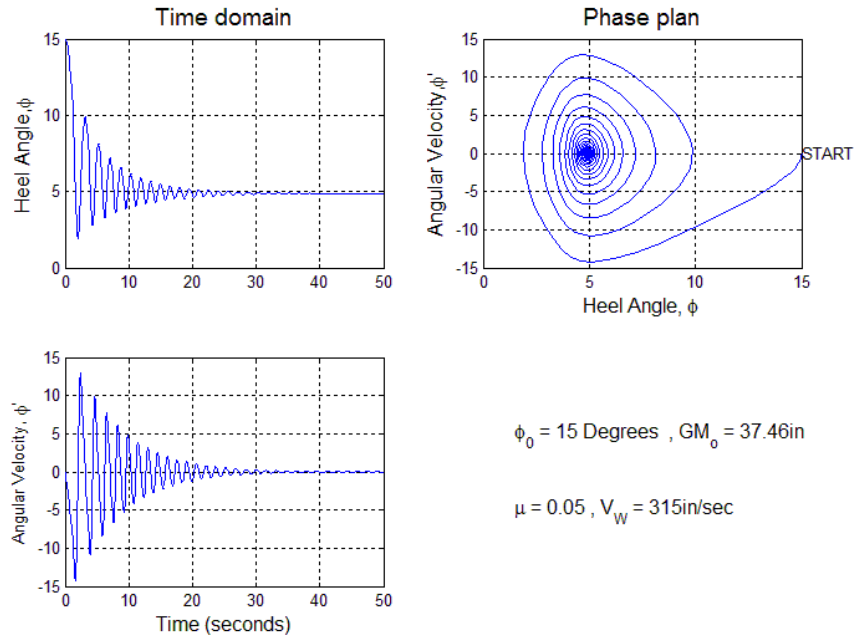


Figure 10.8: Wind Roll: $\phi_0 = 15.00^\circ$, $V_w = 315.00 \frac{\text{in}}{\text{sec}}$, & $\mu = 0.05$

Figure 10.5 illustrates the second case when $\phi_{01} < \phi < \phi_{02}$. The plots for the heel angle versus time, the angular frequency versus time, and the phase plane demonstrate the described behavior. The phase plane plot shows the starting angle, $\phi_0 = 15.00^\circ$, and that in the first roll period the SSF rolls in the opposite direction of the wind until it almost reaches 0° and then it rolls back to angle $\phi \approx 10^\circ$. The SSF float equalizes slightly under 5° . This is the same angle that the SSF float reached an equilibrium state.

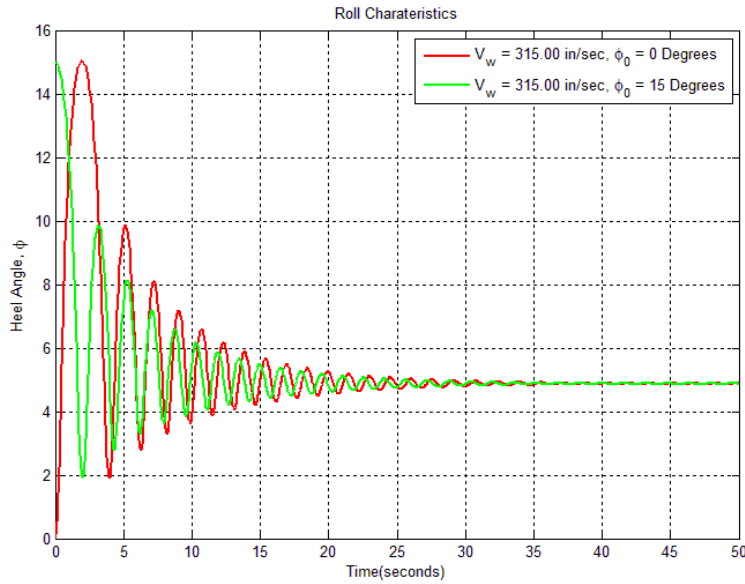


Figure 10.9: Wind Heel Angles: $\phi_{01} = 0.00^\circ$ & $\phi_{02} = 15.00^\circ$

Figure 10.6 overlays the plots for Heel Angle versus Time for the two different ϕ_0 . The SSF equalizes at the same angle given different ϕ_0 and the same wind velocity. From Figure 10.9, it is seen that the offset of the initial angle acts as a phase shift. The curve for $\phi_{01} = 0.00^\circ$ is half a phase behind the curve for $\phi_{02} = 15.00^\circ$, which indicates that the lower the value of ϕ_0 , for the same V_w , the longer it will take for the SSF to reach an equilibrium state.

What if the initial angles were constant and the wind velocity was to vary?

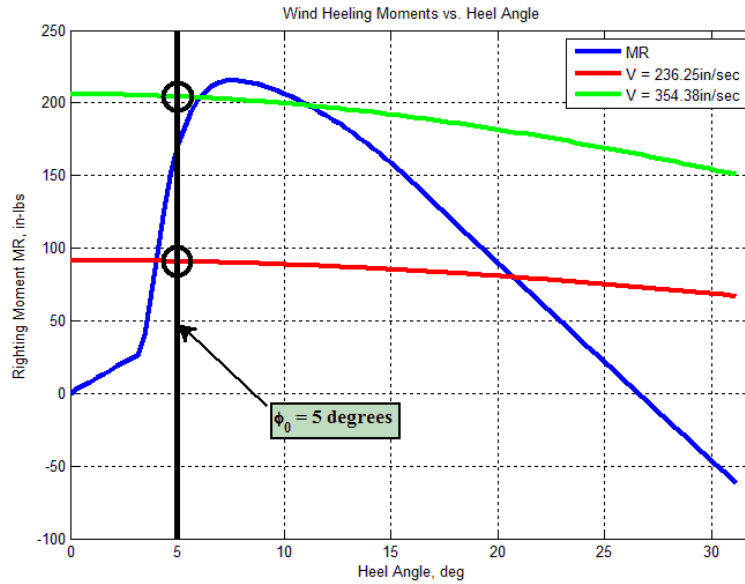


Figure 10.10: Wind Heel Angles: $V_{W1} = 236.25 \frac{\text{in}}{\text{sec}}$ & $V_{W2} = 354.38 \frac{\text{in}}{\text{sec}}$

Figure 10.7 plots the wind heeling moments over the righting moment curve. The initial heel angle, $\phi_0 = 5.00^\circ$, and damping coefficient, $\mu = 0.05$, are constant for both

M_W curves. The red curve is the curve for M_W when $V_{W1} = 236.25 \frac{\text{in}}{\text{sec}}$ and the green

curve is the curve for M_W when $V_{W2} = 354.38 \frac{\text{in}}{\text{sec}}$. The M_W curve for

$V_{W1} = 236.25 \frac{\text{in}}{\text{sec}}$ intersects $\phi_0 = 5.00^\circ$ when $M_W < M_R$ and the M_W curve for

$V_{W2} = 354.38 \frac{\text{in}}{\text{sec}}$ intersects $\phi_0 = 5.00^\circ$ when $M_W > M_R$.

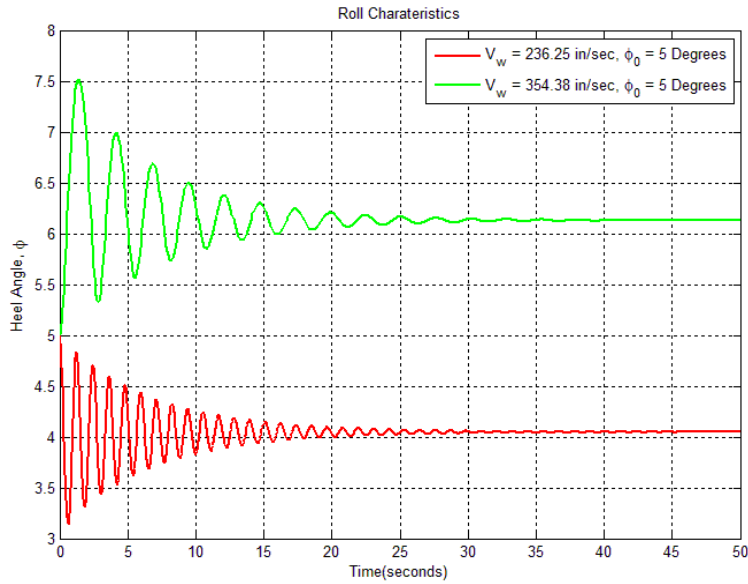


Figure 10.11: $\phi_0 = 5.00^\circ$, $V_{W1} = 236.25 \frac{\text{in}}{\text{sec}}$, $V_{W2} = 354.38 \frac{\text{in}}{\text{sec}}$, & $\mu = 0.05$

Figure 10.6 compares the roll characteristics of the SSF with the same initial heel angle, but with different wind speeds. The red line plots the roll characteristics when

$V_{W2} = 354.38 \frac{\text{in}}{\text{sec}}$ which rolls from 5° to $\sim 3.25^\circ$ and damps out to an angle just above 4° .

The green line plots the roll characteristics when $V_{W2} = 354.38 \frac{\text{in}}{\text{sec}}$ which rolls from 5° to

$\sim 7.5^\circ$ and damps out to an angle $\sim 6.1^\circ$. When the wind speeds varies, the equilibrium angle reached also varies. This is because the wind force is different and will equalize at an angle with an appropriate M_R .

Chapter 11

EXPERIMENTAL DATA

A simple experimental SSF (ESSF) was tested in a backyard pool to verify the calculations in chapters 4-10. This test was not rigorous and meant as a qualitative check on some of the analysis presented in this report.

Table 11.1

Calculated Properties for Experimental SSF.

	Experimental
Mast Weight	9.50 lbf
Mast KG	65.00 in
Ballast Water Weight	21.91 lbf
Ballast Water Volume	606.98 in ³
Ballast Water KG	6.13 in
Total Weight	41.01 lbf
Draught, in	5.63 in
Displacement Volume	1135.90 in ³
KB, in	3.66 in
KG, in	19.77 in
BM, in	35.01 in
GM, in	18.90 in
If, in	26.56 in
GMeff, in	45.46 in
Kempf's Factor	5.77

Table 11.1 presents the properties for the Experimental SSF (ESSF). All properties were calculated using the density of fresh water rather than the density of salt water. Fresh water is slightly denser than fresh water, which decreases the displaced volume and draught. Due to construction issues, the ESSF used a smaller mast than what was used in the analysis. Still, correlations are possible and trends can be verified



Figure 11.1: Experimental SSF

According to calculations, and as seen in Table 11.1, the draught, $T = 5.634in$. A scale was attached to the side of the ESSF to check draught when submerged. This scale measures vertically down from the top of the ESSF. To verify that the calculated draught is correct, the calculated draught is subtracted from the total height of the SSF and then compared to the measurement on the ESSF.



Figure 11.2: Actual Draught of Experimental SSF

$$H_{WL} = H_{TOTAL} - T$$

$$H_{WL} = 6.875in - 5.634in = 1.241in$$

Figure 11.2 shows the actual draught of the ESSF, which is just above 1.39in. The disparity in calculated draught and actual draught is a combination of a slight bend in the mast, which caused the ESSF to list away from the side with the tape measure, and the motion of the water in the pool.

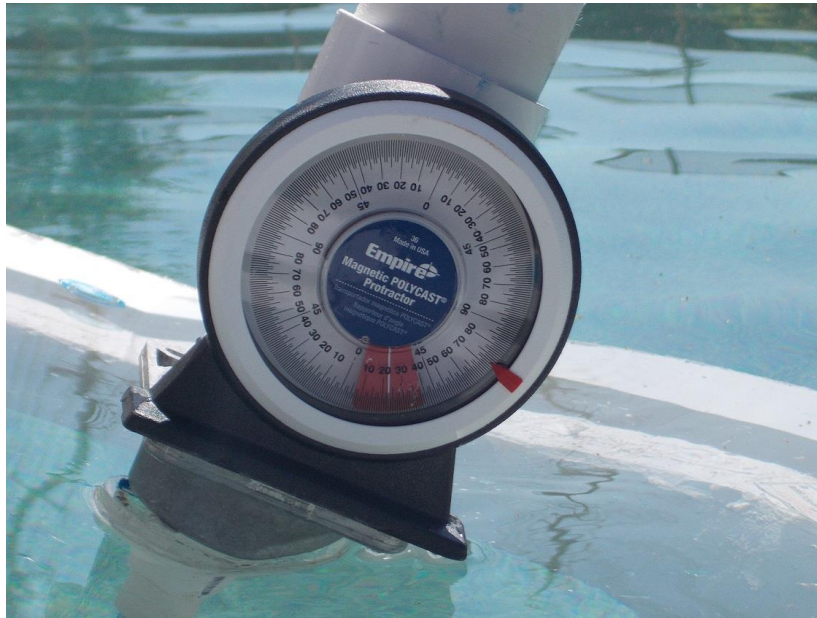


Figure 11.3: Heeled Experimental SSF

Next, the ESSF was heeled to an angle of 22° and allowed to roll back to equilibrium. First, the ESSF rolled past equilibrium and reached a heel angle of $\sim -9^\circ$. It then rolled three more times at low heel angles, between -3° and 3° , before damping out at 0° .

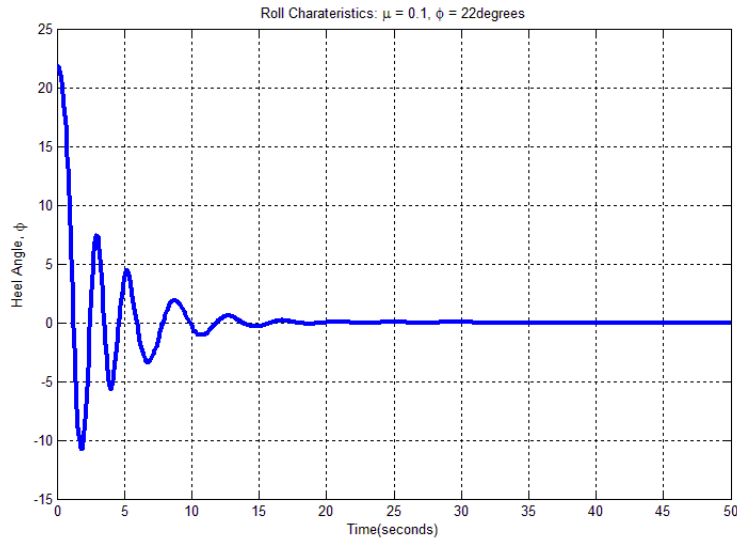


Figure 11.4: Roll Amplitude: Baseline SSF Heeled to 22°

Due to the bend in the mast, the ESSF was unable to return to equilibrium when heeled past 24°, which is close to the predicted value of 26.5° in chapter 8.

Next, the ESSF was subjected to several wave inputs. To create the first wave input, the water was disturbed near the ESSF using different speeds to create different wave phenomena. The ESSF did not succumb to parametric roll and was in no danger of capsizing. The second wave input was created by placing the ESSF in the area of water jets. Once again, no parametric roll resonance occurred and the ESSF did not capsize. Once the ESSF was outside of the induced wave area, it returned to equilibrium.



Figure 11.5: Experimental SSF in Waves

Chapter 12

CONCLUSION AND FURTHER WORK

When a float platform incorporates Suction-Stabilization there is a dramatic improvement in stability. Suction-Stabilization raises the effective metacentric height by approximately 300%, it increases the righting moment between 1000% and 1100%, and it increases the righting lever between 600% and 700% above a float with the same geometry that does not incorporate Suction-Stabilization. The increase in these metrics allows the SSF to withstand higher wind and wave loads than it would in the absence of Suction-Stabilization.

Table 12.1

Comparison: All Geometric Variations.

	No Suction Stabilization	Section 4 Height	Section 4 Diameter	All Section Diameters
Metacentric Height	(-)	(-)	(+)	(+)
Roll Period	(+)	(+)	(-)	(-)
Kempf Factor	(+)	(+)	(-)	(-)
Angle of Vanishing Stability	(-)	(+)	(+)	(+)
Air Entrance Angle	(-)	(+)	(-)	(-)
Righting Moment	(-)	(+)	(+)	(+)
Righting Lever	(-)	(-)	(+)	(+)

(+) - Indicates an Increase from the Baseline SSF

(-) - Indicates a Decrease from the Baseline SSF

The overall stability of the baseline SSF is improved slightly when the height of Section 4 is increased, although at the cost of a lower metacentric height. The reason the decreased metacentric height does not decrease the stability is that the increased Section 4 height allows for a greater volume of trapped ballast water and increases the IST effect.

Stability increases dramatically with the increase of the Section 4 outer and inner diameters and even more so with the increase of the inner and outer diameters of all

sections. However, with the increase of any diameter, without an appropriate increase in Section 4 height, comes the adverse effect of decreasing the air entrance angle and limiting the operable heel angle range. This limit in operable heel angle range is offset by the increased righting moment and righting lever, which requires a much higher load to attain larger heel angles.

From the analysis presented in Chapters 9 and 10 of this report, it is seen that the baseline SSF, which is the worst case presented based on \overline{GZ} and M_R curves, is stable in calm water for heel angles up to the air entrance angle, 26.5° . The baseline SSF is also stable for wind speed up to $V_{w2} = 354.38 \frac{in}{sec}$. Although the various geometries were not analyzed directly under wind load, it is inferred from their respective \overline{GZ} and M_R curves that the geometries explored beyond the baseline SSF would demonstrate improved performance under the same wind loads and remain stable when exposed to higher wind velocities.

Future work needs to be completed on expanding the geometries analyzed in dynamic situations. It is recommended that the following cases are examined.

1. Varying the height of Section 1.
2. Varying the height of Section 4 in cases where all diameters are greater than that of the Baseline.
3. Using a rectangular float rounded corners as opposed to a cylindrical float might help to increase the stability.

4. Changing the material of the SSF body and the top plate to lighter and heavier material might allow for the designer to use the baseline geometry and increase its stability.

It is also recommended that actual wave loads be applied to the SSF to determine what size increases are needed for use in offshore applications. In that same vein, an actual wind turbine should be used in the analysis. This should include the induced forces from both the wind and the rotation of the turbine blades.

REFERENCES

- American Bureau of Shipping. "*GUIDE FOR THE: Assessment of Parametric Roll Resonance in the Design of Container Carriers.*" 2004. American Bureau of Shipping. Houston, TX.
- Avallone, E.A., Baumeister, T., Baumeister, T.III., 1978. *Mark's Standar Handbook for Mechanical Engineers*. 8th ed. New York, NY: McGraw-Hill
- Bangun, E.P., Utsonomiya, T., Wang, C.M. (2010) Hydrodynamic Forces on a Rolling Barge with Bilge Keels. *Ocean Engineering*. 32, 219-232.
- Biran, Adrian. 2003. *Ship Hydrostatic and Stability*. 3rd ed. Oxford, UK: Butterworth-Heinemann (Elsevier)
- Butterfield, S., Jonkman, J., Musial, W., Sclavounos, P.D., and Wayman., E.N. (2006) Coupled Dynamics Modeling of Floating Wind Turbine Systems. Conference paper for Offshore Technological Conference No. NREL/CP-500-39481.
- Butterfield, S., Jonkman, J., Musial, W., Sclavounos, P., and Wayman., E.N. (2007) Engineering Challenges for Offshore Wind Turbines. Conference paper for Offshore Technological Conference No. NREL/CP-500-38776.
- Cheung, K.F., Lee, S.K., Phadke, A.C., Seidl, L.H., Smith, D.A. (2000). Hydrodynamic

- Response of a Pneumatic Floating Platform. *Ocean Engineering*. 27, 1407-1444.
- IMO (1995). *Code on Intact Stability for All Types of Ships Covered by IMO Instruments-Resolution A.749(18)*. London: International Maritime Organization.
- Kliava, Janis, Megel, Jacques. (2010) Metacenter and Ship Stability. *American Journal of Physics*. 78, 738-747.
- Montgomery, James.** (2012). US Patent Application No. 13/242,489. Publication No. US 2012/0090525 A1. Filing Date: September 23rd, 2011.
- National Renewable Resource Laboratory (NREL) (2011). Offshore Wind Resource Characterization. Retrieved from http://www.nrel.gov/wind/offshore_resource_characterization.html
- Redkar, Sangram. (2012). *Suction Stabilized Float (SSF) Progress Report (12/21/2012)*. Arizona State University. Mesa, AZ.
- Taylor, Metin. (2007) On Parametric Resonance of Container Ships. *Ocean Engineering*. 34, 1021-1027.
- Unknown Author. (1987). *Ship Calculations II*. VM156 H36 1987 V. 2. Marine Institute

Library.

Vidic-Perunovic, Jelena. (2011) Influence of the GZ Calculation Method on Parametric Roll Prediction. *Ocean Engineering*. 38, 295-303.

APPENDIX A

UMBRELLA USED AS MAST BASIS

http://www.overstock.com/Home-Garden/Premium-9-foot-Round-Tuscan-Orange-Wood-Patio-Umbrella-1-overstock.com

Shipping Carr Travel Insurance B2B O-Info

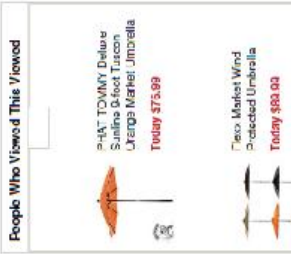
Sign In Join Club O Email Wish List Gift Cards Español

FOR BIDDERS/BUYERS UNDER 18, SEE TERMS & CONDITIONS

SEARCH 0 Item(s)

ALL DEPARTMENTS FOR THE HOME FURNITURE RUSS & DECOR BEDDING & BATH WOMEN MEN JEWELRY & WATCHES HEALTH & BEAUTY ELECTRONICS

Online Shopping Home & Garden Garden & Patio Patio Umbrellas & Shades **Patio Umbrellas**



Premium 9-foot Round Tuscan Orange Wood Patio Umbrella

Write a review

Today **\$92.99**

Item #: 13664722

This 9-foot round patio umbrella brings a tropical feel to your patio or deck while providing you with full UV protection. The sturdy wood frame and polyester rip allow this umbrella to stand up to even the strongest rain, wind, and sun... more

View larger

Qty: 1 [Add to Cart](#)

Add to Wish List Save for Later Delivery Estimate

earn **\$4.65** in rewards on this product

Club O Members Earn 5% in Club O dollars on this Product!

Learn More

Overstock.com Master Card® \$2.1 bonus after activation & 11% into FIFTY

Product Details | **Product Q&A** | **Shipping & Returns**

- Color: Tuscan orange
- Materials: Wood and polyester
- Pole materials: Wood
- Weatherproof
- Shade UV Protection
- Weight: 15 lbs. net wt.
- Dimensions: 36 inches High x 110 inches wide x 100 inches deep

Assembly Required

Buying Guides

- [Tips on Buying a Patio Umbrella](#)
- [How to Store a Patio Umbrella for Winter](#)
- [How to Choose an Outdoor Living Shade](#)

People Who Viewed This Viewed

- **3-1/2" TOWNY Deluxe Sunbrella 6-foot Market Umprella** Today **\$75.99**
- **6-foot Market Wind Protected Umbrella** Today **\$69.99**
- **TropShade 8-foot Flute Aluminum Bronze Market Umbrella** Today **\$83.99**
- **TropShade Flute 3-foot Umbrella Shade** Today **\$53.99**
- **3-1/2" TOWNY Deluxe Sunbrella 6-foot Market 3-foot Market Umbrella** Today **\$93.99**

8-foot 8-foot Patio Umbrella Today **\$51.99**

Dimensions: See description
Materials: Polyester, Wood
Model No.: LC-892043-TUSCAN

Features: English

Material: Wood

Assembly: Assembled

Was this product information helpful? Yes No

Related Categories

- Assembly / Assembler: Patio Umbrellas
- Brand: Laxson & Co. Patio Umbrellas
- Colorway: Brown Umbrella, Patio Umbrella